Deltares

Morphological model for the river Rhine

First (v0) model of the Waal branch

Morphological model for the river Rhine
First (v0) model of the Waal branch

Author(s)
Anke Becker
Anna Kosters
Ana Luisa Nunes de Alencar Osorio
Victor Chavarrias
Willem Ottevanger

Morphological model for the river Rhine
First (v0) model of the Waal branch

Opdrachtgever	Rijkswaterstaat Water, Verkeer en Leefomgeving
Contactpersoon	Arjan Sieben, Michiel Reneerkens, Dénes Beyer
Referenties	
Trefwoorden	Morphological model, Rhine, DVR

Documentgegevens	
Versie	1.0
Datum	20-12-2023
Projectnummer	11209261-003
Document ID	11209261-003-ZWS-0002
Pagina's	120
Classificatie	
Status	final

Auteur(s)		
	Anna Kosters	
	Victor Chavarrias	
	Willem Ottevanger	
	Anke Becker	

Summary

The riverbed (main channel and flood plains) of the Rhine branches is dynamic and changes over time under the influence of morphological processes and human intervention. Currently, morphodynamics in the Rhine branches can be predicted and assessed with the so-called DVR model. For three reasons, this model is however outdated. Therefore, a new model and set of tools is being developed to replace the old one.

In 2023, a first version of the morphological model of the Waal (v0) was set-up based on existing 6th generation hydrodynamic models. Schematizations for three moments have been made: j99 (start of calibration period), j16 (start of validation period), and j19. The latter was used for a wide range of test simulations to test model performance and stability and find appropriate approaches for morphological spin-up, boundary conditions and morphological factors. First calibration runs have been carried out with j99. The results for width averaged bed level changes and sediment transport are promising. Local deviations between model behavior and reality need to be removed in the next phase during more detailed (2D) calibration.

Model stability has been an issue that seriously hampered progress. Several changes have been made to the software in order to improve stability and the workflow of model runs in the Simulation Management Tool (SMT). At the moment, we are still testing these. Looking at current model results, it seems that instabilities result from issues in the software rather than from the model schematizations. We did however identify points of attention in the schematization as well, that need to be looked at in more detail in the coming phase of model development.

The 6th generation hydrodynamic model was changed in several points to make it usable for morphological simulations. The most important one was the definition of main channel roughness. A proposition was made on how to improve the approach to implement main channel roughness in future hydrodynamic models, so that they can be used for morphological simulations as well. These can be tested in the following phase, once the model is more stable and better calibrated.

In parallel to the Waal model, the first model version (v0) for the IJssel has been set-up in the same way as the one of the Waal for the situation in 2016 (j16). The simulations for hydrodynamic spin-up and validation are running at the moment, first morphological simulations are expected to start soon. The results will then be presented in a following report.

All steps in model development and the main steps in analysis of model results have been defined in Matlab scripts to make them reproducible and re-usable for model development for other branches or future scenarios.

Inhoud

1 Introduction

1.1 Background and motivation

The riverbed (main channel and flood plains) of the Rhine branches is dynamic and changes over time under the influence of morphological processes and human intervention. Currently, morphodynamics in the Rhine branches can be predicted and assessed with the so-called DVR model (Duurzame Vaardiepte Rijndelta – sustainable fairway Rhine delta). For three reasons, this model will be outdated in the foreseeable future:

1 The calibration is based on periods before realization of several important interventions (Room for the River, Water Framework Directive).
2 RWS is moving to a new model generation in new software (the 6th generation models in the D-HYDRO Suite software package).
3 There are new data and insights regarding morphological developments.

An up-to-date and reliable model is however needed for river management issues such as:

- project design of interventions in/along the summer bed (normalisation, sediment management),
- impact assessment for evaluation of measures (river engineering assessment framework / licensing),
- analyses of/after monitoring in pilots (sediment management, eroding banks, river widening such as by longitudinal dams, etc.),
- system analyses for long-term scenarios with management variants, e.g. for IRM (Integraal RivierManagement – Integrated River Management) so that estimates can be made of the morphological development on the different river functions.

These are reasons to replace the current modelling instrument for the Rhine branches with a new set of models and tools.

1.2 Objective

The objective of this project is the development of a new modelling instrument that simulates the complex spatial riverbed dynamics in the Rhine branches, enabling us to predict developments and effects of interventions in the riverbed, examine options for long-term (2050-2100) management and policy decisions, and thus shape the river management of the future.

1.3 This report

The development of such a modelling instrument for the entire Rhine branches will take several years. In 2023, a start is made with the steps described in Chapter 2. Chapter 3 gives an overview of the data used for the model set-up. Chapters 4 to 9 describe the model set-up and present validation results. Chapter 10 presents modeling strategies that are needed for future application of the model. Chapter 11 shows conclusions and recommendations for the following steps to be taken in the model development.

1.4 Software

Within this project, the following software is used:

Software package	Version	Used for
D-HYDRO Suite	2023.01 (2.21.17.76916)	Hydrodynamic simulations Morphological simulations
	2.25.07.78558	Morphological simulations
Baseline	6.3.2	Schematization of model geometry
ArcGIS	10.6	In combination with Baseline

2 Approach for model set-up

2.1 General approach of the long-term model development

Spruyt (2023) has made an inventory of the intended use of the new modelling instrument and its required functionality. Based on this, she presents a general approach, which foresees a model development in several steps. These steps are extended as follows for this project:

- v0 This version is a basic model that contains the most important functionality, with the main goal to have a running but not yet too complex model.
- v1 Building on v0, the first model version replaces the existing DVR model. It covers the same functionality, but is based on the latest available data and insights.
- v2 The second model version is based on v1 but extended with new functionality to make the model suitable for more types of applications (e.g. finer grids, exchange of sediment between main channel and flood plains, bank erosion processes, etc.).
- v3 The third model version is used to develop new insights and functionality.

To give structure to this long-term development, several activity areas are defined as presented in Table 2.1 and linked to the stages of model development (v0-v3). The starting point is formed by the existing hydrodynamic model schematizations of RWS (the so-called 6th generation hydrodynamic models).

To effectively carry out the model set-up and associated calibration, we start by setting up submodels for different river branches, which can then relatively easily be merged into an overall model. The intended coverage of the final model is presented in Figure 2.1.

In each year of the model development, specific activities are identified for the different areas of activity per submodel.

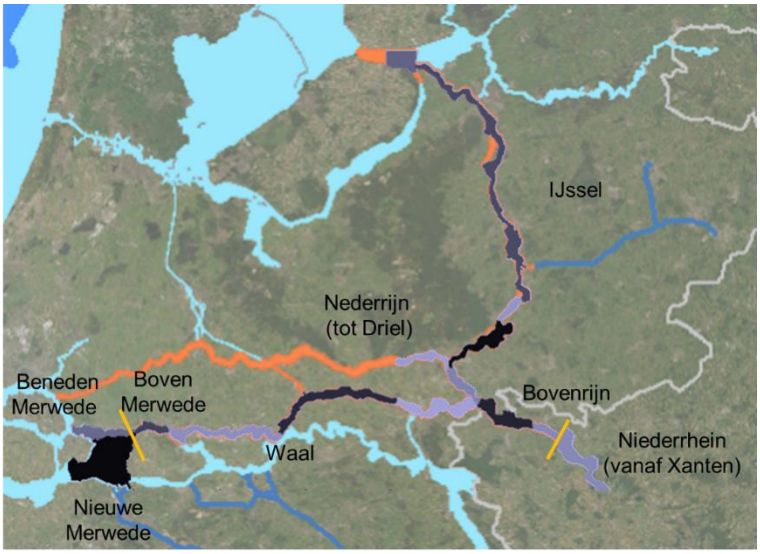

Figure 2.1 Coverage of the sixth-generation hydrodynamic Rhine branches model (orange) and the current DVR instrument (purple areas, the different purple colors indicate the subdomains of which that model consists).

2.2 Overview of the activities carried out in 2023

In 2023, a start was made with the development of the first basic models (v0) of the Waal and IJssel branches. The Waal model was used as example to test methodologies and develop the necessary scripts. Both the Waal and IJssel models helped to identify issues in the existing tools and software used as well as in the model schematizations.

More specifically, the following steps were carried out:

- collection of the data needed to carry out the next steps (Chapter 3),
- modification of the existing hydrodynamic model to make it suitable for morphodynamic simulations (Chapter 4),
- hydrodynamic validation of the modified model (Chapter 5),
- set-up of basic morphodynamic schematizations (v0) of the Waal and IJssel branch (two separate submodels) (Chapter 6),
- “offline calibration” of the Waal branch to get a first impression of the performance of the chosen transport formula in combination with the model schematization (i.e. (gradients in) flow velocities, roughnesses and grain sizes) (Chapter 7),
- running a lot of test simulations to check for model stability and plausibility (findings were directly implemented into the models as described in this report, or collected in the recommendations for future improvement of the models in section 10.5),
- running a specific test simulation for the period of 2019-2022 with the Waal model, with a focus on the morphodynamic behavior around the longitudinal training walls (Chapter 8),
- first steps in the 1D calibration of mainly the Waal branch, including the choice of calibration and validation periods (Chapter 9),
- development of methodologies and tools needed to run the models (Chapter 10), specifically:
    - implementation of the Waal and IJssel models in the SMT (Simulation Management Tool) structure,
    - methodology for spin-up of initial sediment composition and bed levels,
    - making main channel roughness suitable for morphodynamic simulations (first steps).

Model schematizations representing the geometry of three different years were prepared for the Waal (see section 4.1 for more detail):

- 2019: as a first test case, that includes the longitudinal training walls. The choice for 2019 was made before the calibration and validation periods were chosen.
- 1999: This will be the start of the calibration period (1999-2012, section 9.2).
- 2016: This will be the start of the validation period (2016-2022, section 9.2).

In a later stage, the schematization of the IJssel representing the situation in the year 2016 was prepared, because 2016 will be the start of (one of) the calibration/validation period(s). This schematization was not yet tested intensively and is therefore not yet presented in this report.

Table 2.1 Steps in model development.

activity areas	associated activities	model version	done in 2023
data collection	• Collection of all data needed to set-up a model, e.g. boundary conditions, calibration data hydrodynamics and sediment transport and morphology, bed composition, etc.	v0 v1	Waal: boundary conditions, 1D calibration data all branches: discharge distribution; bed composition
morphodynamic model schematization: towards a well-working basic model (v0)	• set-up of a first running model including: a. dynamic river bed b. representative initial bed elevation (e.g. smoothing of bed forms) c. suitable roughness formulation for morphology d. sediment (grain sizes and sediment layers, with focus on active/upper layer) e. secondary flow f. first choice of transport formula and parameters (uncalibrated) g. non-erodible and less erodible layers h. suitable grid resolution • testing phase v0 model, identification of problems and modification of the schematization accordingly	v0	Waal v0 IJssel v0 (both to be continued in 2024)
extending the basic model to a v1 model	• more sophisticated description of a. main channel roughness b. composition and thickness of underlayers, including non-erodible layers • set-up of a dredging and dumping module • testing phase v1 model, and iterative modification of model schematization if necessary	v1	-
development of methodologies and tools for running the model	• approach and tools for model simulation (i.e. Simulation Management Tool) • strategy for model spin-up • strategy and tools for model evaluation and presentation of results • strategy and tools for simplification of model set-up and improving reproducibility	v0 v1	Waal v0 IJssel v0 (both to be continued in 2024)
model calibration and validation	• calibration and validation strategy • adapting the hydrodynamic model to make it suitable for morphodynamic simulations • hydrodynamic validation • “offline” calibration giving a first estimate of morphological response based on the flow field in the hydrodynamic simulations • 1D morphodynamic calibration and validation (focusing on width-averaged, large-scale and long-term trends) • 2D morphodynamic calibration and validation (focusing on 2D patterns in the river bed, such as bank patterns and bend profiles) • validation of dredging and dumping module	v1	Waal v0 (made a start)

activity areas	associated activities	model version	done in 2023
exploring model uncertainties	• influence of unknown physical variables (e.g. roughness in transport, bed composition, active layer thickness) • influence of model settings (e.g. initial geometry/composition and boundary conditions) or modelling concepts (e.g. Hirano model) • influence of simulation strategy and approaches (e.g. methods for optimizing simulation time, schematization of the hydrograph, choice of simulation period)	v1-v3	-
development of modeling strategies and development for future use of the model	• identifying types of application and requirements • development of strategies for application of the model (e.g. choice of scenarios, choices for model settings and geometry, type of interventions) • identifying needs for further development of the model schematization (including needs for knowledge development and data requirements) • implementation and testing	v1-v3	-
verification of model application	• testing the model application in test cases of a. effect of interventions b. planning study (“planstudie”) c. (long-term) forecast of system behaviour • improvement of the model schematization, modeling strategies, methodologies and tools based on the outcomes of the test cases	v1-v3	-
Implementation of new functionality in D-HYDRO	• Identifying requirements of new functionality • functional design of needs • design of implementation • implementation and testing • updating user manuals	v2-v3	-

3 Data

3.1 Observed discharges and water levels

Observed discharges and water levels (daily values) have been delivered by RWS. For the Waal the data covers the period 1999-2022, for the IJssel the period 2016-2022. In 2023, the Waal discharge was used to derive a detailed discharge hydrograph for the period 2019-2022 (section 8.1). For all other simulations, the discharge hydrograph from the DVR model in Delft3D 4, the predecessor of the new model, was used (see section 3.2). In the future, the discharge and water level data can be used to refine the approach for the upstream and/or downstream model boundaries.

3.2 Discharge distribution

The initial version (v0) of the new morphodynamic model of the Waal still makes use of approaches that were derived for its predecessor, the “DVR model” in Delft3D 4. This also applies for the hydrodynamic upstream boundary condition, which is a standardized yearly hydrograph consisting of several stages with constant discharges (Figure 4.11). The same hydrograph is used in v0 of the new model.

Since the DVR hydrograph was originally defined for Lobith on the Boven-Rijn, it had to be translated to the corresponding values on the Waal first. For this translation, information on the discharge distribution for a range of discharges at Lobith, as computed by RWS-ON, was used. Since the discharge distribution at Pannerdensche Kop has changed in the past decades due to continuous incision of the river bed of especially the Waal on the one hand and man-made modifications in the river geometry (e.g. Room for the River measures) on the other hand, it was decided to use two different discharge distributions for the different periods that are to be modelled, i.e. one distribution for more recent periods starting from 2016, and another one for the period between 1999 and 2012.

The distribution for 2016 and later is based on the current Qf-relation (Qf18 stationair), corrected for weir operation, bed level changes (until 01/01/2023), and a closed mass balance at the bifurcation points (‘vereffening’). The Waal discharges corresponding to the nine DVR discharge levels at Lobith were derived based on linear interpolation between the Lobith discharges for which the discharge distribution was computed. The distribution for 1999-2012 was derived in the same way but based on the QH-relation 2000.1 (including corrections to get a closed mass balance at the bifurcation points). The resulting values for both relations are given in Table 3.1 and Figure 4.11.

Table 3.1 Translation of DVR discharge levels to upstream boundary conditions for the Waal pilot model (v0).

Discharge level no.	Q Boven-Rijn (DVR levels) [m^3/s]	Q Waal 1999-2012 [m^3/s]	Q Waal from 2016 [m^3/s]
1	1020	818	829
2	1203	957	972
3	1635	1228	1312
4	2250	1531	1642
5	3053	2065	2132
6	3824	2579	2654
7	4717	3163	3264
8	6151	4137	4231
9	8592	5679	5778

3.3 Grain sizes

Grain size data that covers the entire Waal up to km 952 is available from measurement campaigns from 1995 and 2020 (Figure 3.1). For the new model, the 2020 data will be used. In that campaign, samples have been taken at a distance of 500 m (full and half river kilometers) along the river axis and at a distance of 1.000 m (full river kilometers) along two parallel lines +/-70 m from the river axis (Table 3.2).

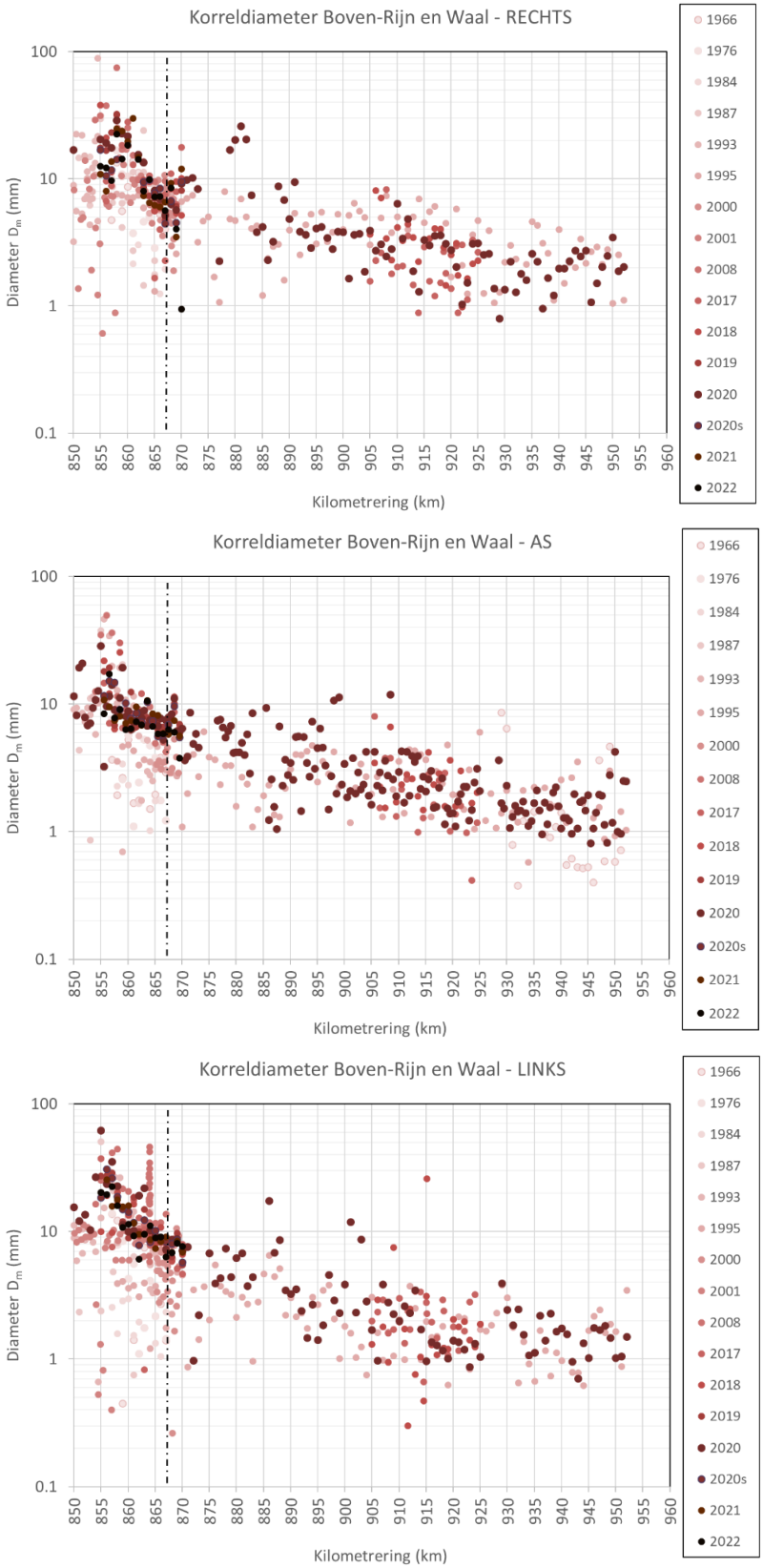

Figure 3.1 Available grain size data for Boven-Rijn and Waal. Top: 70 to the right of the river axis; middle: on the river axis; bottom: 70 m to the left of the river axis.

Table 3.2 Location of data points with sieve curves from the 2020 measurement campaign.

Location	Streamwise coordinates	Transverse coordinate
Left bank	849, 850, … 951, 952	-70 m
Axis	849, 849.5, 850, … 951, 951.5, 952	0 m
Right bank	849, 850, … 951, 952	70 m

3.4 1D calibration data

The following data is available for the 1D calibration, which focusses on long-term and large-scale trends in bed level development as well as yearly sediment transport rates. Furthermore, celerity of bed disturbances is used as a more-easy-to-measure proxy for sediment transport rates.

3.4.1 Trends in bed level change

De Joode (2023) has projected all available multibeam bed level measurements (1 m x 1 m) of the period 1999-2021 onto a grid, which has been defined as (Figure 3.2):

- The length of the cells is 100 m on the river axis and varies slightly towards the outer edges of the main channel due to its curvature.
- The width of the main channel (in between 'normaallijnen') is divided into 8 cells, 4 of which to the left of the river axis (labelled L4-L1) and the other for to the right of the river axis (labelled R1-R4).

De Joode (2023) processed the multibeam data into cell averaged bed elevations and standard deviation per grid cell. This data is used as basis for 1D model calibration.

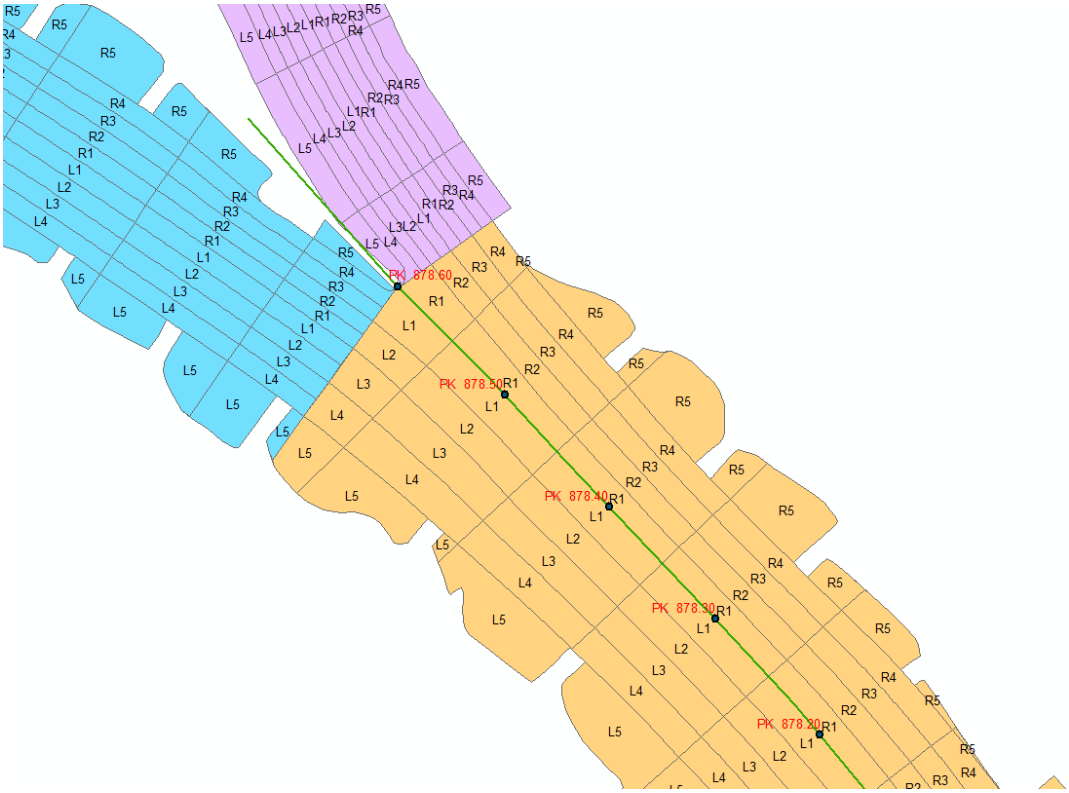

Figure 3.2 Extract from the grid used to analyze bed elevations (from De Joode, 2023).

The morphologically active zone (see section 6.3 for the definition of that) of the new model generally extends slightly into R4 and L4 (Figure 3.3).

Analysis of the data has shown that data coverage is low in the groyne fields (R5 and L5) and around of groyne heads, which mostly fall into R4 or L4 (Figure 3.4). Therefore it was decided to use the data from L3 to R3 for model calibration. Figure 3.4 shows that the data also does not always fully cover the L3-R3 cells. In that case the data of the year that does not provide sufficient coverage is not used in the calibration dataset for the respective cells. A threshold of 99 % coverage has been employed for considering that there is sufficient data for considering the cell. During calibration, data gaps for specific years and cells can be filled by looking at other years that do provide sufficient data for those cells.

As during 1D calibration the focus is laid on width-averaged and large-scale behavior of the model, the data of De Joode was averaged across L3-R3 cells and river sections of 1 km length. Figure 3.5 shows the resulting bed level development for the Waal.

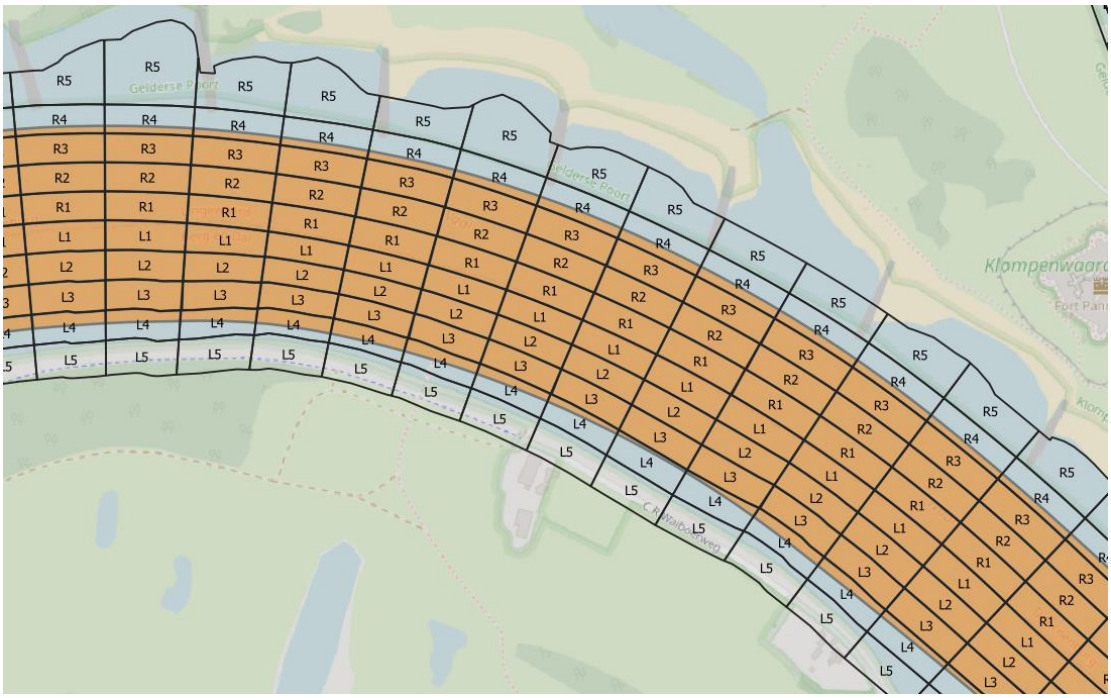

Figure 3.3 Morphologically active part of the river bed in Waal-model v0 (orange area) compared to grid of De Joode (2023).

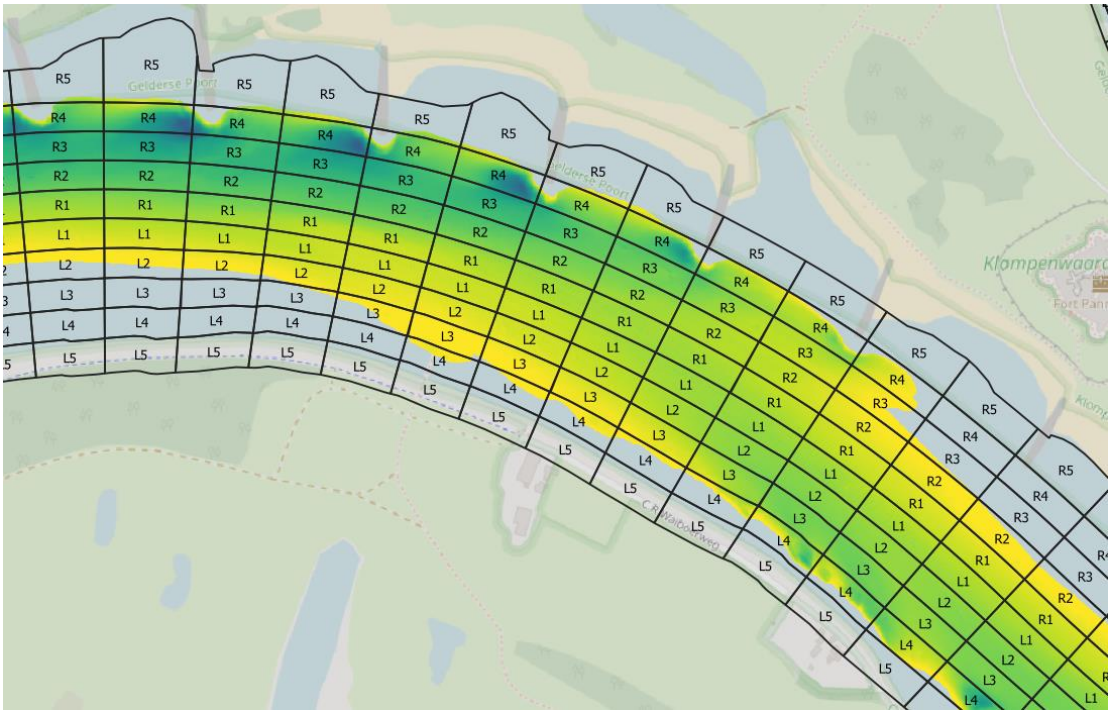

Figure 3.4 Data coverage of autumn 2018 multibeam measurements (yellow-green-blue colors represent the measured bed elevations), which were taken at a moment with rather low discharge and water levels, compared to grid of De Joode (2023, black polygons).

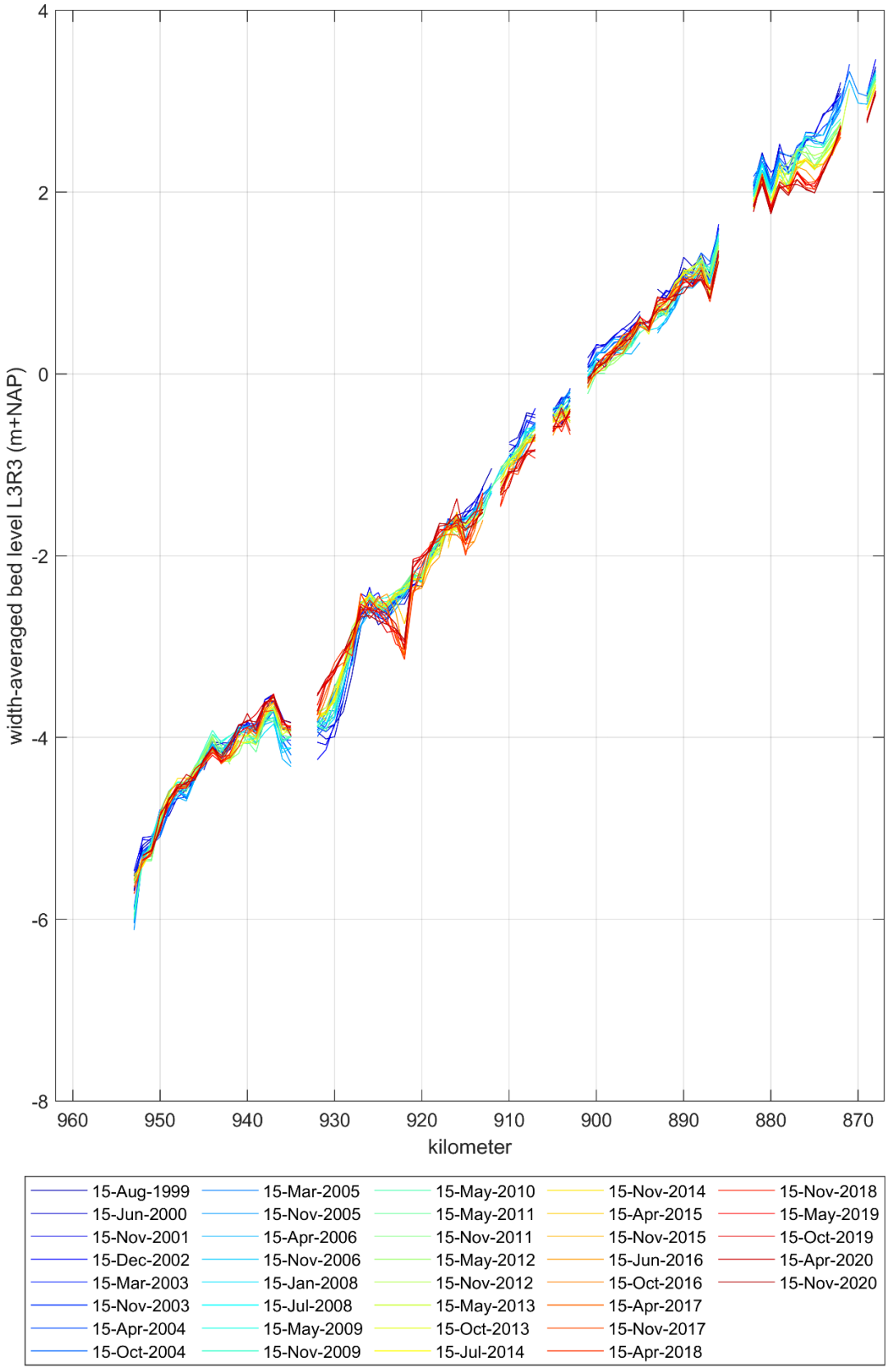

Figure 3.5 Available multibeam bed elevations, averaged over the width of the cross-section (L3R3), for the Waal. The data gaps are caused by river sections with no full data coverage across the entire width from R3 to L3 polygons.

3.4.2 Yearly sediment transport

Frings et al. (2019) estimated the yearly sediment transport per branch of the Rhine delta for a sediment balance of the Rhine (Table 3.3). In the framework of the IRM (Integraal Riviermanagement) project, Sloff (2019) combined the analyses of bed level trends by ten Brinke (2019), Ylla Arbós et al. (2019) and Ottevanger (2019) into a prognosis of bed level changes for the coming decades and then derived sediment transport rates from that. The resulting longitudinal profiles for the Waal and the IJssel are presented in Figure 3.6 and Figure 3.7. The deviations between the estimates stress that these are rough estimates. They will be used in the 1D calibration as such.

Table 3.3 Annual sediment load of the Rhine branches estimated by Frings et al. (2019).

section	kilometers	gravel load (without pores) (m^3/y)	sand load (without pores) (m^3/y)	sum of gravel and sand load (without pores) (m^3/y)
Boven-Rijn	859-867	39,000	232,000	271,000
Boven-Waal	868-886	23,000	208,000	231,000
Midden-Waal	887-915	16,000	198,000	214,000
Beneden-Waal	916-951	6,000	185,000	191,000
Pannerdensch Kanaal	868-878	13,000	36,000	49,000
Boven-IJssel	878-930	2,000	17,000	19,000
Midden-IJssel	930-970	1,000	15,000	16,000
Beneden-IJssel	970-1000	1,000	15,000	16,000
Boven-Nederrijn	878-891	10,000	26,000	36,000
Beneden-Nederrijn	891-922	7,000	26,000	33,000
Lek	922-946	3,000	26,000	29,000

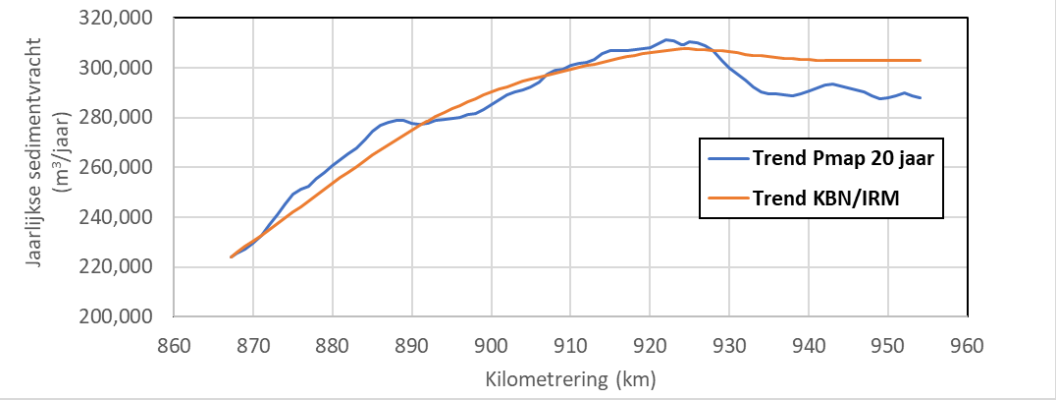

Figure 3.6 Estimate of the longitudinal profile of yearly sediment transport (excluding pores) for the Waal.

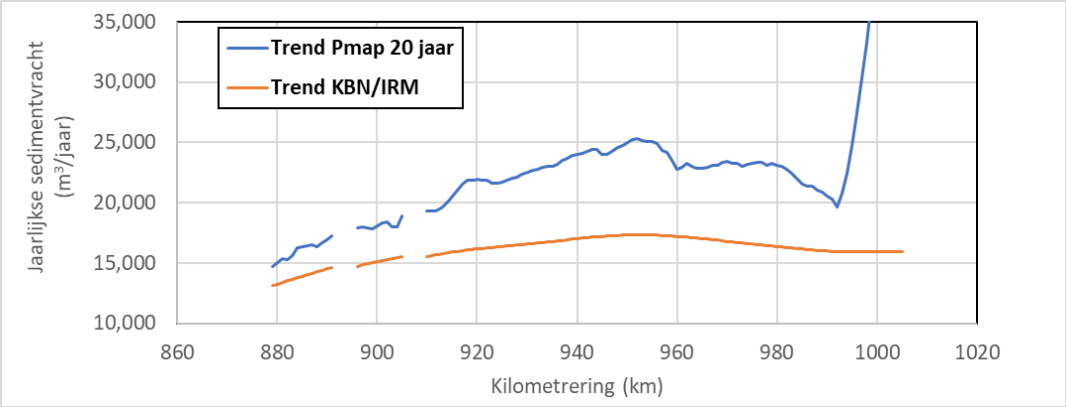

Figure 3.7 Estimate of the longitudinal profile of yearly sediment transport (excluding pores) for the IJssel.

3.4.3 Celerity of bed disturbances

Bed perturbations should migrate downstream with a speed of approximately 1 km/y according to Sieben et al. (2005).

3.5 Fairway maintenance

An inventory of available data on dredging volumes and locations was made for the Waal. Figure 3.8 gives an overview of the data sources and total volumes per year. No data is available for 2003-2004 nor for 2010, which is most probably due to a stop in dredging activities due to a public tendering stop. So in these years, probably no dredging works were carried out. For the years 2009-2013, only yearly volumes are available for the entire Boven-Rijn and Waal together, without further specification of the location. It still needs to be checked whether these have successfully been linked to locations based on ship tracks in an earlier project.

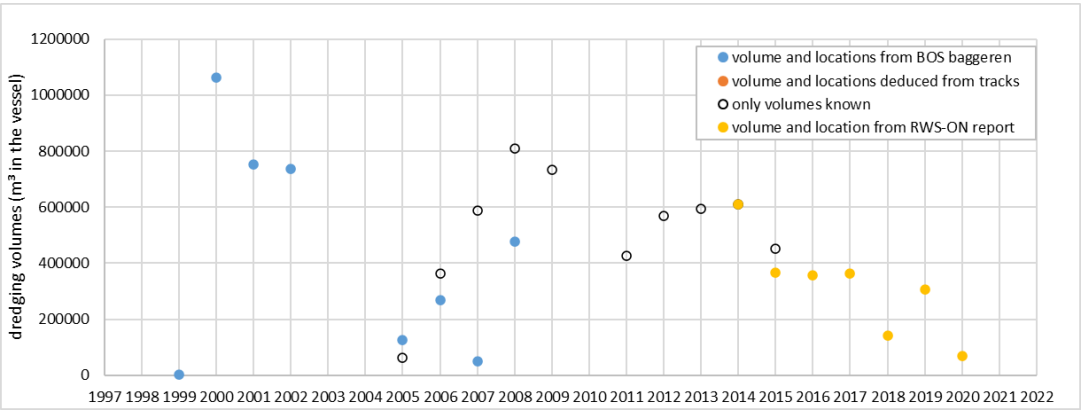

Figure 3.8 Available data on dredging volumes and locations for the Waal.

3.6 Inventory of system behavior

3.6.1 Fixed or semi-fixed layers

The river bed in heavily modified rivers like the Dutch Rhine branches contains areas that are immobile or not fully mobile. They can be divided into two types according to their origin:

anthropogenic:

a) bed stabilization works (e.g. fixed layers and bottom vanes in the Waal)
b) bank stabilization and groynes

natural:

c) steep and stable transition zones between river bed and groyne fields
d) non- or less erodible material in the layers under the river bed

In order to detect these areas, RWS has analyzed bed level changes and slopes along the Waal using multibeam measurements of three moments in time (2002, 2009, 2022). The idea was to identify areas with little mobility by selecting areas with less than +/- 10 cm bed level change in the two periods 2002-2009 and 2009-2022 (Figure 3.9, top and middle). Areas with steep slopes (more than 6 degrees, Figure 3.9, bottom) indicate the presence of human interventions such as bank protection, but also the slopes of e.g. river dunes are found in the images. The values of +/- 10 cm and > 6 degrees have shown to work for identifying locations with removed bank protection on the Maas (Ottevanger et al., 2021), but have not yet been tested for the Rhine branches.

Structures such as groynes, fixed layers and bottom vanes are clearly visible in the maps of the slopes (Figure 3.10). A comparison between the maps of areas with little bed level change to absolute bed levels with hillshades showed, however, that there is a lot of noise in this data. In most of the identified areas, the absolute bed levels do not give a reason to believe that these are less or even immobile. Many of them even show bed forms, which is a clear sign of mobility. On the other hand, the absolute bed levels reveal many places that do not look natural, which can be an indicator for less mobility (Figure 3.11). In general, it is therefore recommended to rather look at absolute bed levels with hillshades than areas with little bed level change, and to do this for as many sets of multibeam measurements as possible. The human eye can obviously identify unnatural zones better than a simple algorithm.

Mainly on the Upper Waal there are areas where are indications for hard layers under a thin layer of sand. According to Deltares' geologists (personal communication T. van Dijk, September 2023), this is probable (while downstream of Nijmegen there is a change in underground material and therefore it is not very probable).

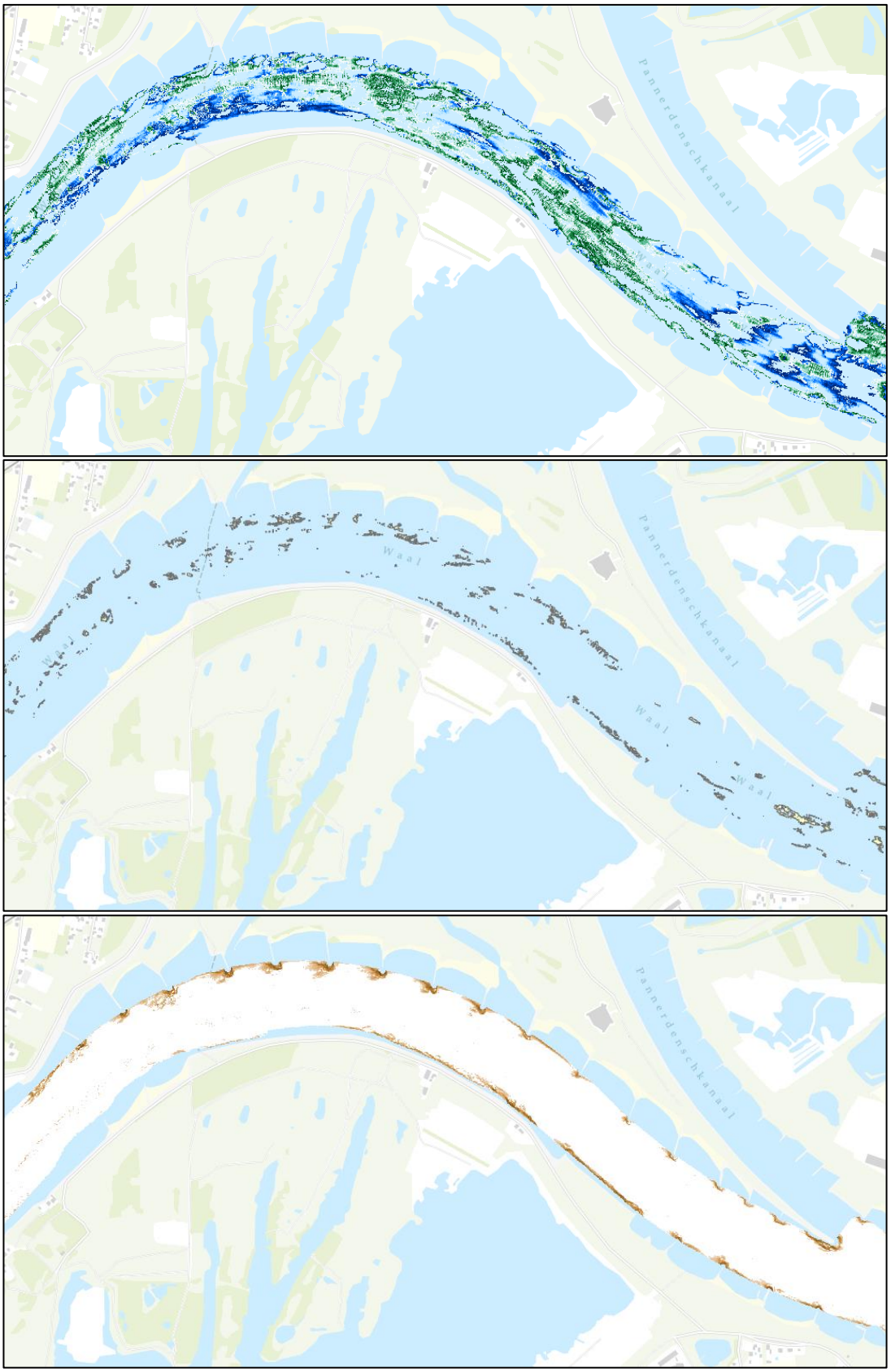

Figure 3.9 Top: Areas with bed level changes of less than +/- 10 cm for two intervals (2022-2009 (green) and 2009-2002 (blue)). Middle: Areas with bed level changes of less than +/- 10 cm in both periods. Bottom: Areas with slopes steeper than 6 degrees. From https://www.arcgis.com/apps/webappviewer/index.html?id=210e8b70b3d640358eee5fc097c6f3e5

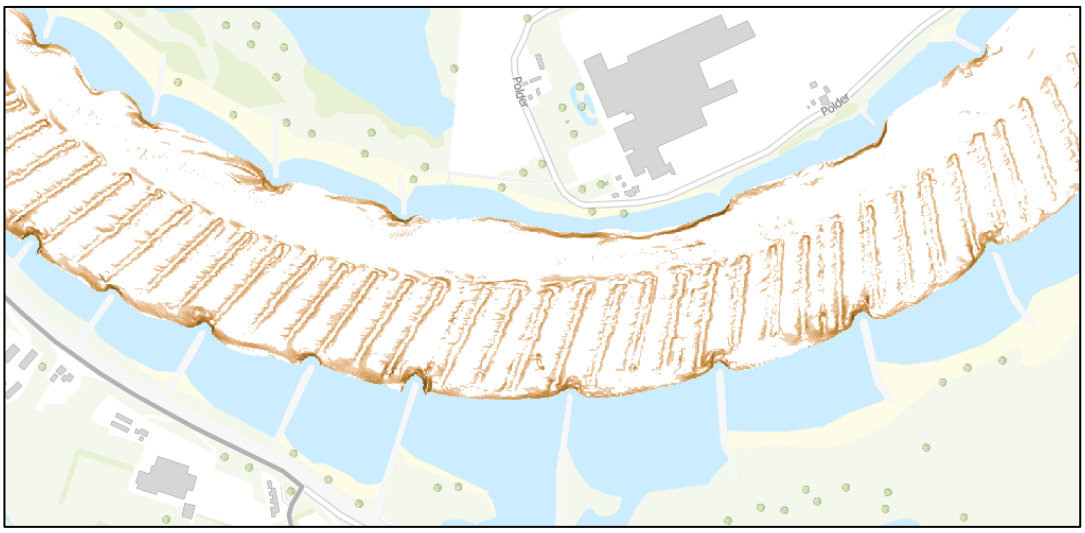

Figure 3.10 Steep slopes (> 6 degrees) around the bottom vanes and groyne tips in the bend at Erlecom on the Waal. From
https://www.arcgis.com/apps/webappviewer/index.html?id=210e8b70b3d640358eee5fc097c6f3e5

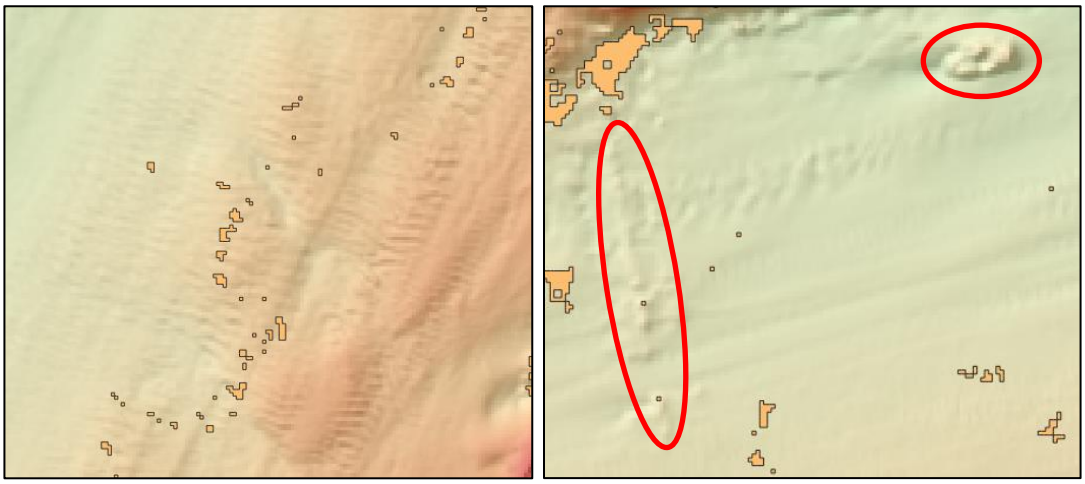

Figure 3.11 Examples for areas with little bed level change (orange polygons) but bed forms (left) and areas with more than +/- 10 cm bed level change that look unnatural and thus immobile (right, red circles).

3.6.2 Important interventions

RWS-ON has provided a list of interventions that have been included in the Baseline schematisations of j19_6 and j22_6 compared to j95_6, including the moment at which these interventions have been carried out (moment of completion of the works). The list also contains interventions that have already been implemented in reality but are not yet included in the Baseline schematizations. This list will be used as background for the interpretation of differences between model results and measurements or of changes in trends.

4 Hydrodynamic model schematizations

4.1 Overview of different schematizations

Three different model schematizations have been prepared for the pilot in 2023:

D-HYDRO model schematization	Derived from Baseline schematization
dflowfm2d-hydr-waal-j99_6-v1a	baseline-rijn-j99_6-v1
dflowfm2d-hydr-waal-j16_6-v2a	baseline-rijn-j16_6-v2
dflowfm2d-hydr-waal-j19_6-v2a	baseline-rijn-j19_6-v2

These schematizations are representative for the situation of 1999, 2016 and 2019, respectively, and will be used to model morphological development in the period 1999-2012, 2016-2020 and 2019-2022.

4.2 Baseline set-up and conversion to D-HYDRO

Baseline-rijn-j19_6-v2 was already available at the beginning of this project. Baseline-rijn-j16_6-v2 is equal to baseline-rijn-j16_6-v1, but converted from Baseline 6.1.1 to Baseline 6.3.2. Baseline-rijn-j99_6-v1 is the result of mixing 8 measures, provided by RWS-ON, in baseline-rijn-j95_6-v1. In order to do this, baseline-rijn-j95_6-v1 was first converted to Baseline 6.3.2. The list of measures is included in Appendix B. All steps are schematized in Figure 4.1.

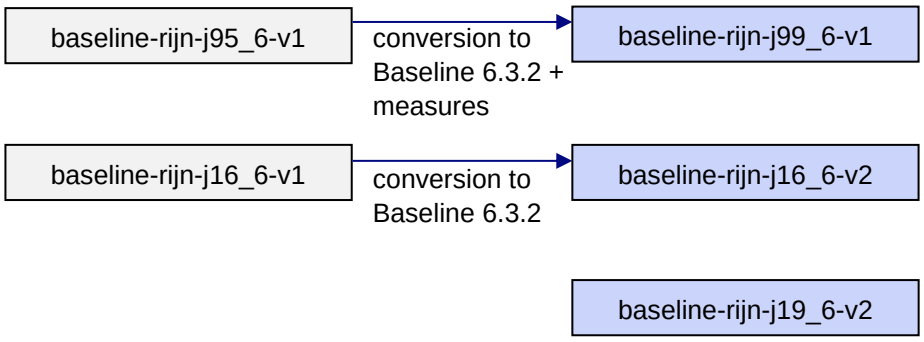

Figure 4.1 Steps to create Baseline schematizations.

The three resulting Baseline schematizations were converted to their corresponding D-HYDRO schematizations using the grid ‘rijntakken_final_v9_net.nc’. To convert only the data within the desired model domain (i.e. the Waal), a shapefile containing the model boundary is used during the conversion from Baseline to D-HYDRO. These shapefiles were constructed by cutting of the model boundaries (or section polygons) of the entire j99, j16 and j19 schematizations at the Pannerdense Kop. The location of the upstream boundary is copied from the Waal branch model that was used during the hydrodynamic calibration for the Rhine (Kosters et al., 2022).

During conversion from Baseline to D-HYDRO, the model boundaries for the Waal are themselves converted to enclosure polygons, a model input file used to delineate the model domain at the start of the computation. By (manually) changing the enclosure polygon, the model domain can still be altered after conversion from Baseline (but only within the original model boundary, not outside of it).

4.3 Modifications within D-HYDRO

After the conversion from Baseline, the following elements of the model geometry have been modified:

4.3.1 Model domain

The Waal pilot model extends from Pannerdense Kop to Hardinxveld, see Figure 4.2. The upstream boundary is located just downstream of the bifurcation (Figure 4.3), to avoid violating the assumption that no sediment transport occurs across closed model boundaries as much as possible. Manual modification of the enclosure polygon for j19 was needed for this. The model boundaries for j99 and j16 already include this modification, so no modification of the enclosure polygon was needed for these models.

Since the model domain covers only the Waal, the connection of Waal and Neder-Rijn/Lek via the Betuwe-section of the Amsterdam-Rijn-canal is closed off. In reality this connection is open at low discharges and closed only during higher flow periods with discharges of more than about 1.200-1.300 m^3/s at Lobith. This is no problem for the morphodynamic model, since morphological development during these periods is very small.

Figure 4.2 Waal pilot model domain.

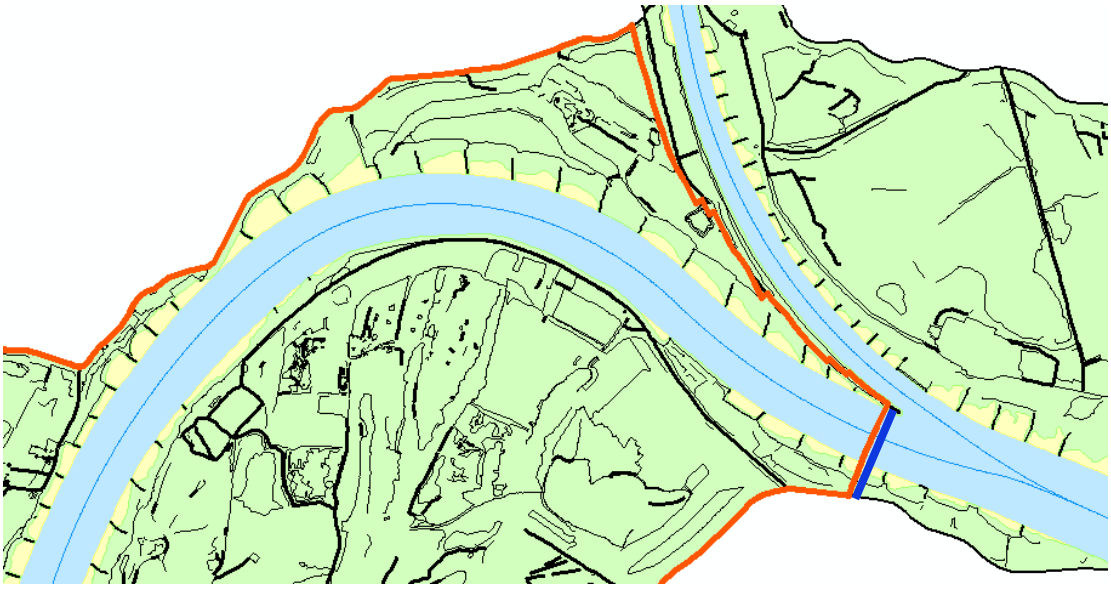

Figure 4.3 Upstream boundary location. The thick blue line indicates the part of the boundary that is open.

4.3.2 Bed elevation

For the hydrodynamic model it was decided to define bed levels at grid cell corner points (`BedlevType = 3` and `Conveyance2D = -1`, see Figure 4.4, lower left).

The bed levels in these points are derived from Baseline by “picking” the elevation at that specific location. In the morphological model, we need to use `BedlevType = 1`[1] (Figure 4.4, top), which defines bed levels in cell centers. Minns et al. (2022) propose to derive the elevations in cell centers from a hydrodynamic simulation[2]. However, these elevations are the minimum of the values on cell edges (Figure 4.4, lower left) and this method therefore leads to structural overestimation of the depth along steep edges (e.g. longitudinal training walls or fixed banks, “gestrekte oever”) and underestimation of water levels as can be seen in Figure 4.5. Letting D-HYDRO determine the bed level in cell centers by the method illustrated in Figure 4.4, lower right, does not seem more promising either, because it still uses a minimum value.

Therefore, it was decided to derive the mean value of the bed levels in the corner points using a script, and impose it as cell center bed level in morphological simulations. Water level difference compared to the original hydrodynamic model was significantly reduced, as is shown during hydrodynamic validation in Chapter 5. In the meantime, the option to pick elevation at cell centers instead of corners became available in Baseline. These could be used directly in the model. For the v0 model of the IJssel, test simulations are running to see whether that gives promising results as well. If so, this option will also be tested for the Waal.

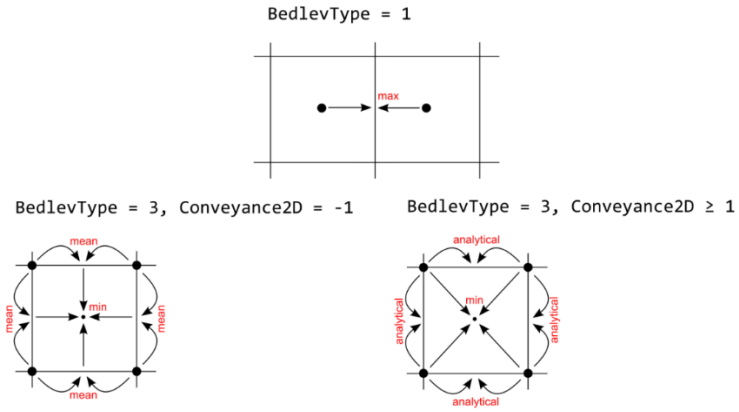

Figure 4.4 Schematic representation of options for representation of bed elevations on the staggered grid in D-HYDRO. The hydrodynamic model uses BedlevType = 3 and Conveyance2D = -1. The morphodynamic model has to use BedlevType = 1.

[1] There is no validated morphology functionality available for bed levels in corner points.

[2] Due to the staggered grid approach in D-HYDRO, bed elevations are needed at several locations in a cell to solve the hydrodynamic equations, including the cell center. Cell center bed elevations can therefore be exported from a hydrodynamic simulation that used elevations at corner points as input.

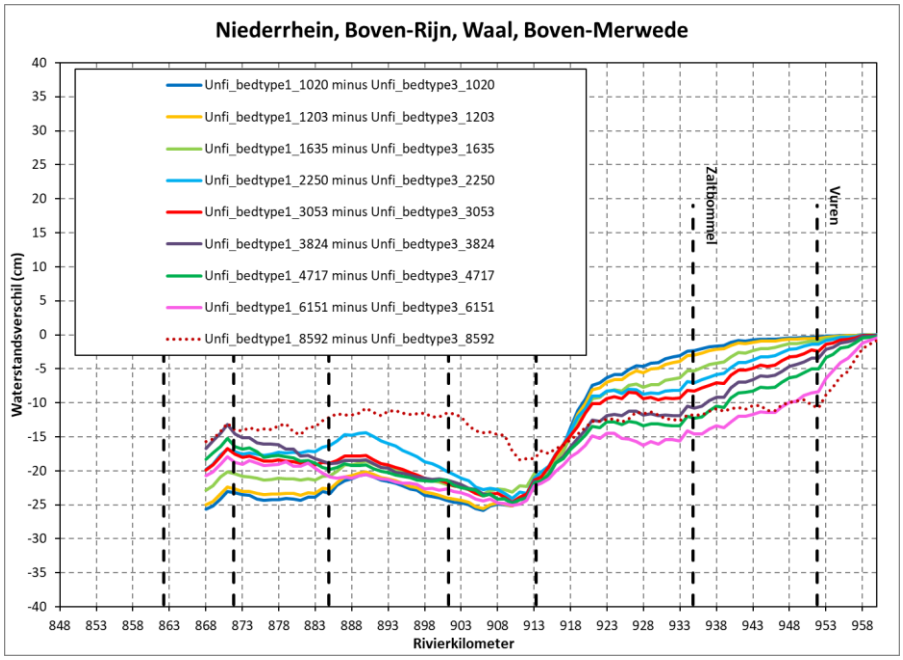

Figure 4.5 Water level difference between quasi steady simulations with the original bed level from the hydrodynamic model (bedlevtype=3) and the bed level converted to cell centers by the model (bedlevtype=1).

In Baseline, the bed elevation within the main channel of the Waal is mainly based on multibeam measurements. The bed level in the three schematizations, j99, j16, and j19, is based on multibeam measurements carried out in August 1999, October 2016, and October 2018 (the start of the 2018/2019 flood season), respectively. Hence, the bed elevation included in Baseline represents one moment in time (a 'snapshot') and contains small-scale features such as bed forms. Our large-scale model of the Rhine branches, however, is too coarse to properly resolve small-scale phenomena such as bed forms. Instead, these are included in a "subgrid" way (e.g. estimating the size of dunes by means of a bed form predictor and taking it into account where relevant, e.g. when deciding if dredging is needed or not).

Thus, the bed level in the model should be a representative bed level without these small-scale temporary phenomena. Therefore, the main channel part of the bed level from Baseline was smoothed using the following steps:

1. averaging of the main channel bed level from Baseline in the polygons created by De Joode (2022) (see description in section 3.4.1). At the edge of the summer bed, the polygons were cut off to not exceed the extent of the morphologically active part in our model.
2. calculating 1 km rolling means along each longitudinal section of De Joode (2023), i.e. L1-L4 and R1-R4 (with L4 and R4 polygons cut off as described above)
3. interpolating (Delaunay triangulation) the resulting values onto the 2D grid of our model (cell centre location).

The filter was only applied within the morphologically active zone of the model (section 6.3) and not to fixed layers e.g. Nijmegen, Sint Andries and Erlecom. Figure 4.6 shows that indeed this method filters out bed forms but not the large-scale patterns such as deep outer bends, and that the bed level at the fixed layers was not filtered (blue line on top of red line).

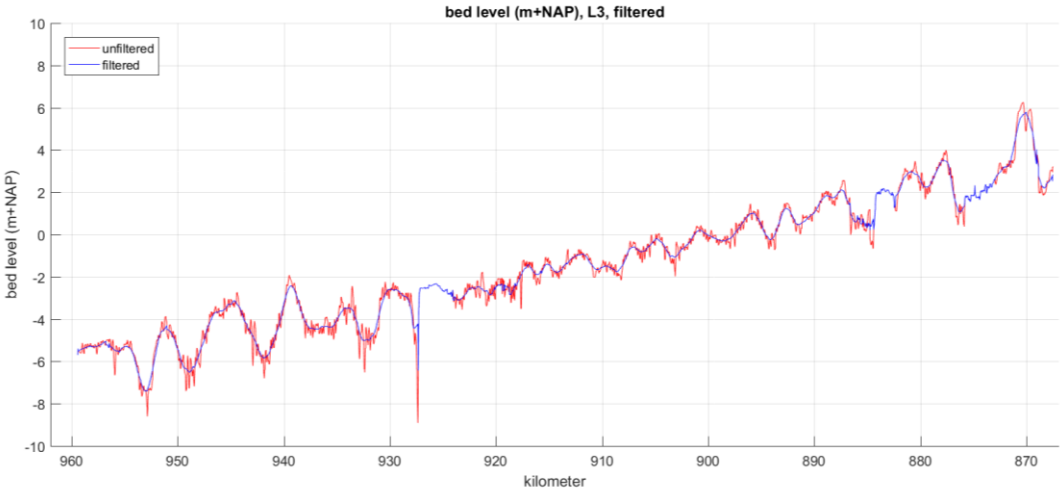

Figure 4.6 Comparison between filtered and unfiltered main channel bed level along a line approximately 70 m to the left of the river axis (L3).

The impact of working with bed levels in cell centers instead of corner points and of the filtering for the main channel on calculated water levels is analyzed in a hydrodynamic validation of the model (Chapter 5).

On the longer term, we need to define based on morphological model results for several branches if filtering is indeed worthwhile. If yes, we also need to define how to get the procedure of determining bed levels in cell centers and filtering the main channel bed into Baseline and/or D-HYDRO, so that it can be used in the hydrodynamic model as well.

In the hydrodynamic simulations used for the first model calibration step (the offline calibration, see Chapter 7), BedlevType = 3 (with Conveyance2D = -1) is used, i.e. bed levels specified in cell corners, in combination with the original bed level from Baseline . For the morphological simulations however, we use BedlevType = 1, with bed levels specified in cell centers (averaged corner point values) and filtered bed levels in the main channel.

4.3.3 Main channel roughness

In the original hydrodynamic model, main channel roughness is defined by means of a base roughness that is multiplied by a calibration factor. Base roughness is constant per section, sections being between several kilometers to about 20 km long. Calibration factors are also defined per section, but the sections for the base roughness and calibration factors do not coincide. This is described in detail by Kosters et al. (2022). An example is presented in Figure 4.7. To ensure a smooth transition of roughness between sections, 2 km transition zones were introduced for the calibration factors. This has not been done for the base roughness yet, since it was not yet technically possible in Baseline when the model was set-up. Therefore, abrupt changes of bed roughness occur at the transitions between roughness sections. Figure 4.8 presents the Chézy values that are calculated for nine different discharges (at Lobith).

These abrupt changes have shown to create strong morphological reactions in the first (not yet calibrated) model runs. This is mainly visible at km 951, where the jump in Chézy value is very large for most discharges, but also at other transitions in base roughness (Figure 4.9 and Figure 4.10). Therefore, the roughness in the pilot model (v0) of the Waal was set to a constant Chézy value of 45 $m^{1/2}/s$. This value was found to give the best representation of water levels (on average) along the Waal (see more details in Chapter 5).

To have full control of model input, furthermore the calibration factors were deactivated, meaning that a constant value of 1 will be used in the entire model domain. In a next phase of model development, after a first calibration, we can experiment with more variability in main channel roughness and work towards a compromise between the input of the original hydrodynamic model and the needs of a morphodynamic model. A proposition for how to do that is made in section 10.4.

The impact of the change in roughness and calibration factors on water levels and flow velocities is analyzed in the hydrodynamic validation of the model in Chapter 5. Note that for morphodynamic simulations a reasonable representation of flow velocities is much more important than correct water levels. Water levels, however, do determine the moment at which the flood plains and side channels are activated.

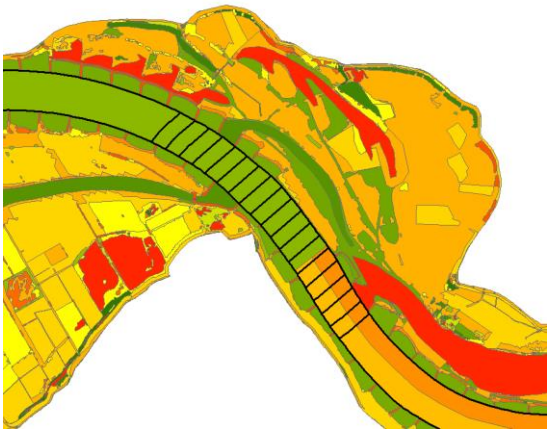

Figure 4.7 Roughness sections (colored polygons) and polygons defining the calibration factor (black lines, including a transition zone) near the bend at St. Andries.

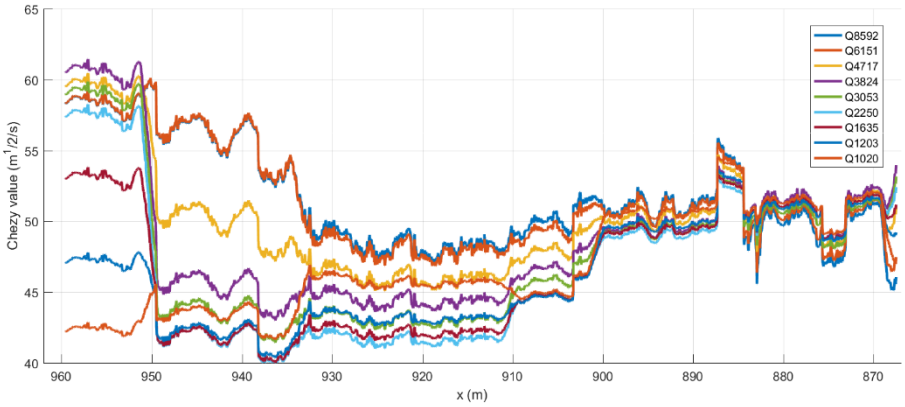

Figure 4.8 Chézy roughness values calculated with the original hydrodynamic model for the 9 discharge levels used in the morphological model (see section 4.4).

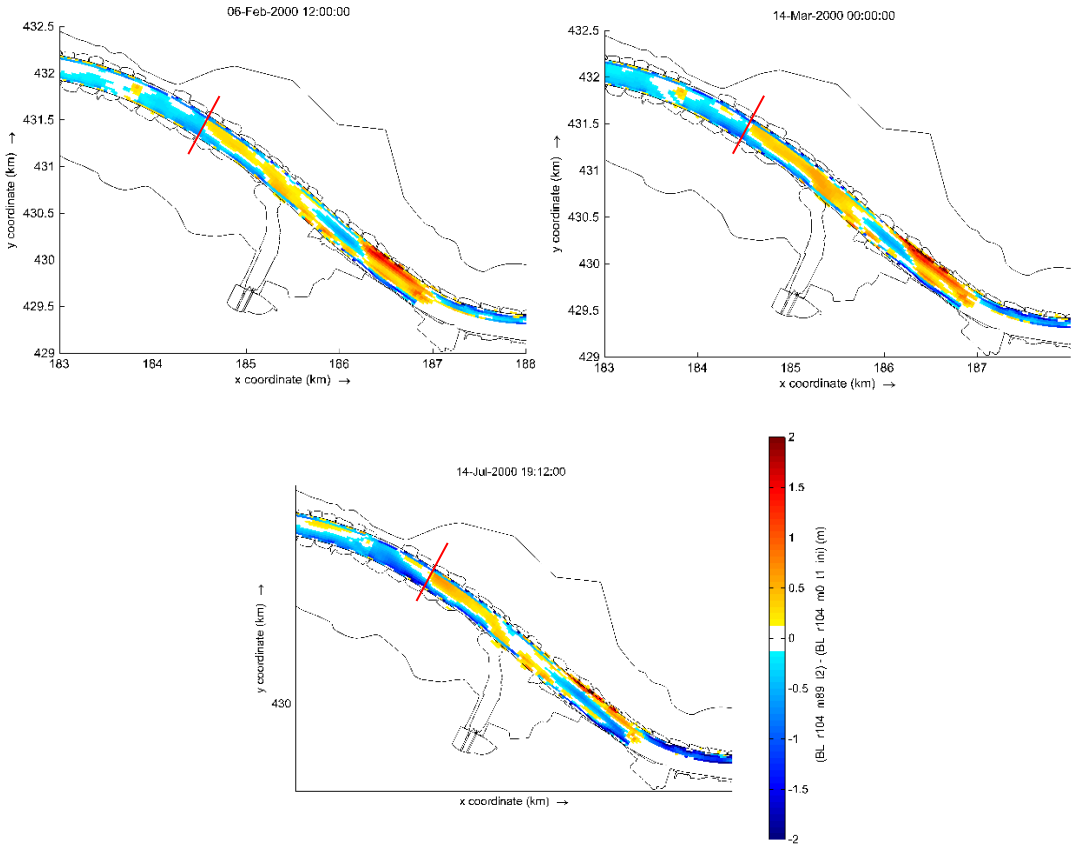

Figure 4.9 Cumulative erosion and sedimentation after 1, 2 and 5,8 years around km 888. The red lines indicate the location of the transition.

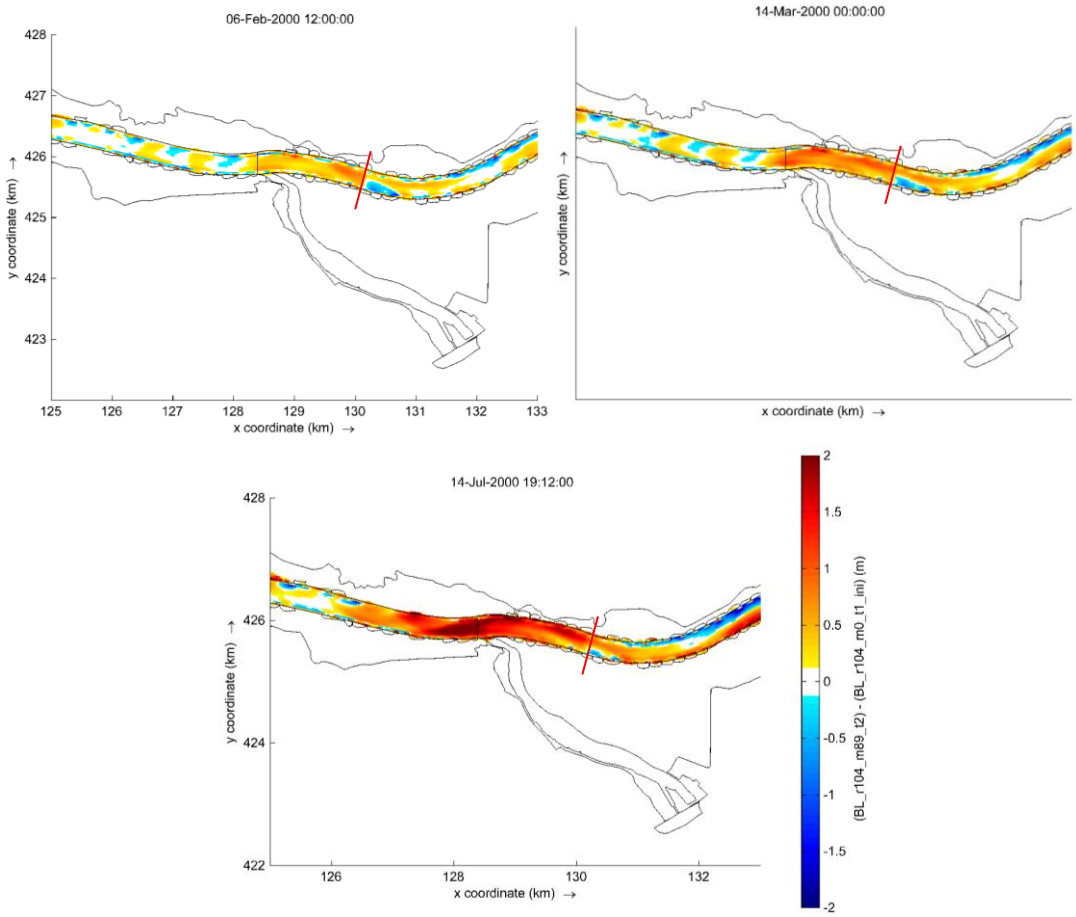

Figure 4.10 Cumulative erosion and sedimentation after 1, 2 and 5,8 years around km 951. The red lines indicate the location of the transition.

4.3.4 Discharge-dependent calibration factors

The modifications described in this section are only relevant for the simulations in which the original calibration factors from the hydrodynamic model are included. As described in Section 4.3.3, it was decided to apply a constant Chézy roughness coefficient in the morphodynamic simulations.

To each calibration section (see section 4.3.3), a calibration factor was assigned that is dependent on the local discharge (for more information, see Kosters et al., 2022). Because of this discharge dependency, a discharge cross-section must be assigned to each calibration section. These cross-sections are located as close as possible to the corresponding water level stations that were used for calibration. Calibration factors are defined for 5 (local) discharge levels. Between these discharges, the calibration factor is determined by linear interpolation.

In the Waal pilot model, the upstream boundary intersects with the smooth transition between calibration sections 2002 and 2003. Hence, a part of calibration section 2002 is present in the model. However, the corresponding discharge cross-section, BR_862.7_QR_Lobith-Pannkop, is not located within the model domain. In all model schematizations (j99, j16 and j19), this cross-section was therefore replaced by WL_868.9_QO_Waal, which is present within the domain but still close to the original cross-section. Furthermore, the discharge levels of section 2002, which corresponded to Boven-Rijn discharges, are replaced by the levels of section 2003, corresponding to the discharge on the Waal. Appendix B gives an overview of the calibration factors (including the changes described in this section).

4.3.5 Inlet structure Lent

To schematize the inlet structure at the upstream end of the side channel at Lent (Nijmegen), a fixed weir (representing the crest of the structure) is used in combination with a pump (representing the 6 culverts within the structure). During the project, it turned out that this schematization did not result in a correct representation of the inlet structure within the latest official software release (2023.01). Pending the solution for this problem, to be implemented in a newer version of the software, the pump was removed from model schematizations j16 and j19 (in j99, the side channel at Lent is not yet present). This means that in the model, there is no flow into the side channel when the water level upstream of the structure is lower than the crest level. In reality, the flow through the culverts in this situation can reach up to 40 m^3/s (estimated) for a discharge of around 4000 m^3/s at Lobith. A deviation of max. 40 m^3/s in the discharge distribution over main and side channel due to removal of the pump was deemed acceptable given the pilot status of the current model.

4.4 Hydrodynamic boundary conditions

The model is forced with a discharge at the upstream boundary and a Qh-relation at the downstream boundary. The upstream model boundary is located on the Waal at the Pannerdensche Kop (Figure 4.3).

The initial version (v0) of the new morphodynamic model of the Waal still makes use of approaches that were derived for its predecessor, the “DVR model” in Delft3D 4. This also applies for the hydrodynamic upstream boundary condition, which is a standardized yearly hydrograph consisting of several stages with constant discharges (Figure 4.11). The same hydrograph is used in v0 of the new model. At a later stage, it will be decided to either use an updated version of that hydrograph, derived from more recent discharge data, or even use a different type of upstream model boundary (e.g. a “normal” hydrograph).

The discharge levels of the DVR model were translated from Lobith on the Boven-Rijn to the Waal as described in section 3.2.

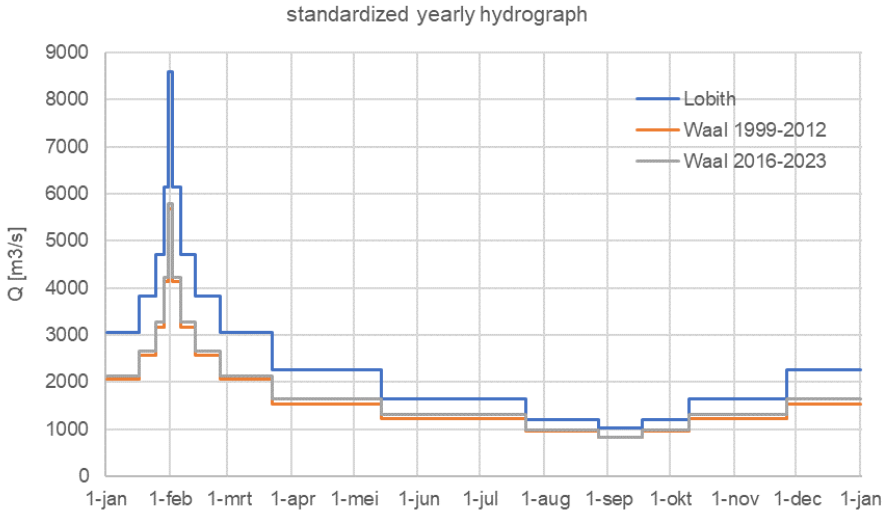

Q Lobith (m^3/s)	no. of days
3824	8
4717	4
6151	2
8592	2
6151	4
4717	7
3824	12
3053	25
2250	53
1635	70
1203	35
1020	21
1203	23
1635	47
2250	36

Figure 4.11 Standardized yearly hydrograph as used in the DVR model for Lobith and converted to the Waal.

The downstream model boundary is located at Hardinxveld. For model schematizations j16 and j19, a Qh-relation derived by Van der Wijk (2022) is used as boundary condition at this location. Van der Wijk derived relations for the current situation, excluding the effect of sea level rise, as well as for a future situation, including a sea level rise of 5 cm.

Because we simulate morphological development in the current situation (2016 – 2023), we use the Qh-relation without the effect of sea level rise, see Table 4.1.

Van der Wijk (2022) derived the Qh-relations with model schematization dflowfm2d-rmm_vzm-j19_6-v2a. An average, idealized tidal signal (slotgemiddelde 2011) was used for the downstream boundary conditions of this model. The resulting flow at Hardinxveld is influenced by tide as well. To derive a Qh-relation, for each Waal discharge (upstream boundary condition of the RMM model), the corresponding discharge at Hardinxveld was taken as the average over two consecutive tidal periods, while the water level was determined by taking the maximum value that occurred during these two tidal periods. Hence, when using the resulting Qh-relation in our Waal pilot model, the water level at the downstream boundary is higher than the average water level that would occur in reality under average tidal conditions. The difference is largest for low river discharge. At a later stage of this project, the tidal influence on morphology will be investigated and, if relevant, represented schematically.

In the period 1999-2012, the relation between discharge and water level at Hardinxveld was different, mainly because the Room-for-the-River-programme, including the Noordwaard project close to Hardinxveld, had not been carried out yet. For simulations with the j99 model, we therefore use the Qh-relation qh_Hardinxveld_j12_5, which was derived with waqua-rmm-j12_5-v1, a WAQUA model schematization without the Noordwaard project (Crebas, 2012). This relation is included in Table 4.2. Figure 4.12 shows the relation together with the one used for j16 and j19. Especially for high discharges, the j99 relation gives significantly higher water levels, with differences reaching up to several decimeters.

Because of issues with model stability in the morphodynamic simulations, it was decided to apply fixed water levels instead of Qh-relations in all morphodynamic simulations. The water levels were derived from the Qh-relations by linear interpolation. The result is technically the same as when using the Qh-relations, because all morphological simulations are composed of series of steady state simulations for the 9 discharge levels (Figure 4.11).

As in the former DVR-model, all simulations are run without lateral in- or outflows. Calibration results need to show if this is acceptable or not. For the Waal it is expected to be OK, but for the IJssel, some of the laterals (Oude IJssel and Twentekanaal) might be important for good results, because the inflows there are significant.

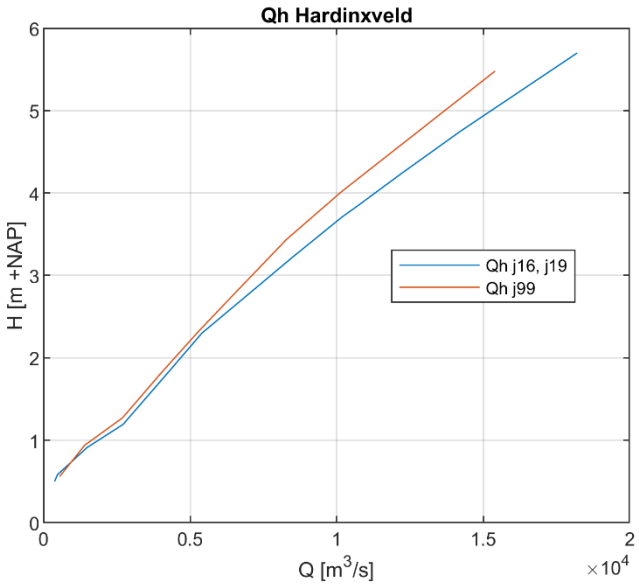

Figure 4.12 Qh relations at Hardinxveld for j16, j19 and j99.

Table 4.1 Qh-relation at Hardinxveld for j16 and j19, excluding the effect of sea level rise (Van der Wijk, 2022).

Q [m³/s]	H [m +NAP]
380.0	0.50
473.9	0.58
1483.7	0.91
2709.5	1.19
4050.7	1.74
5404.0	2.30
6614.6	2.66
8456.3	3.21
10185.1	3.71
10735.9	3.85
11266.9	3.99
12257.9	4.25
14219.3	4.75
18200.0	5.70

Table 4.2 Qh-relation at Hardinxveld for j99, before execution of the Noordwaard project (qh_Hardinxveld_j12_5, Crebas, 2012).

Q [m³/s]	H [m +NAP]
550	0.559
1401	0.937
2697	1.272
3997	1.81
5296	2.324
6473	2.764
8285	3.436
10165	4.017
11435	4.372
15400	5.48

4.5 Initial conditions

For the 2019 Rhine branches model (dflowfm2d-rijn-j19_6-v2a), initial water levels are already available for a set of 12 stationary discharges (ranging from 600 to 16.000 m³/s). For each simulation with the Waal pilot model, an appropriate initial condition was selected from this set, by taking the field of initial water levels closest to the expected stationary state, but not higher than that (see Table 4.3). For example, for the simulation with Q_{BR} = 3.824 m³/s (Q_{WL} = 2.654 m³/s), the initial condition based on a discharge of Q_{BR} = 3.000 m³/s was used. In this way, undesired inundation of storage areas is avoided.

With these initial conditions, stationary hydrodynamic simulations of 15 days were run to let the model adapt to the boundary conditions. The morphodynamic simulations are using the result of this hydrodynamic spin-up as initial conditions via restart files.

Table 4.3 Discharge levels for hydrodynamic and morhpodynamic simulations, and discharge corresponding to the initial water level field.

Q Bovenrijn (DVR levels) [m³/s]	Q Waal [m³/s]	Q ini [m³/s]
1020	829	1020
1203	972	1020
1635	1312	1500
2250	1642	2000
3053	2132	3000
3824	2654	3000
4717	3264	4000
6151	4231	6000
8592	5778	8000

5 Hydrodynamic validation

5.1 Validation simulations

With the Waal branch model of the year 2019, of which the setup was described in chapter 4, nine stationary hydrodynamic simulations are carried out, corresponding to the discharge levels used to schematize the yearly hydrograph for morphodynamic simulations (section 4.4). For these discharge levels, a hydrodynamic validation was carried out by comparing the model after the modifications as described in paragraph 4.3 to the original hydrodynamic model. As additional validation, the discharge through the side channels behind the longitudinal training walls were validated against measurements.

Each discharge is simulated for a duration of 15 days, in order to achieve a stationary situation. Lateral inflow/outflow is not included in the model, just like in the predecessor of the morphodynamic model (the DVR model).

5.2 Effect of modifications to the original model

For the hydrodynamic validation, water levels and flow velocities along the river axis of the morphological model were compared to those of the original hydrodynamic model. In this way, the effect of the following modifications to the original model (see section 4.3) was visualized:

1. defining the bed levels in cell centers instead of at corner points
2. filtering the bed level
3. applying a constant main channel roughness instead of the combination of spatially varying base roughness and space and discharge dependent calibration factor

The following sections present the effect of each of these modifications on water levels and flow velocities. Both parameters are taken on the output locations on full kilometers on the river axis.

5.2.1 Effect of defining the bed level in cell centers

Figure 5.1 and Figure 5.2 show the effect of changing the bed level definition from cell corners to cell centers, which is necessary for morphodynamic simulations. Water levels are raised by 3-5 cm, the change in flow velocities remains limited (about 0.01 m/s on average, with peaks of up to 0.03 m/s).

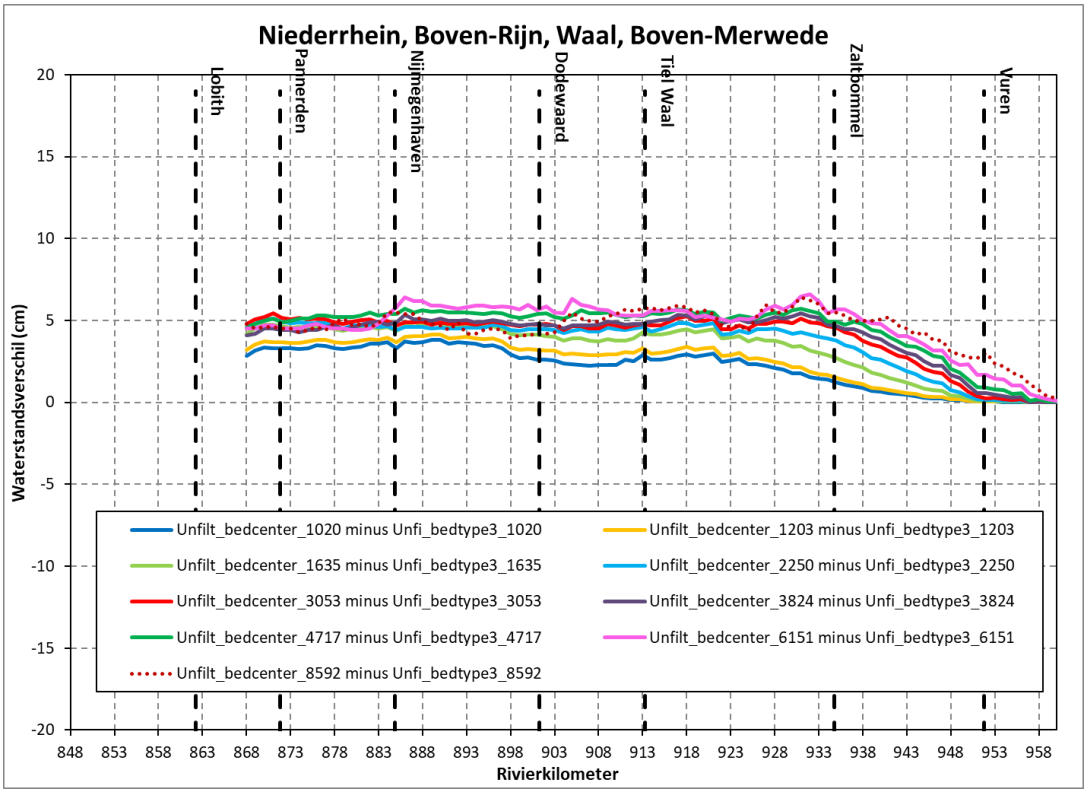

Figure 5.1 Difference in water levels along the river axis between simulations with bed levels in cell centers ("Unfilt_bedcenter", morphological model) and bed levels in cell corners ("Unfi_bedtype3", original hydrodynamic model).

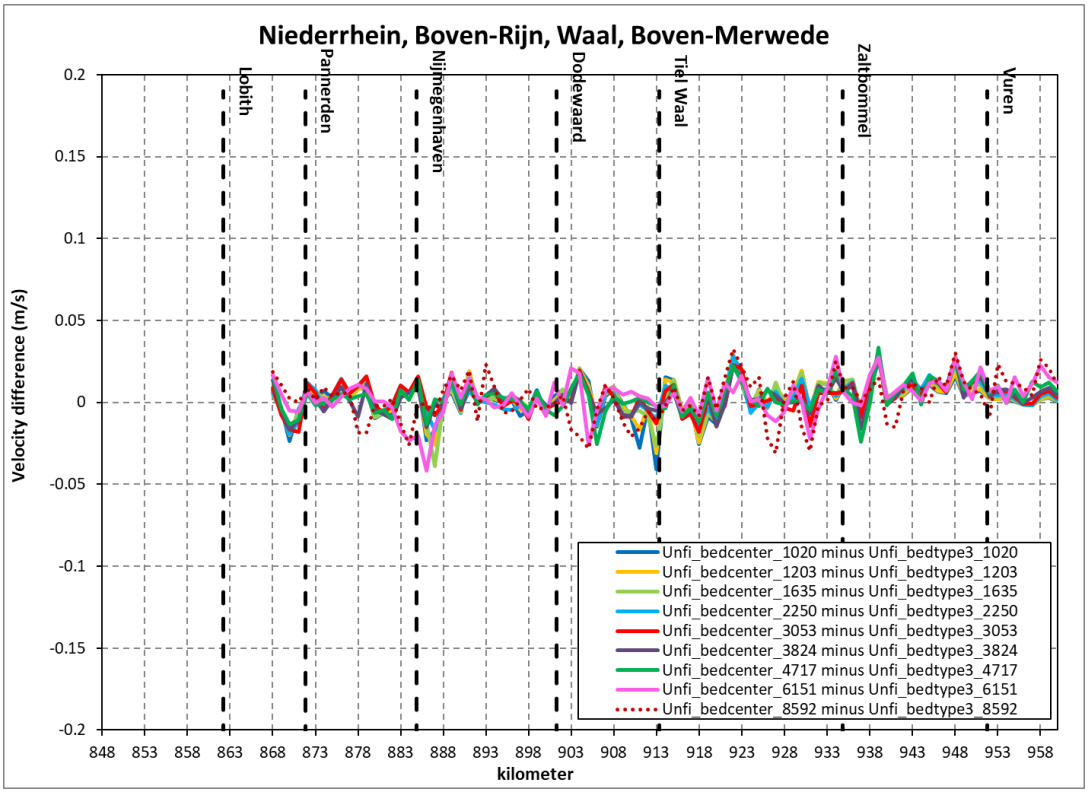

Figure 5.2 Difference in flow velocities (on the river axis) between simulations with bed levels in cell centers ("Unfilt_bedcenter", morphological model) and bed levels in cell corners ("Unfi_bedtype3", original hydrodynamic model).

5.2.2 Effect of filtering the bed level

To evaluate the influence of bed level filtering, at first model results of simulations with filtered and unfiltered bed level, both using a bed level definition in cell centers, are compared (Figure 5.3 and Figure 5.4). This shows the influence of purely the filtering. In a next step, Figure 5.5 and Figure 5.6 show the difference with the original hydrodynamic model, i.e. the effect of both filtering and changing the definition of bed levels from cell corners to cell centers.

The filtering of the bed level removes local variations and thus reduces the resistance of the bed level. This might need to be compensated in the roughness in the following phase. Therefore, water levels after filtering are about 5 cm lower than before filtering (for the lowest two discharge levels up to 9 cm). Combined with the effect of defining bed levels in cell centers instead of corners, water level differences are reduced to 0-2 cm (for the lowest two discharge levels up to -5 cm). In both comparisons, velocity differences range between +/- 0.02 m/s, with some local peaks of up to +/- 0.06 m/s. With total flow velocities ranging between 1 m/s for the lower discharges and 1.5-2.0 m/s for the higher discharges, that results in relative changes of about 1-2%, with peaks of up to 3-6%. This is acceptable for the morphodynamic simulations.

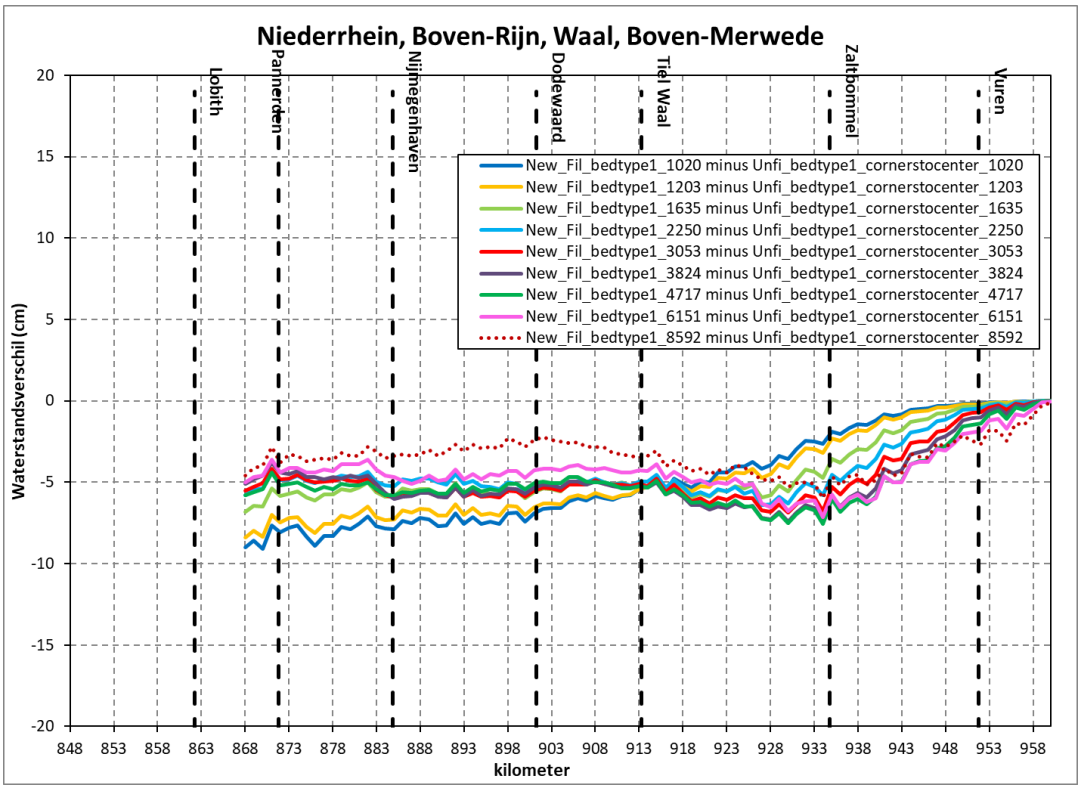

Figure 5.3 Difference in water levels (on the river axis) between simulations with unfiltered ("Unfi_bedtype1") and filtered bed levels ("New_Fil_bedtype1"). In both cases, bed levels are defined in cell centers.

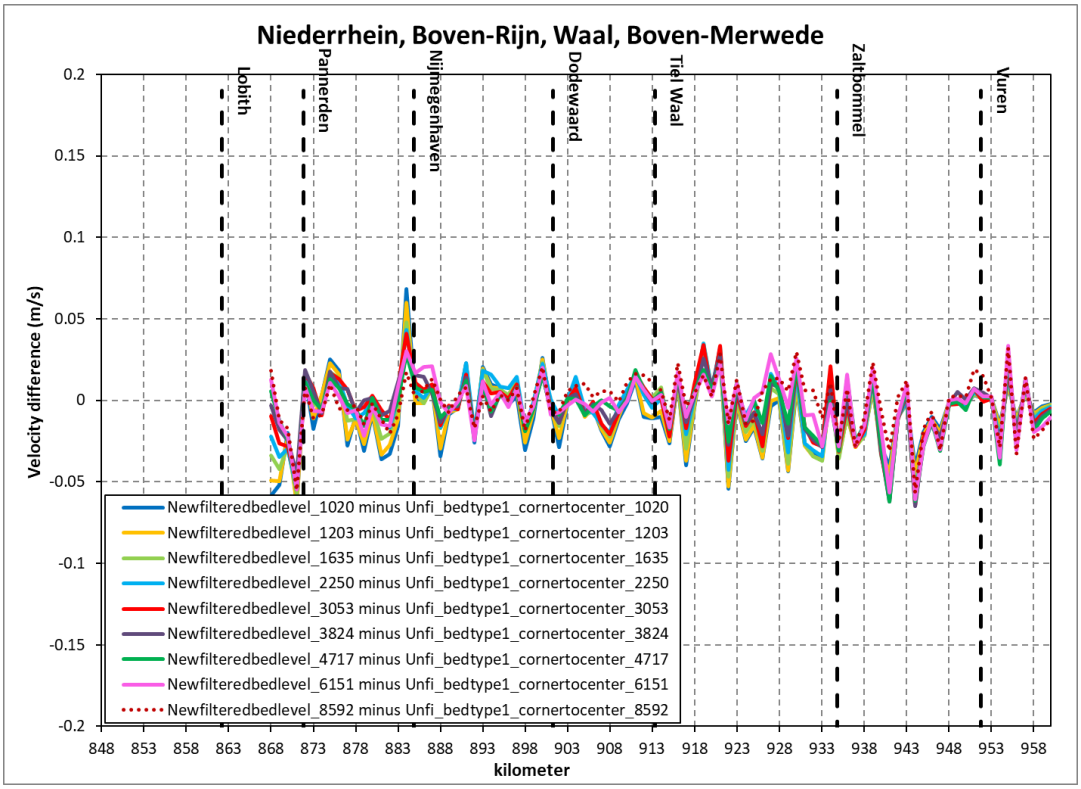

Figure 5.4 Difference in flow velocities (on the river axis) between simulations with unfiltered ("Unfi_bedtype1") and filtered bed levels ("NewFilteredbedlevel"). In both cases, bed levels are defined in cell centers.

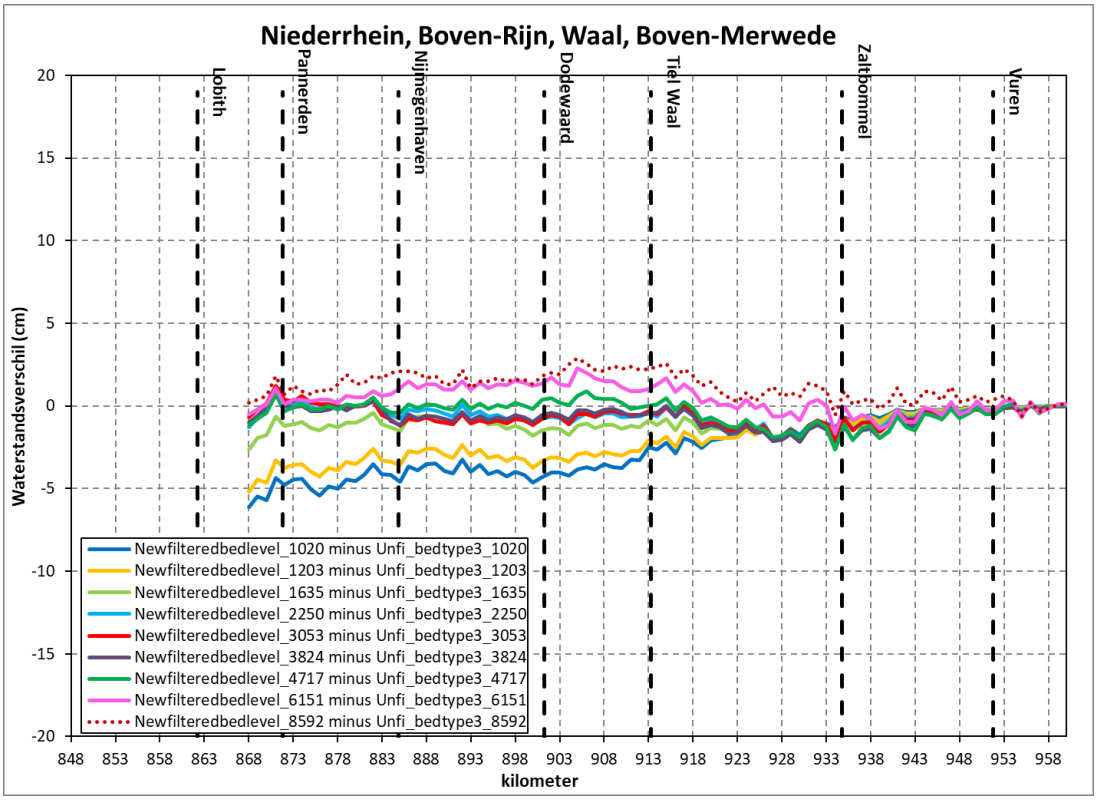

Figure 5.5 Difference in water levels (on the river axis) between simulations with filtered ("NewFilteredBedlevel", defined in cell centers) and unfiltered bed levels ("Unfil_bedtype3", defined in cell corners).

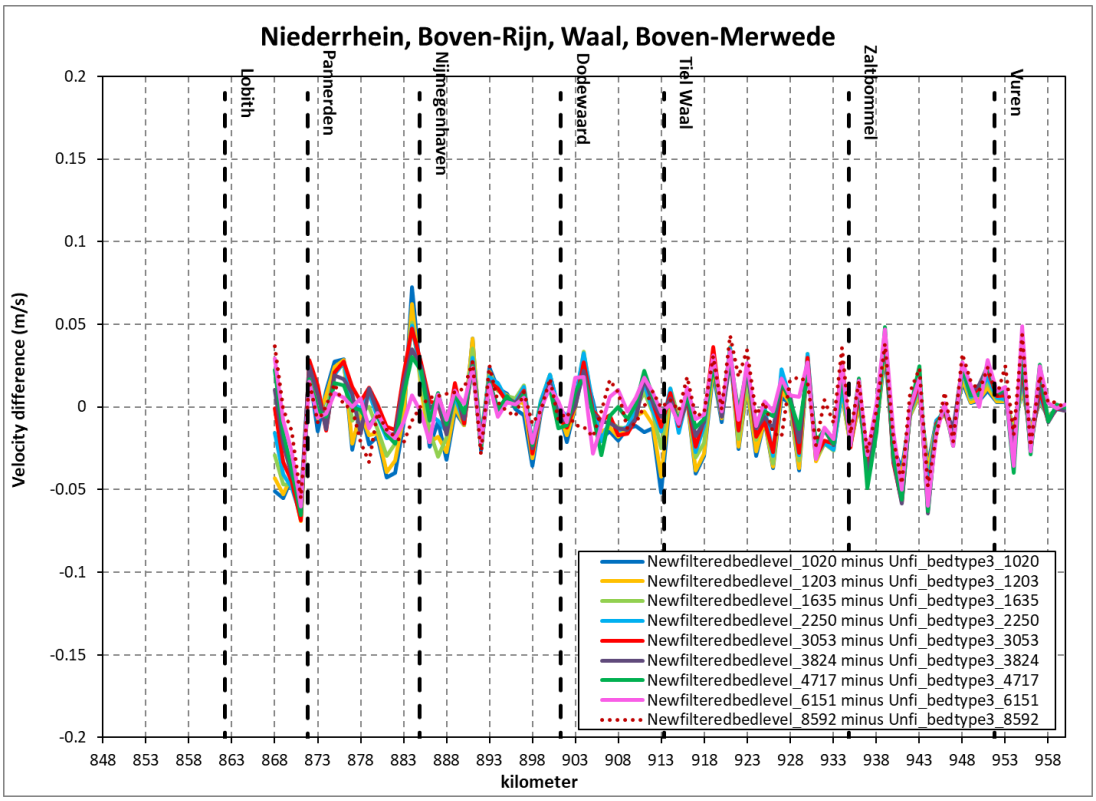

Figure 5.6 Difference in flow velocities (on the river axis) between simulations with filtered ("NewFilteredBedlevel", defined in cell centers) and unfiltered bed levels ("Unfil_bedtype3", defined in cell corners).

5.2.3 Effect of applying a constant main channel roughness

Another modification in the original settings of the model was to first turn off the use of the calibration factor and then set a constant main channel roughness value of 45 $m^{1/2}/s$. In both cases the changes were made keeping the bed level in cell corners and without filtering. Figure 5.7 and Figure 5.8 show the effect of not using the calibration factor anymore on water levels and flow velocities. For the lower discharges (up to 2.250 m^3/s, which is close to the yearly average discharge), water levels increase along the entire Waal. For discharges above average the water levels decrease on the Midden-Waal, and for flood discharges (6.151 and 8.592 m^3/s) also on the Lower Waal. This is reflected in the flow velocities, which reduce where the water level has increased, and vice versa.

Figure 5.9 and Figure 5.10 compare the results of the model without calibration factor and with constant main channel roughness to the original hydrodynamic model. Figure 5.11 and Figure 5.12 present the absolute water levels for that comparison. In general, the impact on water levels is similar as before. But the increase of water levels in the Upper and Lower Waal becomes stronger if also the base roughness is modified. And the increase of water levels in the Midden Waal for lower discharge is reduced.

The value of C = 45 $m^{1/2}/s$ was chosen because it gave best water level results (on average along the entire Waal) especially for the medium discharges. A good representation of water levels for these discharges is important because it defines the moment at which the flood plains start to flow, and because these discharges contribute most to the morphological development. After all, they are high enough to create morphological changes, and they are run for longer periods than the very high discharges, which run only a few days (Figure 4.11).

In a next phase of model development, after a first calibration, we can experiment with more variability in main channel roughness and work towards a compromise between the input of the original hydrodynamic model and the needs of a morphodynamic model. A proposition for how to do that is made in section 10.4. It is important to keep in mind discharge distribution across the bifurcations in the Rhine branches system when making a choice.

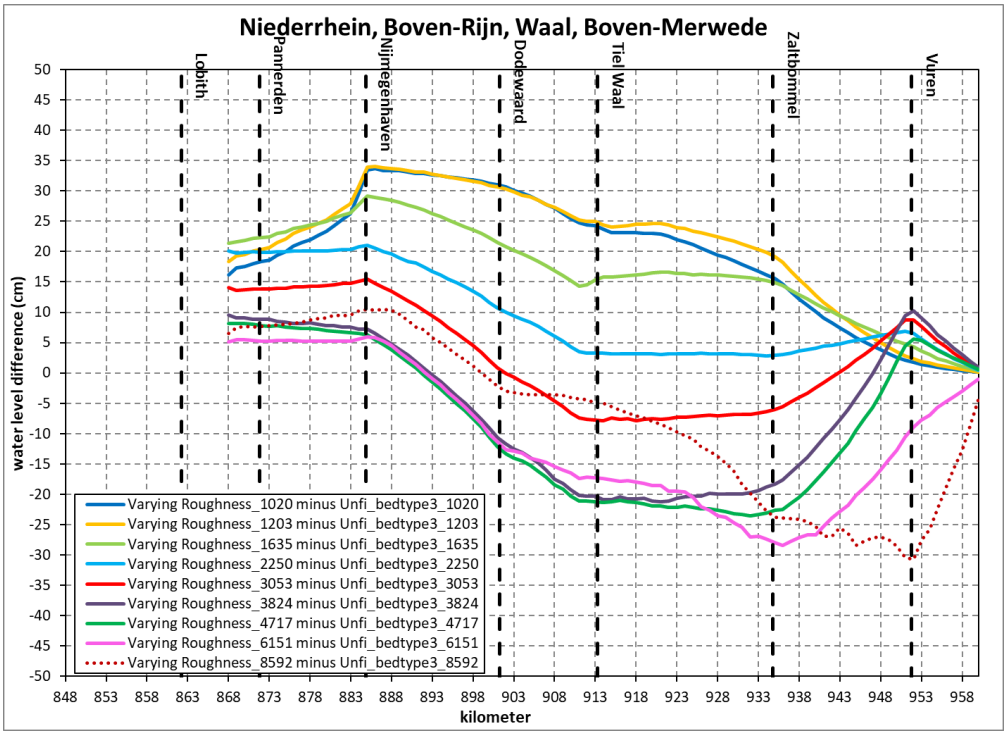

Figure 5.7 Differences in water levels between the simulations without calibration factor ("Varying roughness") and with calibration factor ("Unfi_bedtype3", original hydrodynamic model).

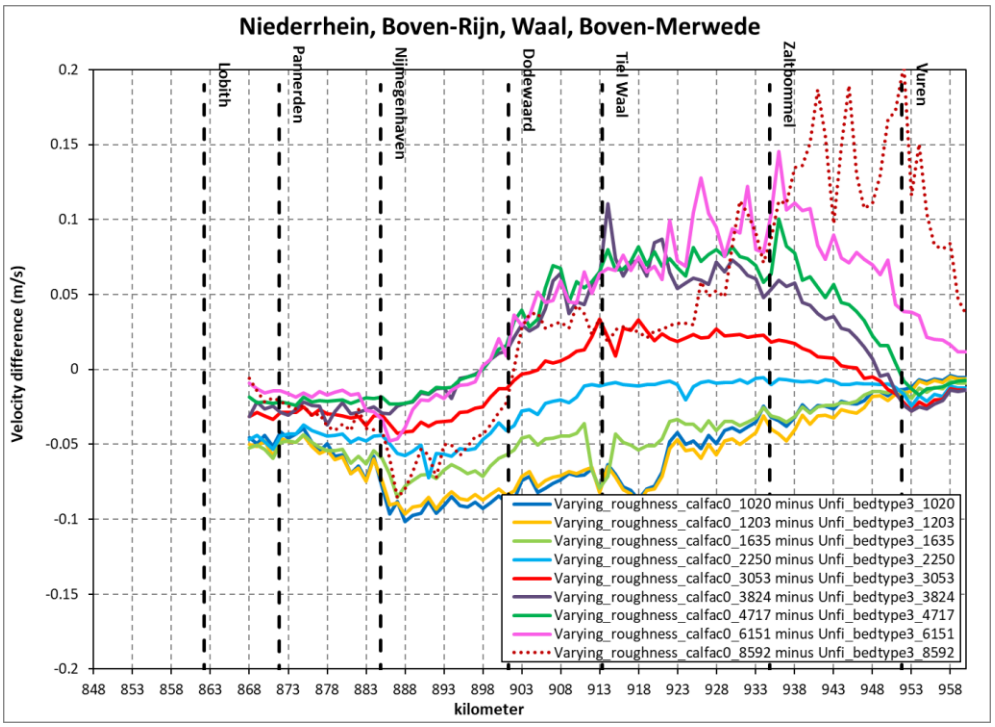

Figure 5.8 Differences in flow velocities between the simulations without calibration factor ("Varying roughness") and with calibration factor ("Unfi_bedtype3", original hydrodynamic model).

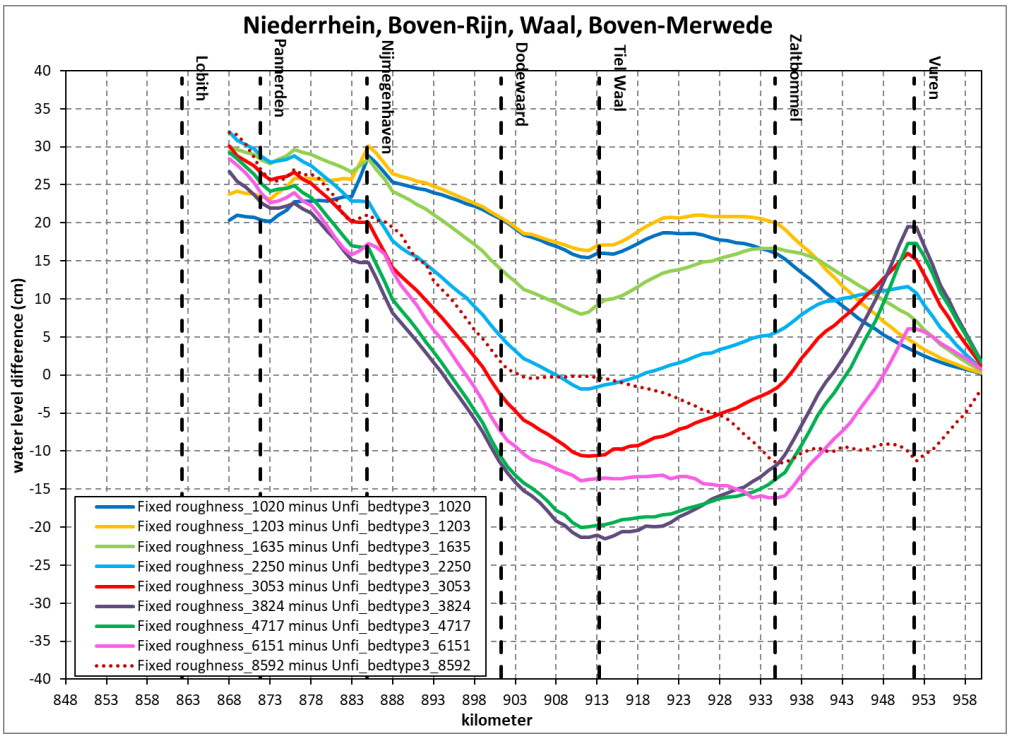

Figure 5.9 Differences in water levels between fixed roughness (C = 45 $m^{1/2}/s$ and no calibration factor) and the original hydrodynamic model ("Unfi_bedtype3", varying roughness and calibration factor).

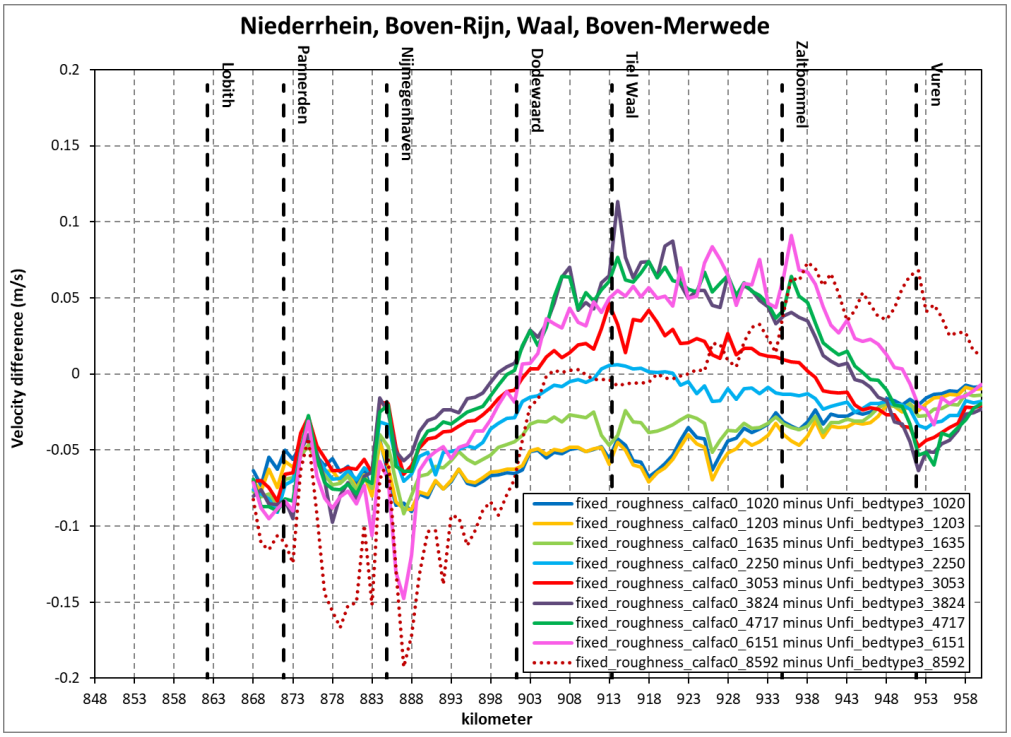

Figure 5.10 Differences in flow velocities between fixed roughness (C = 45 $m^{1/2}/s$ and no calibration factor) and the original hydrodynamic model ("Unfi_bedtype3", varying roughness and calibration factor).

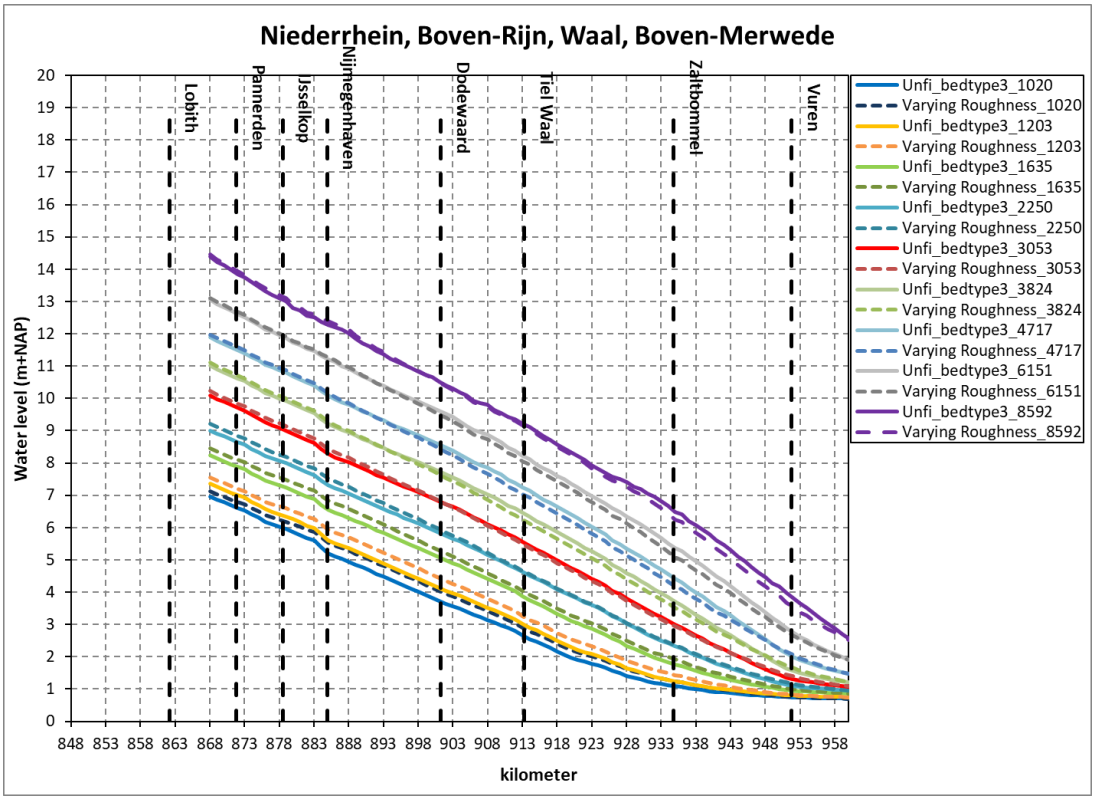

Figure 5.11 Water levels between the simulations without calibration factor ("Varying roughness") and with calibration factor ("Unfi_bedtype3", original hydrodynamic model).

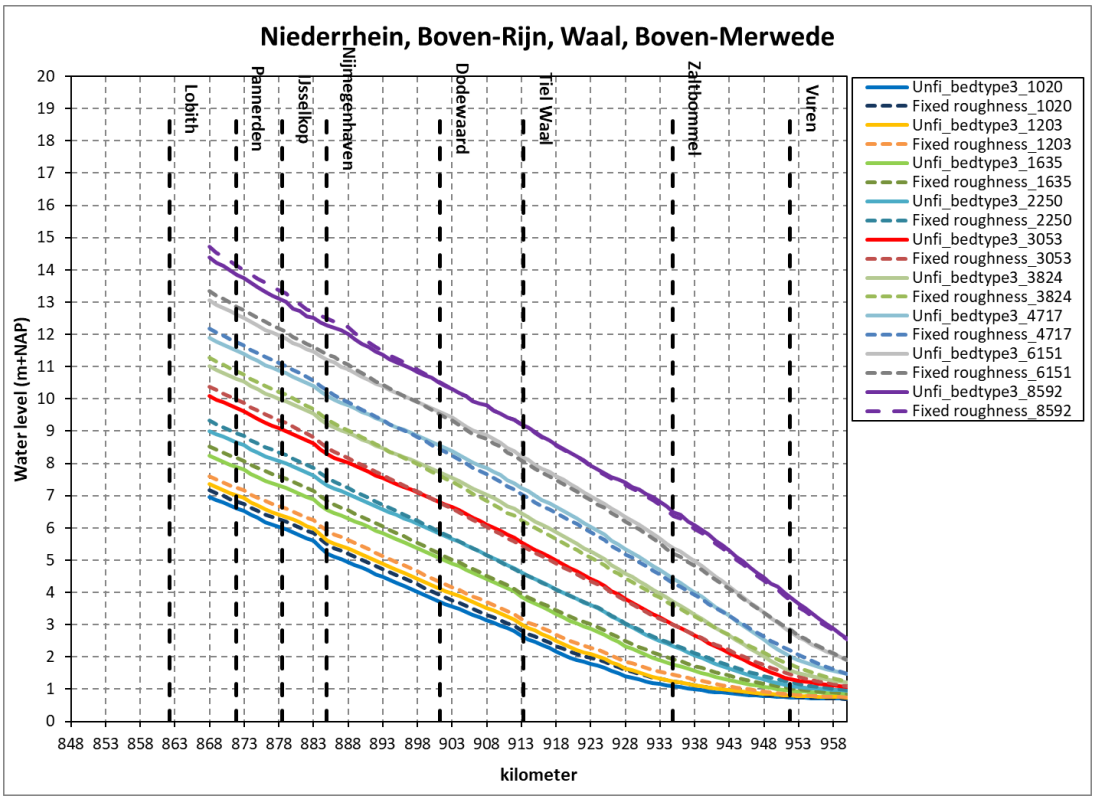

Figure 5.12 Water levels for fixed roughness (C = 45 $m^{1/2}/s$ and no calibration factor) and the original hydrodynamic model ("Unfi_bedtype3", varying roughness and calibration factor).

5.3 Discharge distribution at longitudinal training walls

For morphological development in the area of the LTW's (longitudinal training walls), located along rkm 911 - 922, the discharge distribution between main and side channels is important. It was decided to carry out a simple validation of the discharge distribution within this project, as this had not been done previously (within D-HYDRO).

5.3.1 Data

Validation data are the same as used in Section 3.3.2 of De Jong, Chavarrías and Ottevanger (2021). The dataset is based on the data compiled by Sieben (2020), but only uses those measurements in the main channel that can be paired to a corresponding measurement (i.e. taken at the same day and rkm) in the side channel and vice versa. This means approximately half of the total amount of 650 measurements was discarded. De Jong, Chavarrías and Ottevanger also distinguish three different periods, for which the precise configuration of the LTW inlet structures differ. In the current analysis this distinction is omitted, as De Jong, Chavarrías and Ottevanger show that the effect of changes in configuration is not visible in the data.

5.3.2 Model simulations

The validation was carried out for the same sets of simulations as used in section 5.2.3. In this way, the effect of (1) switching off the calibration factor and (2) setting a constant Chézy roughness coefficient on the LTW discharge distribution can be determined.

To determine the discharge distribution in the model, use was made of output cross-sections that were already included in the model. This means that for each LTW, one cross-section is available for the discharge in the side channel. The corresponding total discharge (main and side channel) was taken from the closest river kilometer cross-section (WL_913.00_QK, WL_916.00_QK and WL_920.00_QK).

5.3.3 Results

Figure 5.13, Figure 5.14 and Figure 5.15 show the discharge distribution for each LTW for the three sets of simulations compared to the ADCP measurements described in section 5.3.1. Validation of the discharge distribution for Waal discharges > 3500 m^3/s is not possible since no measurements are available for this discharge range. We also observe that in several cases, the measured discharge distribution for a single LTW varies, depending on the exact measurement location (river kilometer). This is the case for the side channel at Dreumel when the total discharge is larger than 1500 m^3/s and for the side channel at Ophemert along the entire discharge range. This is because the LTW's have multiple inlets, which means the side channel discharge can vary along one LTW.

Generally, we see a good agreement between modelled and measured discharge distribution, with the main channel roughness having a relatively small effect on the results. Switching off the calibration factor increases the discharge fraction going into the side channels for the three lowest discharge levels. This behaviour is as expected, because the calibration factors on the Waal are smaller than 1 for these discharges. Hence, switching off the calibration factors increases the roughness of the main channel, resulting in a larger portion of the discharge going into the side channels. For larger discharges, the effect is the other way around as calibration factors are generally larger than 1.

Setting a constant Chézy coefficient of 45 $m^{1/2}/s$ decreases the fraction into the side channel again (compared to the model without calibration factors), except for the highest two discharges, where no clear effect is visible.

A clear discrepancy between model and measurements is that for the lowest two discharges, no discharge is going into the side channel at Wamel according to the model, while a fraction of about 0.01 to 0.04 was measured here. A possible cause for this is that the inlet structure configuration was changed in April 2019. The new configuration is included in the model, while the measurements in question were carried out in September/October 2018, so before the configuration change. It is also possible that the measurements are less accurate in this range, as measured side channel discharges are only in the order of 10 m^3/s.

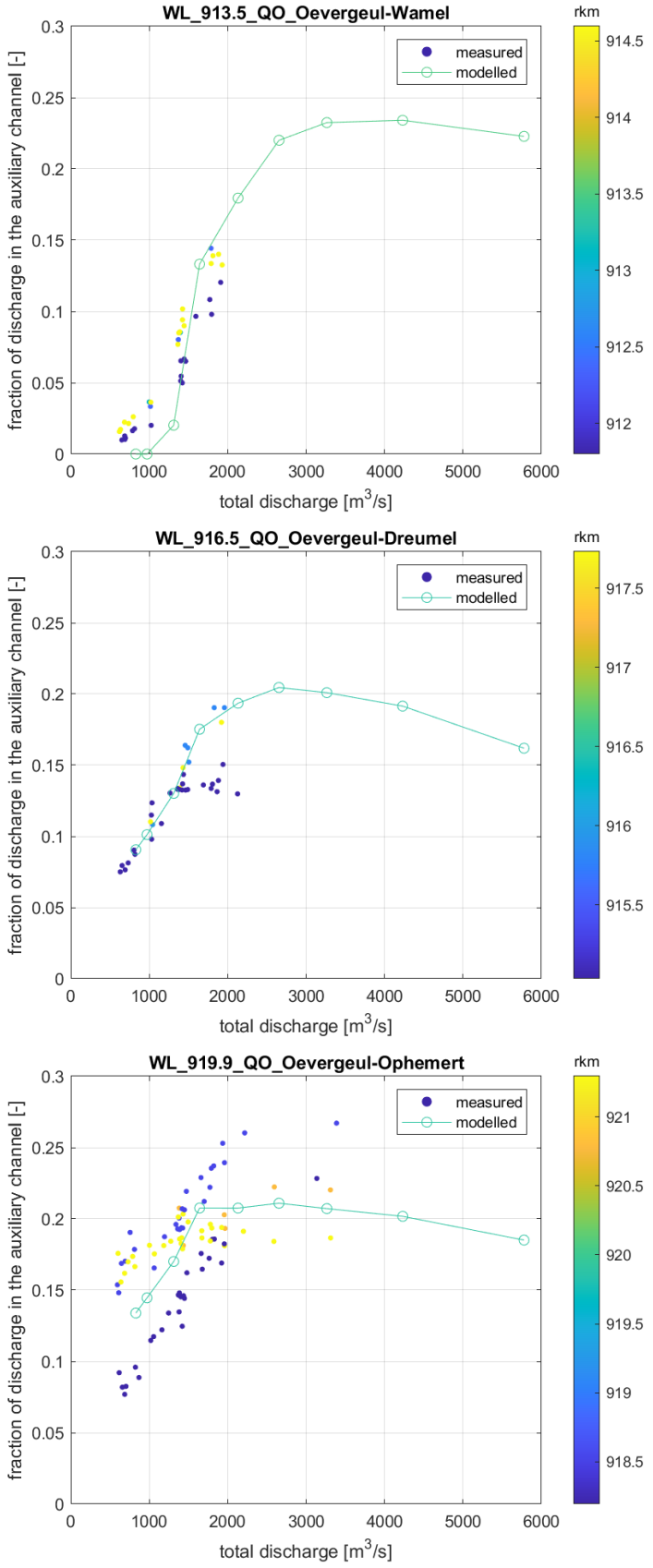

Figure 5.13 Discharge distribution at the LTW's, original roughness of hydrodynamic model. Note that line and dot colours indicate the river kilometer.

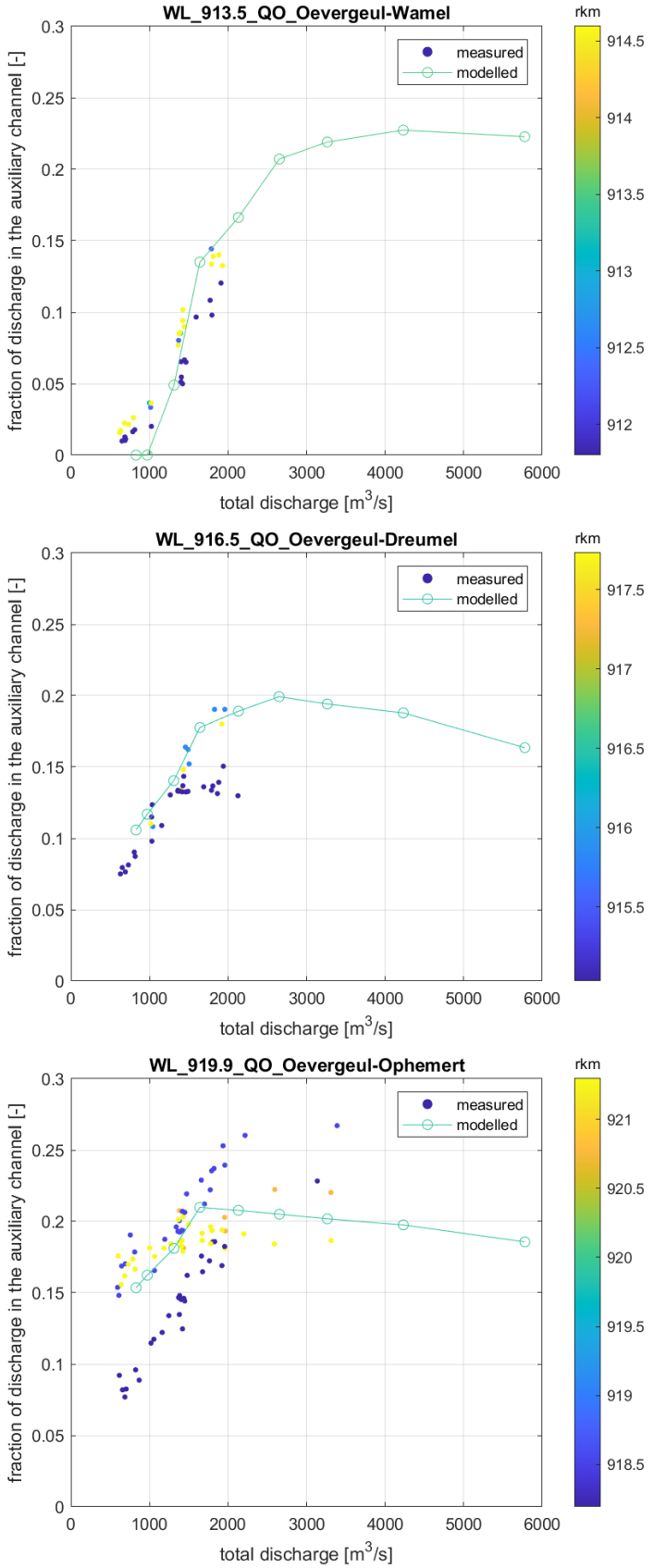

Figure 5.14 Discharge distribution at the LTW's, original roughness of hydrodynamic model, without calibration factor. Note that line and dot colours indicate the river kilometer.

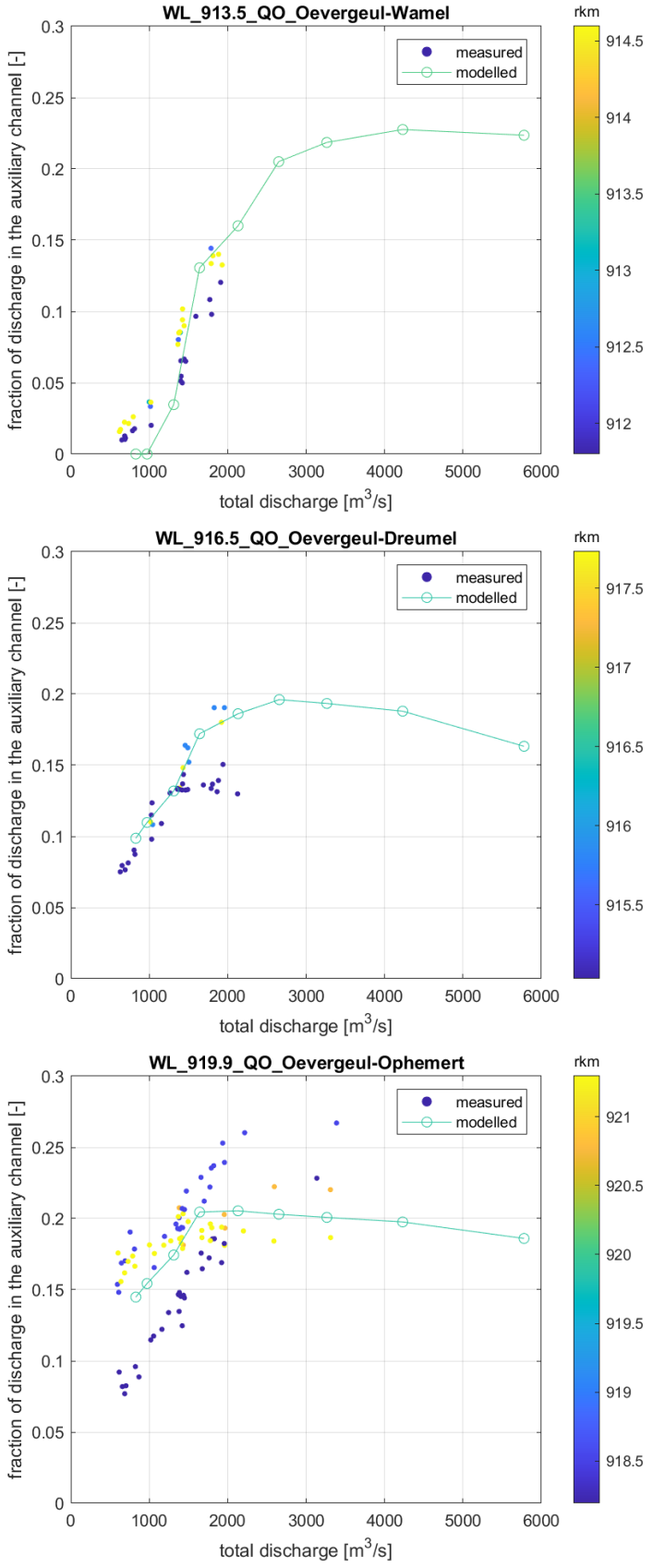

Figure 5.15 Discharge distribution at the LTW's, C = 45 $m^{1/2}/s$. Note that line and dot colours indicate the river kilometer.

6 Morphological schematization

6.1 Implementation of graded sediment

6.1.1 Active layer and underlayers

In D-HYDRO, morphodynamic changes for mixed-size sediment (graded sediment) are modelled using the active layer model (Hirano, 1971). In this model, the part of the bed that interacts with the flow is represented by the active layer. Only sediment in the active layer can be set into transport. Sediment in the active layer is perfectly mixed. Computed changes in mean bed elevation per cell result in vertical mixing of sediment between the active layer and the underlayers, and in between underlayers.

D-HYDRO allows to specify spatially and temporally varying active layer thickness, e.g. to model changes in dune height. In the v0 of the Waal model, however, we will use a constant active layer thickness in order to reduce model complexity and over-parametrization. In the future, we will investigate the impact of the active layer thickness. Based on the results of that analysis, the active layer thickness might be modelled as being dependent on water depth in later model versions. Simulations with the DVR model (predecessor of the new model) have shown that making the active layer thickness directly dependent on the predicted dune heights leads to circular dependencies and therefore unplausible results (Niesten et al., 2017).

As in previous modeling efforts (e.g. Chavarrias et al., 2020), an active layer thickness of 1 m is chosen.

In the DVR model, four layers (1 active + 2 sublayers + 1 thick lowest layer) were used. That turned out to be rather few, it lead to fast mixing of sediment into the lowest thick layer. Therefore, we use a total of 7 layers in the new model: the active layer with an initial thickness of 1 m and 6 layers below with a thickness of 0.5 m for the first 5 and 10 m for the lowest one. The initial sediment composition is prescribed for all these layers. The number of underlayers and their maximum thickness is defined accordingly (.mor file) in order to avoid any sediment transfer between layers and immediate mixing during the first time step.

6.1.2 Sediment fractions

The new morphodynamic model does not only need to assess local morphological developments of the navigation channel, but also the large-scale and long-term morphological development of the Rhine river system in the Netherlands. Therefore it is important to account for the entire variety of processes that play a role in different reaches from upstream till downstream. Most relevant in this respect is the occurrence of grain-size variation and its relevance for sediment-transport processes. Characteristic for the Rhine River is a downstream fining of sediment when looking at it on the length-scale of the German Niederrhein and Dutch Rhine branches, see for example Figure 3.1. The Rhine in Germany (Niederrhein) can be considered as a gravel river, whereas it shows a transition towards a sand-bed river in the Dutch Rhine branches. In the transition zone between the German border and the upper-Waal, Pannerdensch Kanaal and upper-IJssel and Neder-Rijn, both gravel and sand play an important role in sediment transport and morphology. The river bed of the further downstream-located branches is composed of sand. In the tidal low-land part the interaction between sand, silt and mud becomes important.

Therefore, it was decided to apply graded sediment in the entire model. This means that different sediment fractions, from coarse to fine, and their interaction, are modelled separately. The sediment fractions included in the model are shown in the Table 6.1. The boundaries of the fractions are based on the sieve sizes used in the 2020 measurement campaign (Onjira, 2023). In future model versions, we intend to reduce the number of fractions to about 12.

For the finest fraction the minimum diameter is taken as half of the maximum diameter. The maximum diameter of the coarsest fraction is set to the value of 0.125 m.

Table 6.1 Sediment fractions included in the first model schematization (v0).

Name	Minimum diameter [m]	Maximum diameter [m]
Fraction01	0.000008	0.000063
Fraction02	0.000063	0.000090
Fraction03	0.000090	0.000125
Fraction04	0.000125	0.000180
Fraction05	0.000180	0.000250
Fraction06	0.000250	0.000355
Fraction07	0.000355	0.000500
Fraction08	0.000500	0.000710
Fraction09	0.000710	0.001000
Fraction10	0.001000	0.001400
Fraction11	0.001400	0.002000
Fraction12	0.002000	0.002800
Fraction13	0.002800	0.004000
Fraction14	0.004000	0.005600
Fraction15	0.005600	0.008000
Fraction16	0.008000	0.011200
Fraction17	0.011200	0.016000
Fraction18	0.016000	0.022400
Fraction19	0.022400	0.031500
Fraction20	0.031500	0.045000
Fraction21	0.045000	0.063000
Fraction22	0.063000	0.125000

6.1.3 Initial sediment composition in top layer

The initial sediment composition in the top layer is derived from the data from the 2020 measurement campaign (section 3.3). The characteristics of the sieve curves at the different measurement locations vary considerably due to measurement inaccuracies and physical (e.g. sorting) processes on the river bed (see Sloff, 2022, for a description of these processes and a detailed analysis of the 2020 data). For use in the morphological model, they need to be interpolated in space to achieve a full coverage of the computational grid area. The data should also be smoothed to filter out the enormous spatial variability which cannot be reproduced by the model due to the absence of smaller scale processes. This is similar to the reasoning for the filtering of initial bed levels as described in section 4.3.2.

Initially, three different ways of interpolation and filtering were explored:

1. T-SNE: Measurement data was filtered using the T-SNE algorithm (van der Maaten and Hinton, 2008) and predictions via mixture modelling using logistic regression output as weights (see Appendix A for details and result). Afterwards, the filtered data was interpolated as follows: At locations on the left side of the channel (transverse coordinate < -70 m) the left bank values are interpolated by the distance along the channel. At the right bank (transverse coordinate > 70 m) the treatment is similar, but based on the right bank information. For the central portion linear interpolation based on a Delaunay triangulation of the streamwise and transverse distance.
2. Rolling Mean: Measurement data was first averaged across the width of the main channel. To prevent any bias, only locations with data on all three positions (river axis, left and right side) were considered, i.e. only the full river kilometres (section 3.3). Then, a 10 km rolling mean was calculated for the variation in longitudinal direction. The result is applied on the computational grid as constant across the width.
3. Linear Interpolation: A simple linear interpolation of the raw measurement data without filtering was done as well.

The simple linear interpolation (option 3) does not seem desirable since it regards each measurement as “the truth”, without taking into account the relatively large uncertainty in the measured data.

The rolling mean is based on all grain size data from 2016-2020, so including the data from the sediment nourishment project. This was done because the 2020 campaign contains a few very coarse samples on the Boven-Rijn/Waal that would influence the mean too much. The nourishment project’s samples for the Boven-Rijn/Waal do not show these coarse values. The statistical approach T-SNE should be able to consider this without needing additional data. Another important difference between the rolling mean and the T-SNE is that the rolling mean is based on width-averaged data, so left and right side and center of the main channel use the same composition. In the statistical approach, an interpolation in space is made, so that differences in grain sizes between e.g. left and right side are included in the model (Figure 6.1).

Since we suppose that the structural difference between left and right bank is caused by navigation, an effect that the model is not able to mimic, and because (at the moment) the T-SNE approach does not add any additional information (e.g. grain size variations induced by river bends) compared to the simple rolling mean, we chose to use the rolling mean approach in the model. This is similar to the approach used in the DVR model. It would have to be investigated how the T-SNE approach could be modified in order to reproduce the influence of bends. In this way, an initial sediment composition that is closer to reality and thus needs less spin-up could be produced. This would be preferable in terms of simplicity of model use and to avoid undesired influences of spin-up (section 10.3).

Note that the initial sediment composition might have to be modified during calibration.

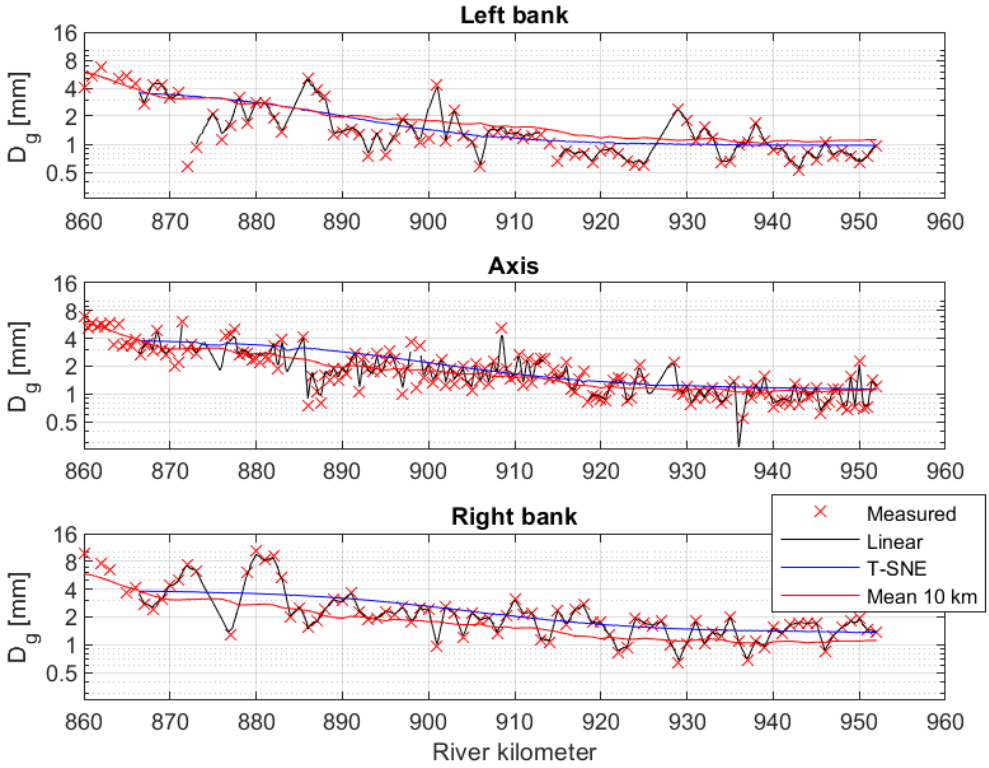

Figure 6.1 Geometric mean of the sieve curves derived from the 2020 measurements (red crosses) and derived using the three methods described above (solid lines).

6.1.4 Initial sediment composition in underlayer

There is not enough data available to define the composition of underlayers in the Waal. Therefore, we will use the same (initial) composition for the underlayers as for the top layer.

6.1.5 Hiding and exposure

Hiding and exposure is a relevant process in transport and sorting processes in poorly sorted sediments. Due to hiding processes fine sediments are hidden behind coarse grains and have a lower mobility, whereas the coarse particles are more exposed and get a higher mobility. This effect is accounted for by a modification factor on critical shear stress in the transport formula. For hiding and exposure, the ration between grain-size of a fraction Di and the median grain-size Dm of the sediment mixture is used to increase (for coarse fractions) or reduce (for fine fractions) the critical shear stress.

The hiding exposure used is the Ashida & Michiue formulation (same as in DVR model, see e.g. Becker, 2021):

$$\xi = \begin{cases} 0.8429\frac{D_m}{D_i} & \text{if } D_i/D_m < 0.38889 \\ \left(\frac{{}^{10}\log 19}{{}^{10}\log 19 + {}^{10}\log\left(D_i/D_m\right)}\right)^2 & \text{otherwise} \end{cases},$$

with D_i the characteristic grain size of the sediment fraction considered [m] and D_m the mean grain size of the total sediment mixture [m].

Since the hiding and exposure factor works on the critical shear stress, it is only used in sediment transport formulations that contain a critical shear stress (e.g. Meyer-Peter-Müller, see section 6.2).

6.2 Sediment transport formula

In principle, the choice of a suitable sediment transport formula is part of the calibration of a model. For the first version (v0) of the Waal and IJssel model, experiments were run with the settings used in previous calibration efforts for the DVR model (Sloff et al., 2009) and for a 1D morphological model for the Rhine branches developed for the Integrated River Management (IRM) programme (Chavarrías et al., 2020). These settings are presented in Table 6.2.

Sloff et al. (2009) found that the formula of Meyer-Peter and Müller (1948) was well suited for the upstream part of the DVR model (Boven-Rijn, Pannerdensch Kanaal, Boven-Waal). The model domains further downstream were never modelled using graded sediment. When developing the fully graded sediment 1D model for IRM, Chavarrías et al. (2020) found that it was impossible to correctly predict both the sand and gravel load for all Rhine branches with only one load relation. They decided to use the formula of Engelund and Hansen (1967) for the sand fractions and the one of Meyer-Peter and Müller for the gravel fractions, as these were most accurate for the independent fractions.

Model calibration results will have to show which of these performs best for the Waal and IJssel models, and if the settings still need to be modified.

Table 6.2 Sediment transport formulations tested in the first model version (v0).

Abbreviation	Sediment transport formula	Parameters	Source
IRM00	Fractions 1 – 11: Engelund-Hansen (EH) Fractions 11 – 22: Meyer-Peter-Müller (MPM)	a = 0.18, n = 5 a = 2.56, b = 1.5, θ_c = 0.025, μ = 1	Chavarrías et al. (2020)
DVR00	Meyer-Peter-Müller (all fractions) (MPM)	a = 5, b = 1.5, θ_c = 0.025, μ = 0.7	Sloff et al. (2009)

with:

$$S_{EH,i} = \frac{a \cdot 0.05 u^n}{\sqrt{g} C^3 \Delta_i{}^2 D_i}$$

$$S_{MPM,i} = a D_i \sqrt{\Delta g D_i} (\mu \theta_i - \xi_i \theta_c)^b$$

with u the flow velocity magnitude [m/s], C the Chézy friction coefficient [$m^{1/2}/s$], Δ_i the relative density of the sediment fraction considered [-], D_i the characteristic grain size of the sediment fraction considered [m], μ the ripple factor, θ_c the critical Shields parameter, ξ_i the hiding and exposure factor for the sediment fraction considered, and n, a and b calibration parameters.

6.3 Fixed layers, constructions and morphologically active area

In general, in the v0- and v1-version of the new model we follow the approach used in the DVR model, i.e. only the main channel of the river is morphologically active, because morphological processes in the flood plains and e.g. of side channels in the flood plains are more complex due to vegetation. More research is needed to model these processes sufficiently well (see Spruyt, 2023).

In the flood plain, sedimentation can take place, and sediment that has been deposited there during the simulation can be moved away again, but at the start of the simulation no sediment is present in the flood plain and thus no erosion can take place. All grid cells neighboring the tips of groynes are also made inactive in the same way, because the bed level of these cells contains parts of the groynes. If these cells were kept active, the groynes would erode at the beginning of the simulations.

According to our current approach, man-made fixed layers or naturally immobile areas are implemented into our morphological model in the same way. Since this approach makes them have a significant influence on the behavior of the surrounding river bed, it is recommended to only implement them at locations that are very clearly immobile and that are of significant size. Therefore, in the first model version only the fixed layers at Nijmegen and Sint Andries as well as the bottom vanes at Erlecom are made immobile. This first model version (v0) will be used for offline and 1D calibration.

6.4 Secondary flow

In the simulations including sediment transport and morphology, secondary flow is switched on, without coupling it back to hydrodynamics. The calibration parameter for bend effects is initially given the same value as was used in the DVR model (e.g. the model used in Becker (2021)):

- Espir = 1,0

6.5 Bed slope effects

The parameters for taking into account bed slope effects are initially given the same values as were used in the DVR model (e.g. the model used in Becker (2021)):

- AShld = 1.1
- BShld = 0.5

In a next phase of the model development, the values will be used as calibration parameters for calibrating 2D bank patterns.

6.6 Upstream boundary conditions (morphology)

In a river model, with flow in only one direction, a morphological boundary condition has to be prescribed at the upstream model boundary. In the Waal model, that is the boundary at Pannerdensche Kop (section 4.3.1). D-HYDRO offers different possibilities for prescribing these. Tests were made with two different configurations:

1) The sediment influx was prescribed per fraction. The results of the “offline” calibration for the most upstream kilometer of the Waal were used for that. The influx differs per discharge level, but is for now prescribed as constant across the width of the boundary.
2) The rate of bed level change was prescribed. A constant rate was derived from the bed level measurements processed by De Joode (2023). The trend was derived for the most upstream 100 m section of the Waal as shown in Figure 6.2, from which the trend for the entire period of analysis was chosen (-1.4 cm/y). In combination with a bed level trend one also has to impose information on upstream sediment composition. It was assumed that composition stays constant.

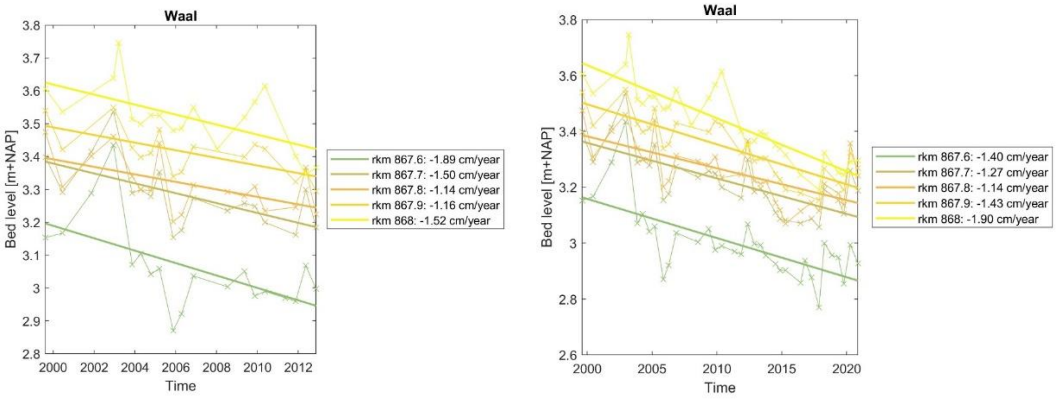

Figure 6.2 Bed level trend during calibration period 1999-2012 (left) and the full period of analysis (1999-2021, right) in the most upstream 100 m sections of the Waal.

Figure 6.3 shows that the second option results in a far too high sediment inflow from the boundary, with an influence that propagates significantly far downstream[3]. It also results in significant changes in sediment composition that do not seem realistic (not shown in this report).

Sediment inflow is also too high using the first option, but to a lesser extent, and sediment composition stays close to the initial composition (see 9.3.4). However, the first option gives a wrong distribution across the cross-section and results in strong sedimentation on the right side and erosion on the left side of the main channel. This only reaches about 400 m into the model domain (two groyne fields, Figure 6.4) and is therefore found acceptable for the current model version. For future improvements, we recommend to distribute the sediment inflow per cell and find an optimum value for the amount of inflow (after sufficient 1D and 2D calibration). It seems to be difficult to impose a bed level change that produces a realistic sediment inflow (amount and composition), although that needs to be investigated further.

[3] In the j99 model used for calibration, this problem does not occur. This needs to be investigated further.

Figure 6.3 Sediment transport along the Waal for different types of upstream boundary conditions using schematization j19_6. Top: sediment transport per fraction prescribed; bottom: bed level change in combination with constant sediment composition in active layer prescribed.

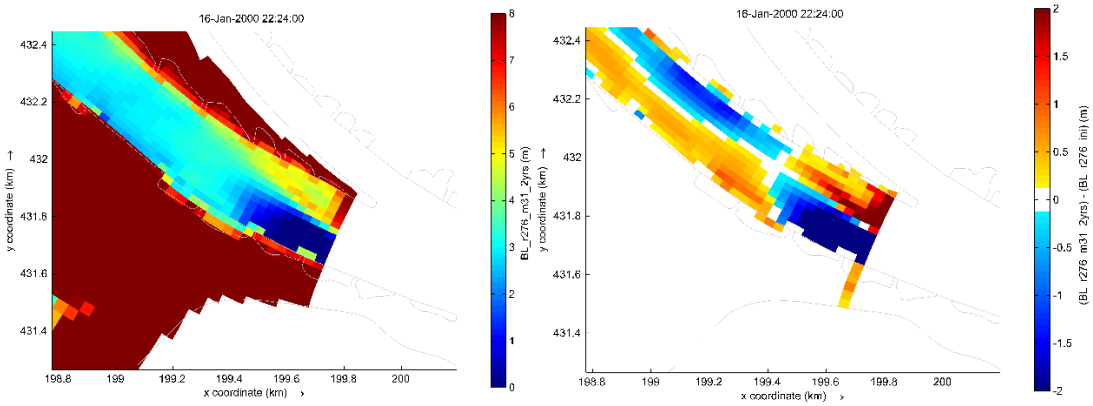

Figure 6.4 Bed level at the upstream boundary after two years of simulation with j19_6 (left) and cumulative sedimentation and erosion.

7 Offline calibration Waal

7.1 Methodology

Within the offline calibration, sediment transport is calculated based on hydrodynamic model simulations. This means that the computed sediment transports are not translated into bed level changes in the model, which in turn would influence hydrodynamics. Because this feedback mechanism is not included, we call this an offline calibration. The objective is to compute the expected sediment transport of an average year for varying sediment transport relations and parameters.

For the offline calibration use was made of the bed level schematization from Baseline without further modification, so bed level specified in corners and no averaging procedure. Given the uncertainty in sediment transport, the limited differences in velocity due to these adjustments are not expected to have any significant impact on the conclusions regarding yearly sediment transport rates.

The basis of the offline calibration is formed by the steady-state hydrodynamic results for nine different discharge levels as described in section 4.4. The final state of each hydrodynamic simulation (i.e., the steady-state for each discharge) is used to construct a schematized hydrograph as in the SMT (Section 4.4). As in this case there is no coupling between hydrodynamics and bed level changes, the order in which discharge levels occur does not influence the results. We can therefore simply take the total duration of each discharge level within the standard hydrograph, without dividing this duration over different periods through the year.

The hydrodynamic output is combined with morphodynamic input regarding the characteristic sediment sizes and the bed composition, defined as the available sediment volume per fraction in each grid cell. For the offline calibration, the rolling mean interpolation of the data from the 2020 measurement campaign was used (see Section 3.3 and 6.1.3) in combination with 22 sediment fractions (Section 6.1.2).

For each flow field (i.e., for each discharge level), the sediment transport rate is computed given the morphodynamic input. The yearly sediment transport is obtained by multiplying each sediment transport rate by the duration of each discharge level.

Within the offline calibration, the two settings for the sediment transport formula described in Section 6.2 (IRM00 and DVR00) were tested.

Section 5.2.3 treats the influence of different main channel roughness definitions on modelled water levels and flow velocities. To also gain insight in the effect of these roughness variations on modelled sediment transport, the offline calibration was carried out for the three sets of hydrodynamic simulations described in Section 5.2.3.

In this first calibration step, we are interested only in along-channel gradients in sediment transport. For this reason, calculated sediment transports are averaged across the width of the main channel (between *normaallijnen*), and for each river kilometer (the river kilometer being in the center of the section). Results are compared to the data described in Section 3.4.

7.2 Results

7.2.1 Original roughness definition

Figure 7.1 presents yearly sediment transport along the Waal for the standardized yearly hydrograph, as calculated with the offline method using the hydrodynamic simulations with the original roughness definition (including a base roughness and a calibration factor that are both varying along the main channel). The black lines in the figure correspond to the values reported by Frings et al. (2019). As Frings et al. (2019) also report values for sand and gravel separately, the total sediment transport is divided accordingly in Figure 7.2 and Figure 7.3. In terms of absolute values, we observe the following:

Although DVR00 gives larger sediment transports than IRM00, for both formulas the order of magnitude of the computed total yearly transport corresponds to the values reported by Frings et al. (2019). The gravel transport is very similar for both formulations, but much higher than the numbers reported by Frings et al. (2019). According to IRM00, sand and gravel transports are equal on the Boven-Waal, while Frings et al. report a sand transport that is 9 times higher than the gravel transport in this section.

For sand DVR00 gives much higher values and steeper gradients than IRM00 on the Midden-Waal and Beneden-Waal. Around rkm 910, the transport resulting from DVR00 is even two times as high as the transport based on IRM00. Compared to the values by Frings et al. (2019), the computed sand transport is lower in the Boven-Waal for both transport formulas. Further downstream, the computed transport gets closer to Frings' values (on average).

Regarding gradients in sediment transport, the following remarks can be made:
The computed gradients are in agreement with the prognosis by Sloff (2019), i.e. erosion in Boven- and Midden-Waal, while no long-term trend or even some sedimentation is expected in the Beneden-Waal. For reference, the trends following from the analysis of bed level trends ("Pmap analysis", Sloff 2019) are also included in the figure.
Overall, we see an increase in sediment transport from the upper boundary to around rkm 930. Further downstream, the rates decrease rapidly. This rapid decrease, especially between rkm 949 and 957, is unexpected. Further analysis reveals that in this section, water depth sharply increases and velocities decrease in downstream direction, especially for low to average discharges. This is because:

- Bed levels, averaged over the width of the main channel, are decreasing rapidly in this section. It is to be investigated if these bed levels are representative for a longer period, or if they are influenced by short-term changes, e.g. due to dredging.
- This section is influenced by tides, especially when river discharges are low. The use of a Qh-relation or a constant water level at the downstream boundary does not do justice to the hydrodynamic conditions that occur in reality. Furthermore, the Qh-relation overestimates the average water level at the downstream boundary, again mainly for low discharges. This is because the Qh-relation is based on the maximum water level occurring over a tidal period, instead of the average water level (Van der Wijk, 2022). The lower the discharge, the larger the tidal range at Hardinxveld and the larger the difference between the average and the maximum water level.

A sharp decrease in sediment transport rates is observed in the section around the longitudinal training walls (LTW's), roughly along rkm 913-921. In the online morphodynamic computations, we would expect sedimentation in this section, which is actually one of the intentions of the LTW's. Based on section 5.3 of this report, which shows that the discharge distribution between main and auxiliary channels is well captured in the model, we conclude that the observed transport gradient is not the result of too much discharge flowing into the auxiliary channels.

Gradients in sediment transport are largely related to gradients in bed sediment composition. Up to rkm 920, grain sizes are generally decreasing in downstream direction, while sediment transport rates are increasing. Further downstream, gradients in bed sediment composition are less prominent, and transport gradients are more related to changes in flow velocity.

As described in Section 4.3.3, preliminary morphodynamic simulations showed artificial sedimentation and erosion patterns, introduced by sudden changes in roughness at the transitions between base roughness and calibration sections. To avoid these effects and simplify the interpretation of model results, a constant Chézy roughness coefficient was applied in the remainder of the project. To investigate the effect of (1) eliminating the calibration factor and (2) applying a constant base roughness coefficient, the offline calibration was repeated with these changes as well. The results are discussed in the following two sections.

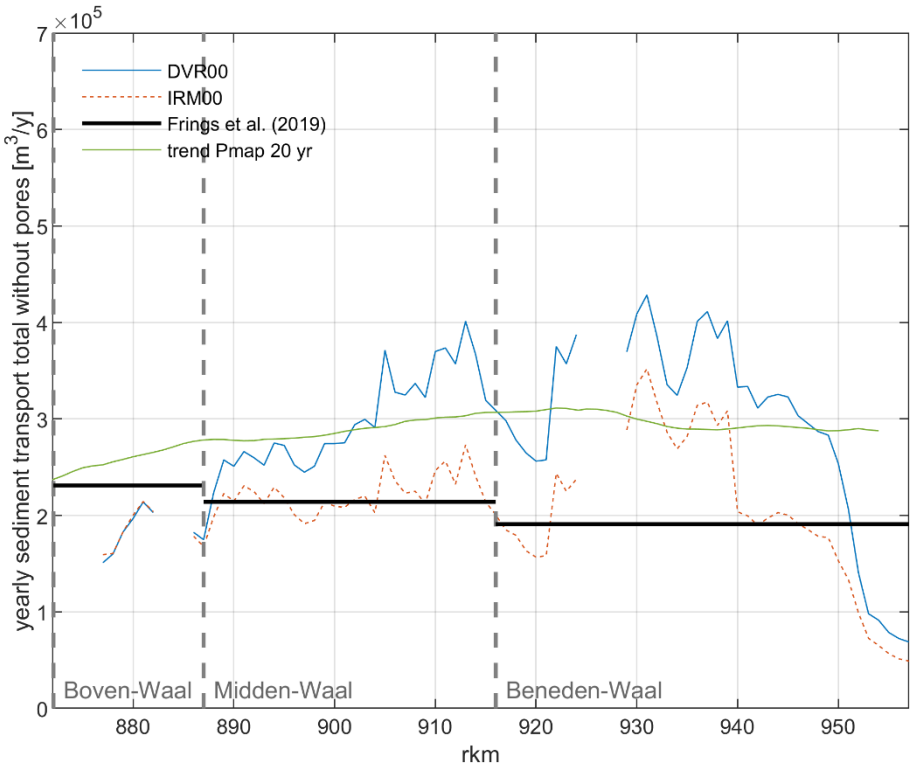

Figure 7.1 Total sediment transport without pores for the standardized yearly hydrograph, as calculated with the offline method. Hydrodynamic conditions follow from model simulations with the original hydrodynamic model roughness. Computed transports at the locations of fixed layers are not shown because averaging over the main channel width (half alluvial, half fixed) yields unrealistic values in these cases.

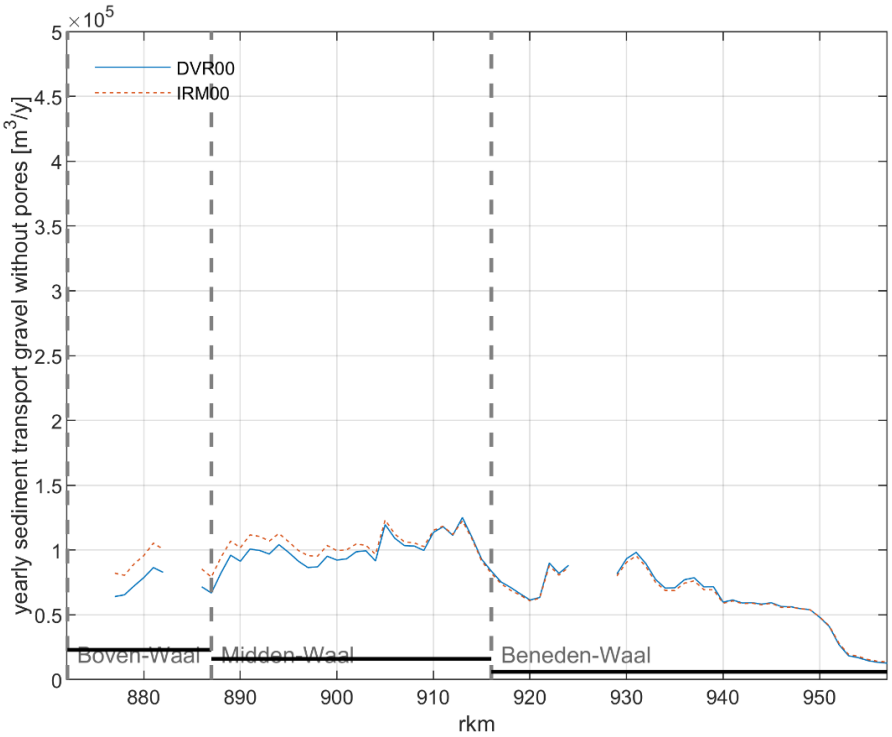

Figure 7.2 Gravel (D > 2mm) transport without pores for the standardized yearly hydrograph, as calculated with the offline method. Hydrodynamic conditions follow from model simulations with the original hydrodynamic model roughness. The black lines correspond to the values reported by Frings et al. (2019). Computed transports at the locations of fixed layers are not shown because averaging over the main channel width (half alluvial, half fixed) yields unrealistic values in these cases.

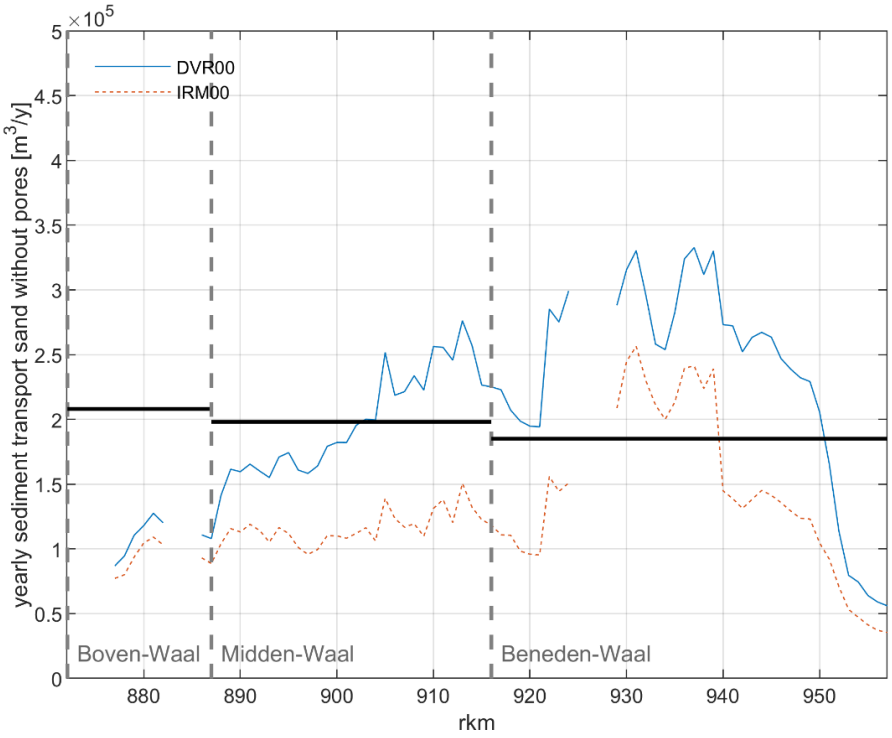

Figure 7.3 Sand (D < 2mm) transport without pores for the standardized yearly hydrograph, as calculated with the offline method. Hydrodynamic conditions follow from model simulations with the original hydrodynamic model roughness. The black lines correspond to the values reported by Frings et al. (2019). Computed transports at the locations of fixed layers are not shown because averaging over the main channel width (half alluvial, half fixed) yields unrealistic values in these cases.

7.2.2 Influence of calibration factor

Figure 7.4 shows total yearly sediment transport when the calibration factor is omitted. Compared to Figure 7.1, the transport rates are generally larger up to rkm 935. The increase is largest on the Midden-Waal. This effect can be explained by looking at the calibration factors more closely (see appendix B). From our offline analysis, we know that the discharge levels 1635 m^3/s and 2250 m^3/s in the standard hydrograph (see e.g. Figure 4.11) have the largest contribution to the yearly sediment transport, because they have a relatively long duration. Corresponding discharges on the Waal are 1312 and 1642 m^3/s. For these discharges, calibration factors are generally smaller than 1. Omitting these factors effectively increases the roughness, which leads to an increase in sediment transport.

In the LTW section, the increase in transport rates compared to the simulation with calibration factors is less pronounced, because calibration factors for 1312 and 1642 m^3/s are very close to 1 in this section.

From rkm 935 onward, sediment transport is lower than in the case with calibration factors, until rkm 952. In the most downstream section (rkm 952 – 957), transports are higher again. Overall, these changes result in a somewhat smoother transport gradient along the Beneden-Waal. This is because a sudden roughness transition for discharge levels M1 and M2 (which are most important for morphology) at Vuren (around rkm 951.8) is eliminated by setting all calibration factors to 1. In the original simulation, calibration factors for these levels are 1.0 and 1.1 upstream of Vuren, while downstream they are 0.8 and 0.9. This led to a sudden decrease in roughness for these discharge levels, resulting in a drop in sediment transport. This analysis corresponds to the results of the preliminary online morphodynamic computations (including the calibration factors), which show large sedimentation rates around Vuren, see Figure 4.10.

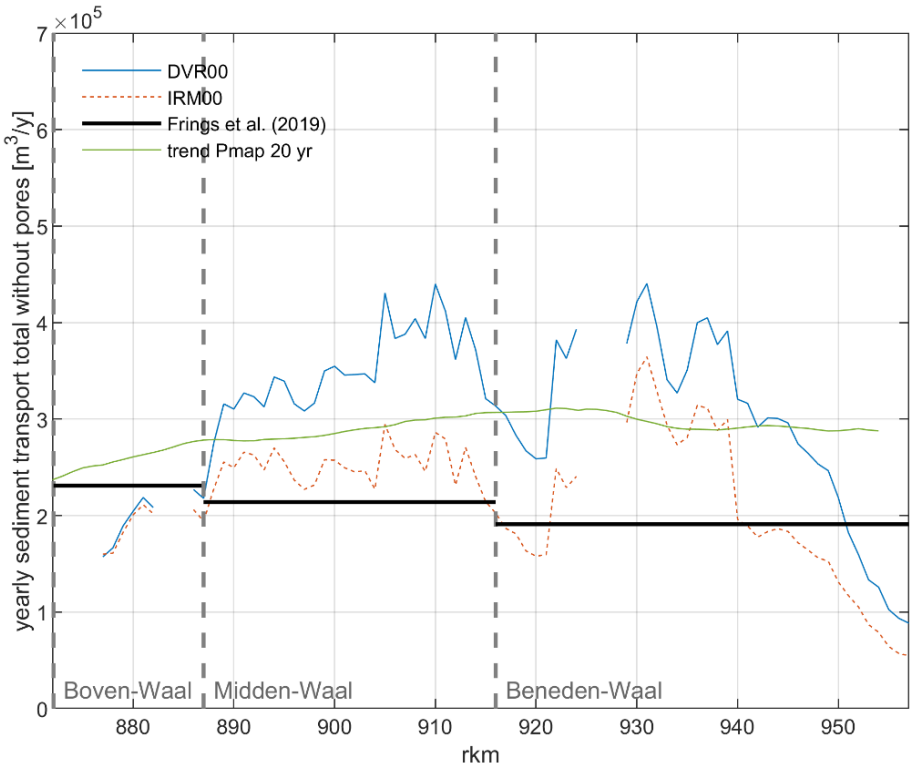

Figure 7.4 Total sediment transport without pores for the standardized yearly hydrograph, as calculated with the offline method. Hydrodynamic conditions follow from model simulations without calibration factor. Computed transports at the locations of fixed layers are not shown because averaging over the main channel width (half alluvial, half fixed) yields unrealistic values in these cases.

7.2.3 Influence of background roughness

When we not only eliminate the calibration factors, but also replace the varying background roughness by a constant Chézy roughness coefficient of 45 $m^{1/2}/s$ throughout the domain, the gradients in sediment transport become even smoother, see Figure 7.5. Yearly sediment transport rates increase on the Boven-Waal and the Midden-Waal up to rkm 900, as well as on the Beneden-Waal from rkm 940 onward, compared to Figure 7.4. In between (rkm 900 - 940), the rates decrease. Sudden changes in sediment transport at rkm 888, 904, 939.5 and 951 are eliminated. Figure 7.6, which gives an overview of the α-values in the Van Rijn roughness formulation as used in the original model, shows that these sharp gradients were caused by sudden transitions in the background roughness at the mentioned locations.

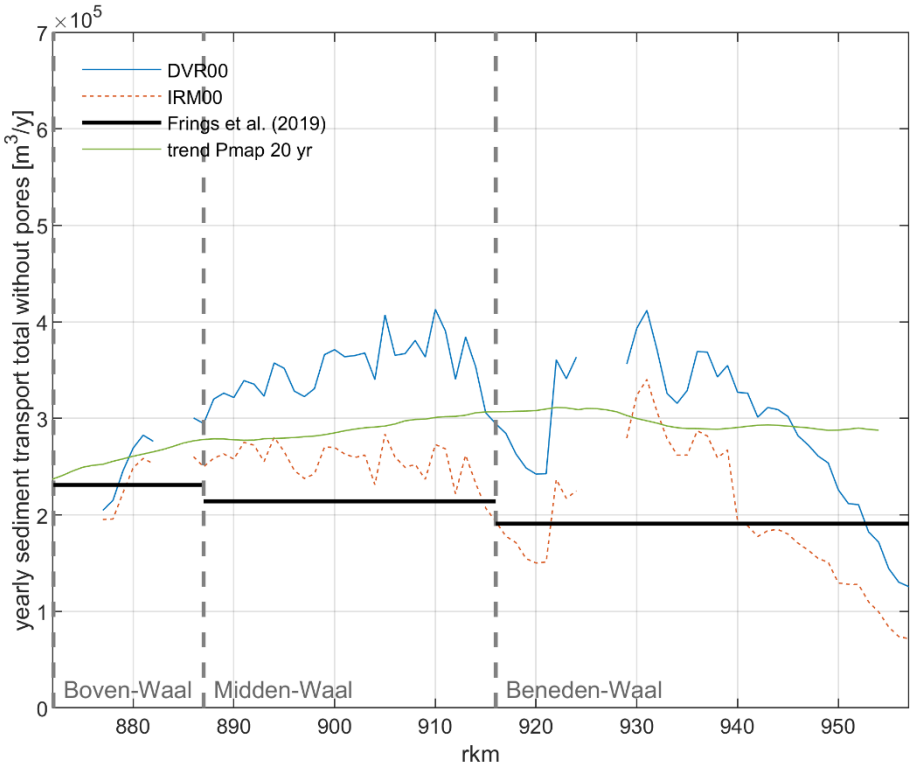

Figure 7.5 Total sediment transport without pores for the standardized yearly hydrograph, as calculated with the offline method. Hydrodynamic conditions follow from model simulations with a constant Chézy coefficient of 45 $m^{1/2}/s$. Computed transports at the locations of fixed layers are not shown because averaging over the main channel width (half alluvial, half fixed) yields unrealistic values in these cases.

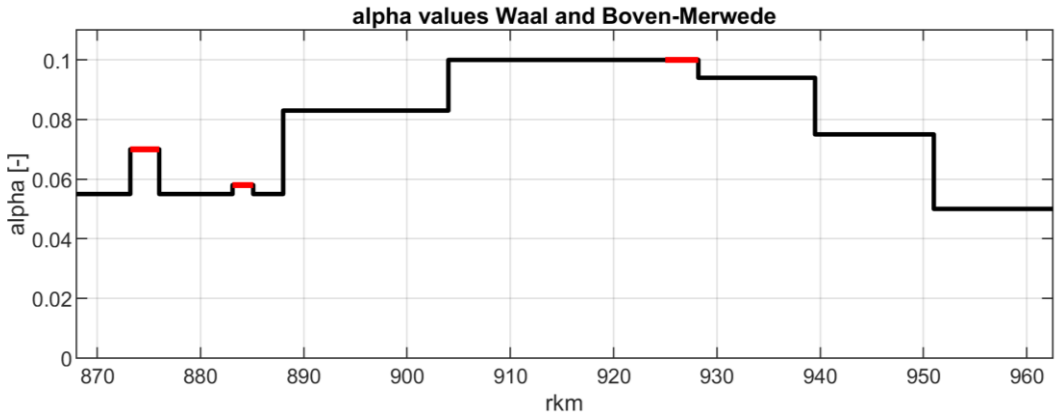

Figure 7.6 Values of coefficient alpha in the simplified Van Rijn roughness predictor, for the original hydrodynamic model. Red lines indicate the values in the alluvial part of the river along fixed layers.

7.2.4 Sediment transport as function of total discharge

Next to computing yearly sediment transport rates, the offline analysis can be used to investigate sediment transport as a function of river discharge. Figure 7.7 (left panel) shows this variable for rkm 952, for the case with constant Chézy roughness. As we would generally expect, sediment transport rates increase non-linearly with discharge at this location, because flow velocity in the main channel also increases with discharge. However, at some locations the offline analysis shows a different behaviour, see for example Figure 7.7 (right panel) for rkm 908. Here, sediment transport increases with discharge up to Q_{Lobith} = 4000 m^3/s, after which transport rates decrease and then stay constant with increasing discharge. This pattern is visible at multiple locations and generally doesn't change between the different roughness schematizations. This means this behaviour is not caused by changes in roughness due to discharge-dependent calibration factors, but is rather a direct result of river geometry. Up to bankfull discharges, velocities in the main channel indeed increase with discharge, but when floodplains become submerged and start carrying flow as well, the velocity in the main channel may decrease. This can explain the decreasing rates for increasing total discharge. This behavior was confirmed for rkm 908; modelled flow velocities in the main channel indeed decrease for the two highest discharge levels compared to the level below. However, a recent model validation with ADCP-measurements (Gradussen, 2023) shows that the model grossly underestimates main channel flow velocities at this location for a Waal discharge of 4500 m^3/s, because the geometry of the floodplain is not up to date. Hence, the pattern shown in the right panel of Figure 7.7 may not be an accurate representation of reality. Further investigation of model accuracy is needed at other locations that show a similar decrease in sediment transport for increasing discharge. Where needed, the model geometry should be updated.

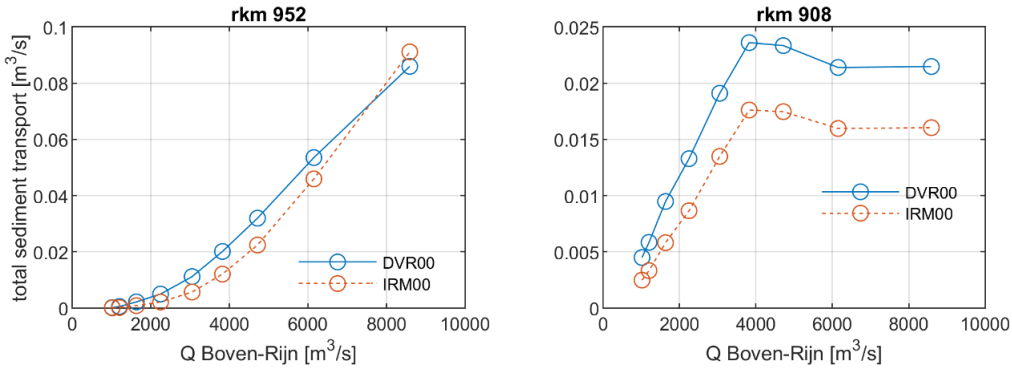

Figure 7.7 Sediment transport per discharge level in the offline calibration, for rkm 952 (left) and 908 (right).

7.2.5 Choice of roughness field

Based on the offline computations, we find that the use of calibration factors and background roughness values that vary per section may lead to large gradients in roughness at the section boundaries, which are physically unrealistic. In morphological simulations, these gradients will then lead to gradients in sediment transport, and therefore unwanted sedimentation and erosion patterns. Using a constant roughness instead prevents this unwanted behaviour. However, this also leads to different overall gradients in sediment transport, which may be less representative of the actual behaviour.

For this first pilot model, a constant roughness may be applied for simplicity. With this approach, sudden roughness transitions are avoided and results can be interpreted more easily. At a later stage, a more detailed roughness field may be applied based on the findings presented in this chapter and the results of morphological simulations with the pilot model (see proposition in Section 10.4).

7.2.6 Choice of sediment transport formula

The principal aim of the offline ‘calibration’ of the pilot model was to present first insights in the computed sediment transport with different transport formulations, without having to carry out time-consuming morphodynamic model simulations.

Although we indeed see significant differences between the two formulations used in our analysis (taken from IRM and DVR), it is not possible to already know which transport formula (including calibration coefficients) will perform best in the online computations. Both formulations result in sediment transport rates of the right order of magnitude and capture the expected gradients in sediment transport. Further analysis with the morphodynamic pilot model is necessary to make an informed decision regarding the transport formula.

Results from the offline calibration that need further attention in the online analysis are:

- The overestimation of gravel transport compared to the values of Frings et al. (2019). Calibration of the morphodynamic model based on measured bed levels and sediment composition will give more insight into the accuracy of these numbers.
- The sharp decrease in sediment transport in the LTW section. The 2D morphodynamic behaviour in this section must be explored in detail.
- The rapid decrease in transport rates near the downstream model boundary. Morphodynamic simulations will reveal if these gradients lead to realistic morphological behaviour.

First results of morphodynamic simulations are presented in Chapter 9. In the next phase, the offline calibration tool can be used to experiment with transport formula settings based on those results.

8 Verification run 2019-2022

8.1 Discharge hydrograph

For the 2019 – 2022 simulation, use is made of the discharge levels within the standardized yearly hydrograph as described in section 4.4 and 3.2. These discharge levels are used to schematize the actual time series of discharges that occurred in the period 2019 – 2022. This was done by rounding the daily averaged discharges at Lobith to the most representative discharge level in terms of sediment transport capacity, under the assumption that sediment transport scales with the discharge to the power 5/3 (which holds for the formulation of Engelund-Hansen). The result is shown in Figure 8.1. Note that due to the scaling based on sediment transport capacity, the schematized discharge levels may be lower than one would expect based on a non-weighted classification. The grey line in Figure 8.1 shows the subsequent translation to the Waal discharge levels, following Table 3.1.

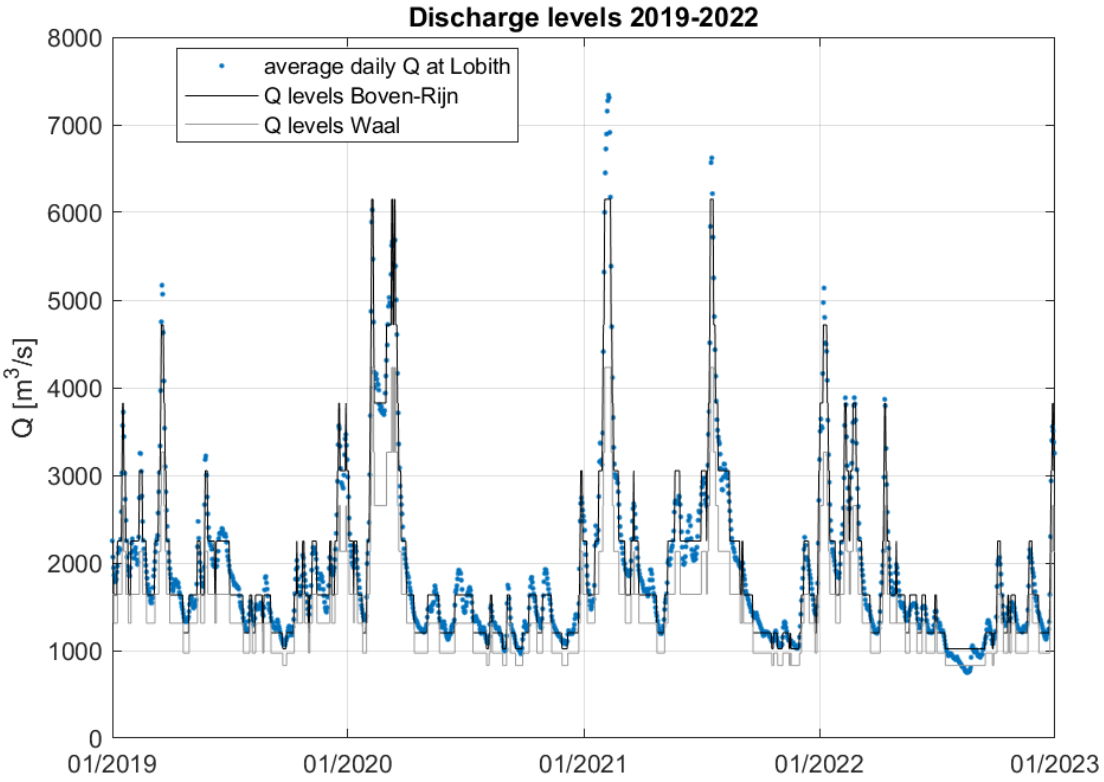

Figure 8.1 Discharge schematization for the 2019 – 2022 simulation, based on daily averaged discharges at Lobith. The grey line shows corresponding discharges for the Waal, based on Table 3.1.

8.2 Analysis of model results

8.2.1 Stability

Figure 8.2 shows the model time step during the simulation. The time step is usually 10 or 12 seconds, but can also reach much lower values (down to just 0.25 seconds) without leading to an error. At this stage it is not clear if the small timesteps are caused by large or even physically unrealistic morphological changes, or by a numerical artifact. There is no clear correlation with the discharge applied at the upstream boundary.

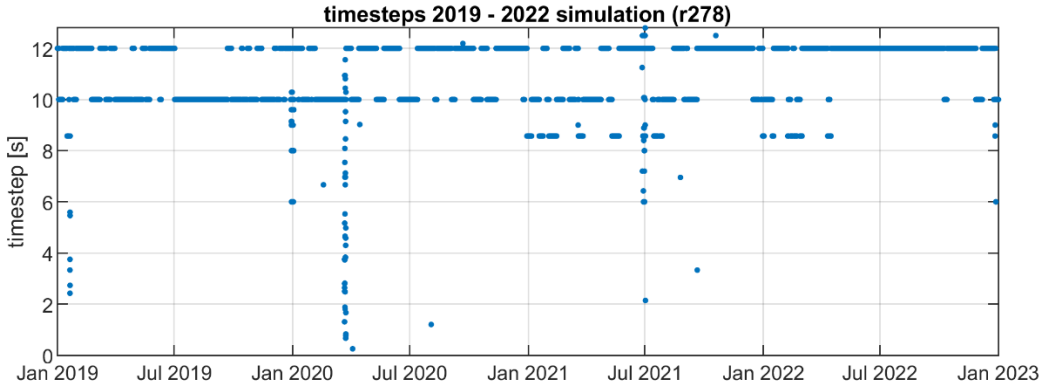

Figure 8.2 time step 2019 – 2022 simulation.

8.2.2 Plausibility

The order of magnitude of modelled bed level changes is according to expectation. We see up to 3 m sedimentation and erosion over the course of 4 years. In this section, a few locations that stand out in terms of morphological changes will be investigated in more detail. Figures for the entire branch are included in Appendix D.

The first location of interest is the upstream boundary, see Figure 8.3. Strong sedimentation is visible at the right side of the main channel. Section 6.6 explains that this is the result of applying a constant boundary condition (sediment influx per fraction) along the width of the boundary. A refinement of the boundary condition is needed to realistically simulate sediment influx at the upstream boundary.

A second unexpected pattern in bed level changes is observed in the transition zone between main channel and groyne fields, see Figure 8.4. Especially in the ~10 km reach close to the downstream boundary, sedimentation and erosion hotspots are visible at these locations. Figure 8.5 shows flow velocity vectors for three of the groyne fields depicted in Figure 8.4. It seems that due to the limited grid resolution parallel to the groynes, the expected 2D flow pattern within the groyne fields (with one or two eddies) is not captured correctly in the model. This may yield unrealistic velocity and sediment transport gradients.

In the remainder of this section, we focus on morphological development around the longitudinal training walls (LTWs), as depicted in Figure 8.6 and Figure 8.7. Large bed level changes are observed mainly downstream of the second LTW (near Dreumel, Figure 8.6). Near the left bank an eroding stretch develops, with lowering of bed levels up to 6 m locally (as an exception to the generally much smaller changes in the rest of the model domain). In the remainder of the main channel, an increase in bed level of up to 1.5 m occurs. The pattern is probably caused by the abrupt change in channel geometry, with the auxiliary channel alternating between the left and the right bank. At the outlets of Wamel and Ophemert sedimentation occurs locally as well, but the changes are much less pronounced.

In the auxiliary channel at Dreumel some sedimentation is observed, while the main channel alternatingly shows erosion and sedimentation at this location. The main channel sections at LTW Wamel and Ophemert mainly show erosion, while the morphological development in the auxiliary channels is relatively small at these locations.

In a later stage of this project, model results will be compared to observed bed level changes in these areas for calibration and validation purposes.

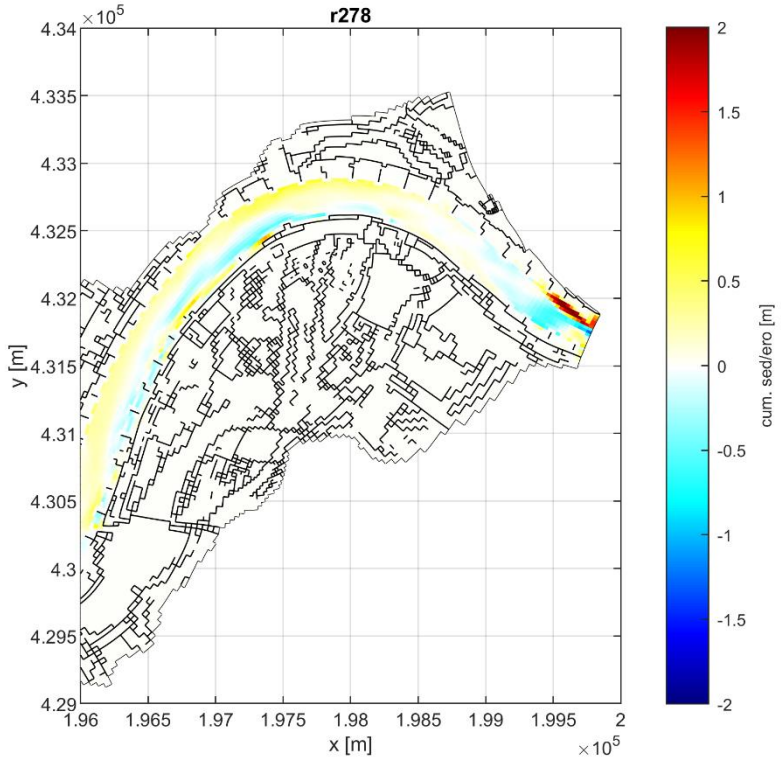

Figure 8.3 Bed level changes 2019 – 2022 near the upstream boundary.

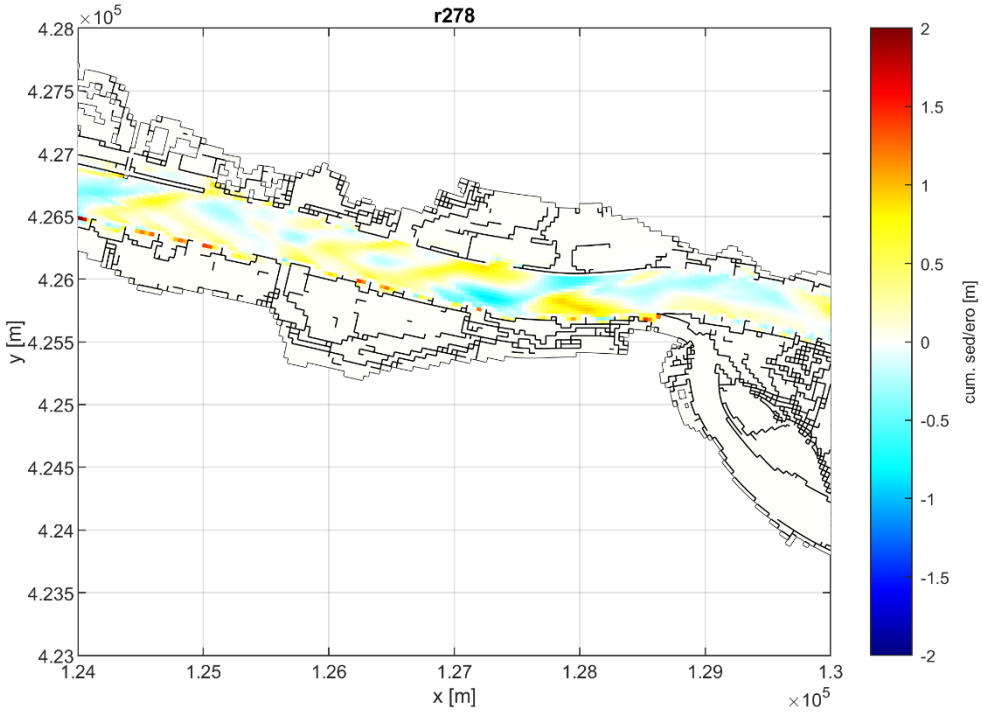

Figure 8.4 Bed level changes 2019 – 2022, sedimentation/erosion between main channel and groyne fields.

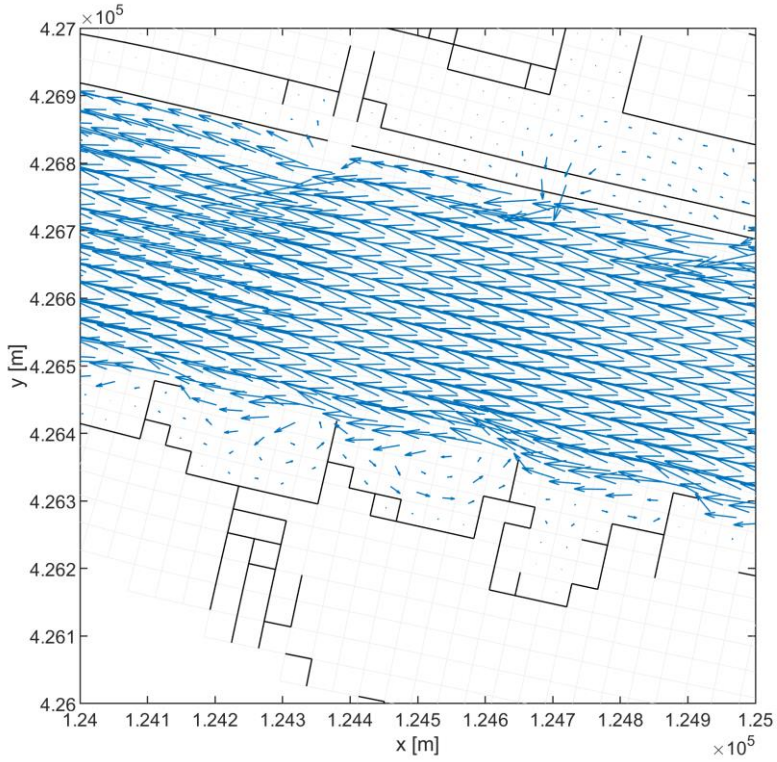

Figure 8.5 Velocity field for a small part of the domain shown in Figure 8.4, for Q_{Lobith} = 2250 m^3/s.

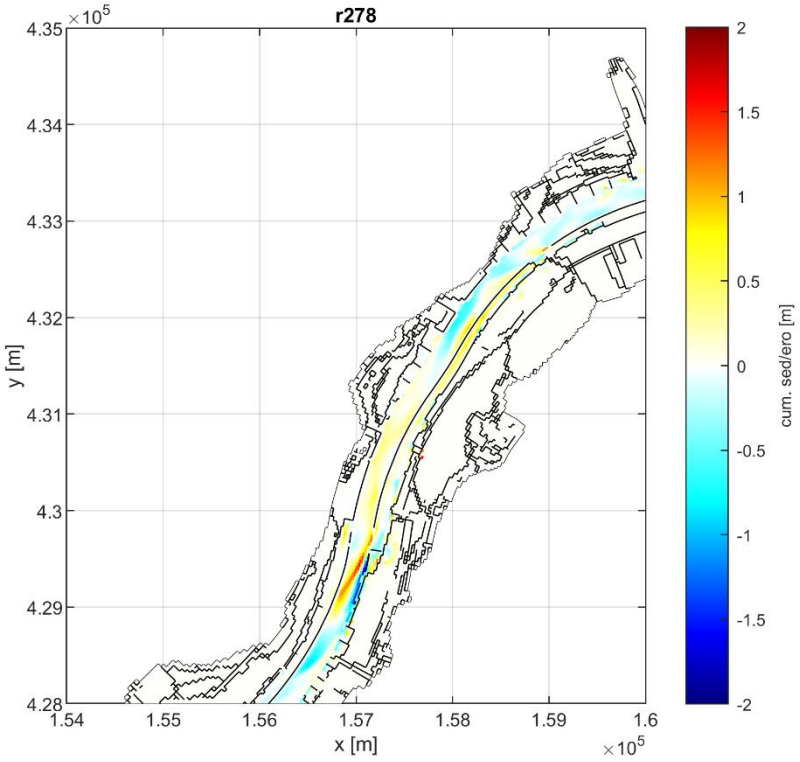

Figure 8.6 Bed level changes 2019 – 2022 around longitudinal training walls.

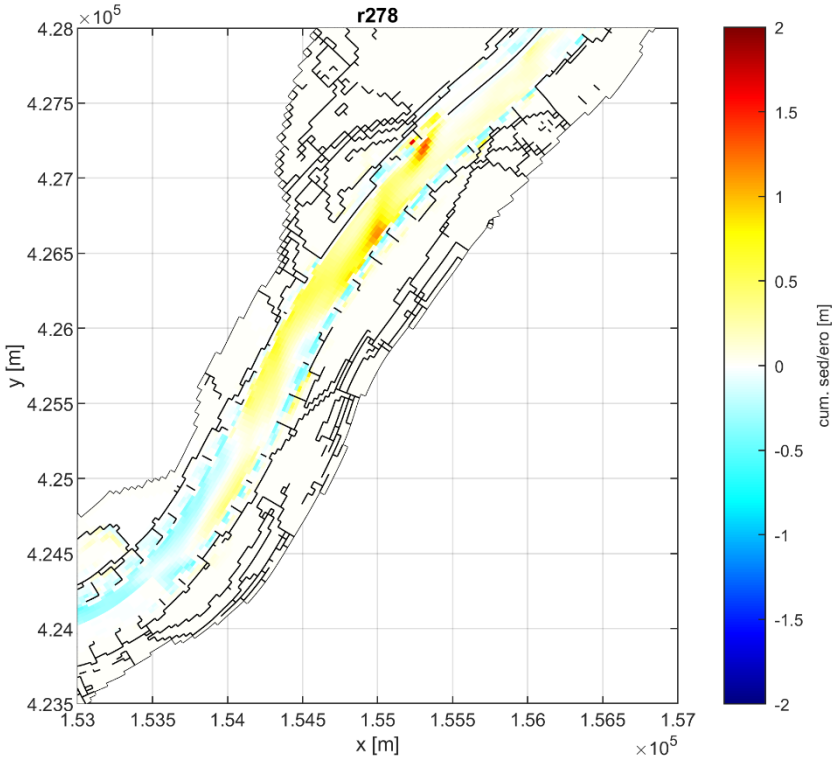

Figure 8.7 Bed level changes 2019 – 2022 around longitudinal training walls.

9 First steps in 1D calibration

9.1 Calibration procedure

Calibration will be carried out in 2 steps, a 1D and a 2D calibration, as described in the “plan van aanpak” (Spruyt, 2022). The 1D calibration focusses on the following parameters:

1. Yearly sediment transport rates and transport gradients (longitudinal profiles of sediment transport)
2. width averaged bed levels and bed level trends (longitudinal profiles L3R3 per km)
3. celerity of bed disturbances per river section

The 2D calibration is meant to adjust

4. 2D patterns, e.g. transverse slope in bends (longitudinal profiles along the river axis and lines to the left (L3) and right (R3) of the river axis)

For the 1D calibration, simulations without and with dredging and dumping will be run. We will not impose observed dredging volumes and locations onto the model, because they are uncertain. Instead, the simulations with dredging and dumping will use the general strategy that has been defined for the old DVR model already (and updated with more detailed polygons for the nourishment studies of 2021 and 2022). One step in the calibration is to check if the modelled dredging volumes are in the same order of magnitude (per river section) as the observed volumes. In that way, the model is made suitable to test different strategies for dredging and dumping as well.

If data about sand mining is provided by RWS, the mined volumes in the model can be checked against observed volumes as well. To this end, an extra simulation containing both dredging & dumping and sand mining will be run.

In the following sections, the first morphological simulations for the calibration period (see section 9.2) are analyzed. Since the simulations do not yet cover the full calibration period due to instabilities, a full 1D calibration is not yet possible. The simulations do, however, give an indication on how far the model results will still need to be tuned and what model input parameters could be used for that. Note that these results are coming from simulations that start from initial bed levels and composition without prior spin-up.

9.2 Calibration and validation periods

For the Waal branch, an analysis of bed developments and dredging activities by Sieben (2023) has shown that the following periods can be regarded as approximately homogeneous:

- 1999-2012
- 2016-2020

We suggest to use the first (and longer) period for calibration and the latter and shorter period for validation. The following paragraph presents first results for the period 1999-2003, the start of the first calibration period. So far, all simulations carried out became instable after a few years, so that it was not possible to run the full calibration period yet.

9.3 1D calibration – first results

9.3.1 Yearly sediment transport rates and transport gradients

Sediment transport of sand and gravel upstream of the Waal should be around 370.000 m³/y including pores and increase towards approximately 510.000 m³/y at km 925 (Sloff, 2019, and section 3.4.2). From there towards km 935, historic bed level measurements were translated into a drop in sediment transport of about 10.000 m³/y, and from km 935 yearly sediment transport is expected to stay approximately constant. Figure 9.1 shows the yearly sediment transport along the Waal for the first years of simulations using the two sediment transport formula proposed in section 6.2. Both show the gradient of increasing transport between the upstream end of the Waal towards km 910, but using the formulation from the DVR model that gradient is far too big. Both results also show that between km 935 and 960, sediment transport decreases significantly, while it should stay roughly constant. In the model, the decrease in grain size along that river section can obviously not compensate for the decrease in flow velocity (Figure 9.4). Both transport formulae result in a negative gradient in sediment transport between the upstream model boundary and km 877 which is unexpected. It needs to be investigated further how this is caused. The sediment inflow via the upstream boundary could be the reason. Figure 9.2 presents the yearly sediment transport for the sand and gravel fractions separately for the IRM settings, and Figure 9.3 shows the transport per discharge level in the third year of simulation. The biggest contribution to the yearly transport comes from the medium and higher discharge levels.

Figure 9.5 shows that there is still some room for a stronger decrease in grain sizes towards the downstream end of the model. However, it is expected that this will by far not be enough to eliminate the decrease in sediment transport. The hydrodynamic validation shows that in the reach between km 930 and 950, the gradient in flow velocities is overestimated in our model (compared to the original hydrodynamic model) due to applying a constant main channel roughness. This is mainly the case for the medium and high discharges (from 3.053 ³/s at Lobith upwards), which have the main contribution to the yearly sediment transport. Correcting that, e.g. by applying a smooth transition in roughness in longitudinal direction, is expected to have a clear influence on the transport gradient, because velocities influence the transport with a power of 5 in this sandy reach, for which mainly the formulation of Engelund-Hansen is applied (if the IRM formulations are used).

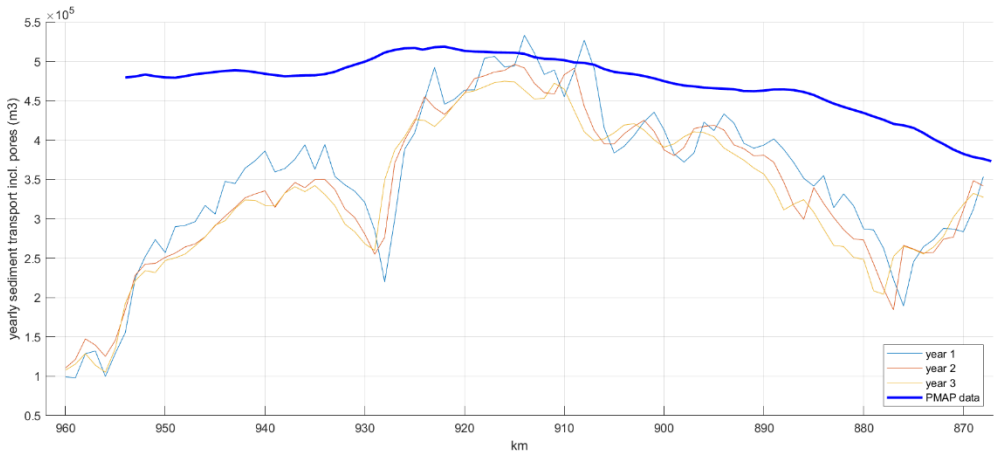

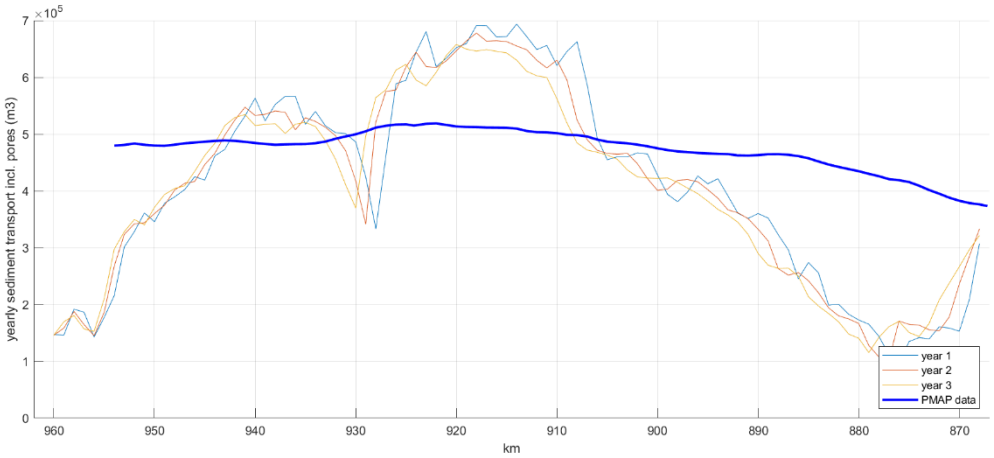

Figure 9.1 Yearly sediment transport rates (total for all fractions) using the IRM (top) and DVR (bottom) settings for the transport formula.

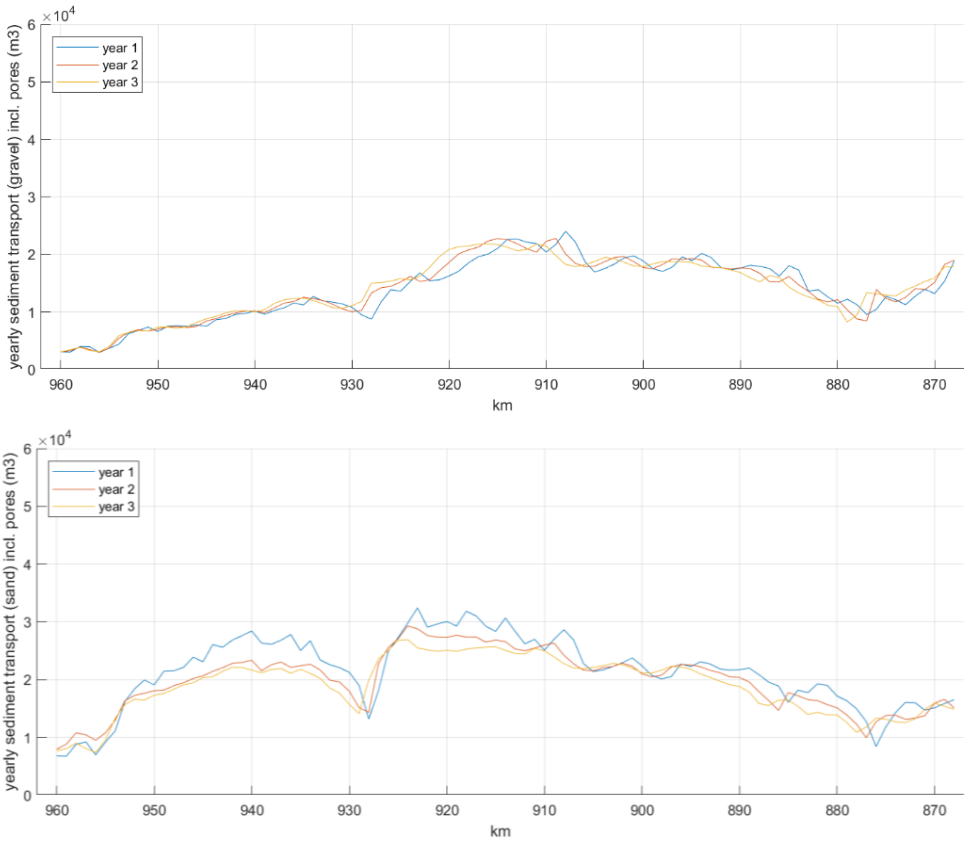

Figure 9.2 Yearly sediment transport rates for gravel (top) and sand (bottom) fractions using the IRM settings for the transport formula.

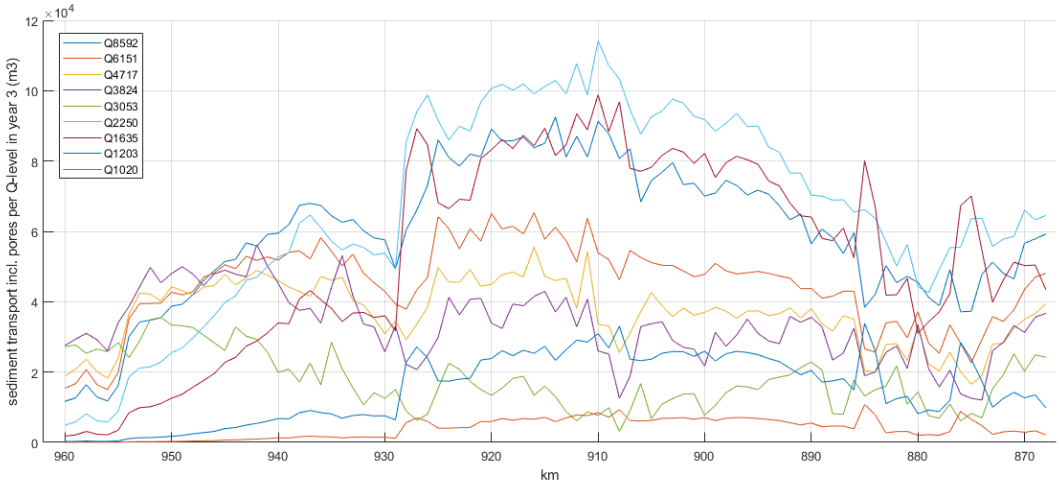

Figure 9.3 Yearly sediment transport rates per discharge level during the third year using the IRM settings for the transport formula.

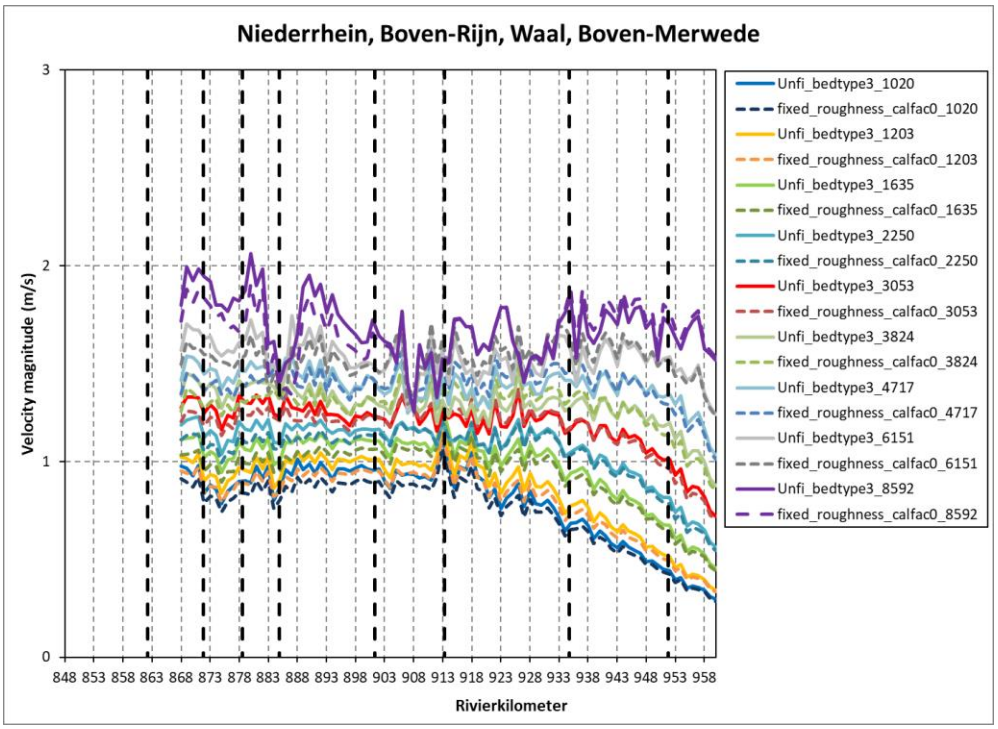

Figure 9.4 Flow velocities along the river axis for the 9 discharge levels used in the morphodynamic simulations. Original hydrodynamic model ("Unfi_bedtype3") vs. model with fixed roughness and without calibration factor ("fixed_roughness_calfac0_").

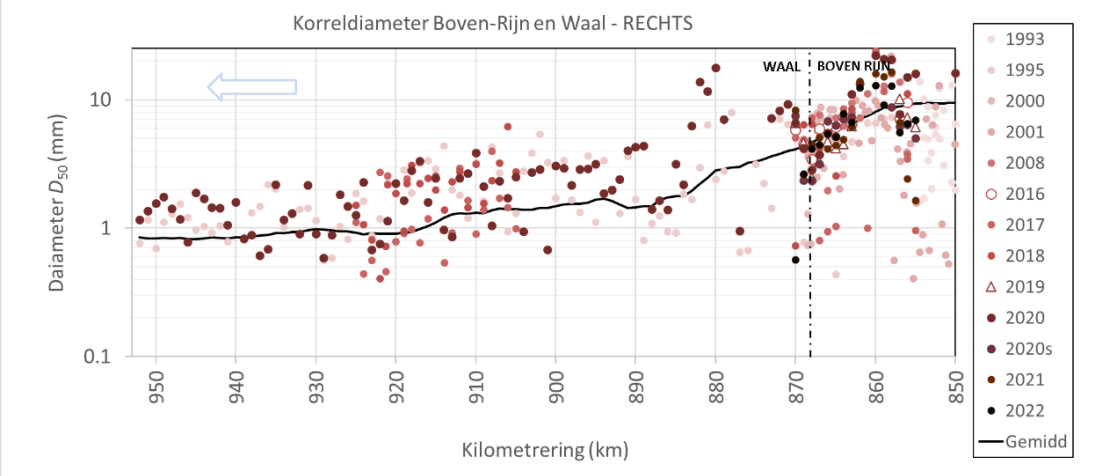

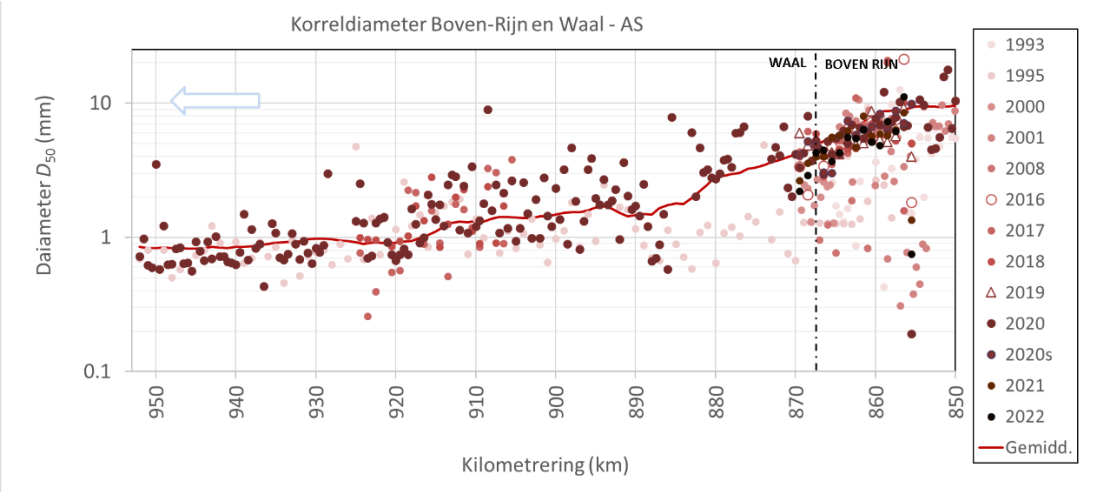

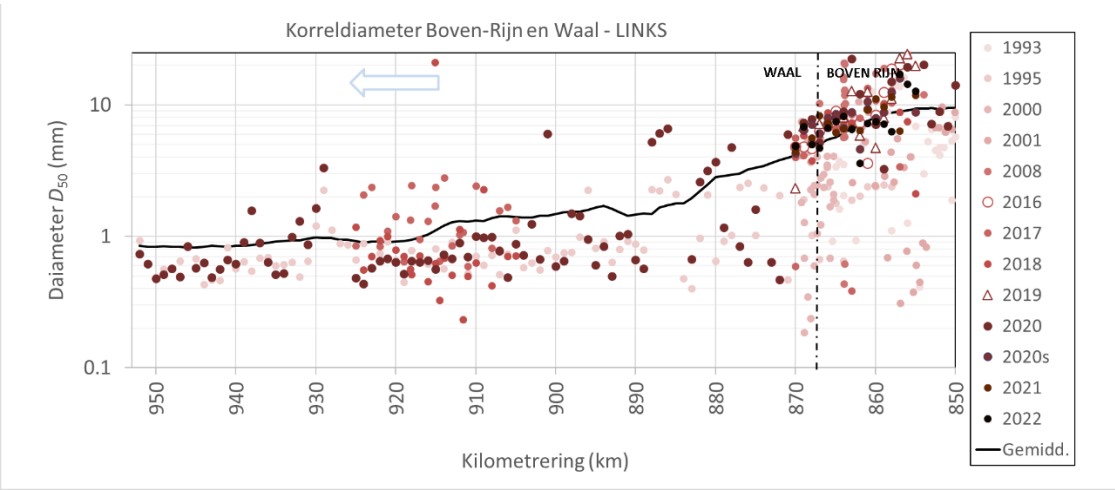

Figure 9.5 Median sediment diameter D_{50}. Dots: from measurements; black/red line: initial composition in the model.

9.3.2 Bed level development

Figure 9.6 compares the width- and km-averaged bed level development in the model to measurements. Figure 9.7 presents the modelled width-averaged (R3L3) and km-averaged bed level change. The large spike around km 928 is caused by initial adaptation (spin-up) of the fixed layer at Sint Andries, which ends at that location.

The somewhat smaller spikes at km 885 and km 876 are caused in the same way by the fixed layer at Nijmegen and the bottom vanes at Erlecom, respectively. It is expected that these trends vanish in a simulation that starts from a well spun-up bed level and bed composition.

Due to the increasing sediment transport, there is an eroding trend between Pannerdensche Kop and km 920. Around km 908, a ‘bump’ in the bed level develops and then propagates downstream. In the measurements, this is not clearly visible, because there is not enough data available to cover the entire width of R3-L3.

Downstream of km 928, the ‘dip’ in the bed levels is slowly eroding in the model. This ‘dip’ is present around the Martinus Nijhoff bridge (A2) at Zaltbommel, where the main channel is narrower than upstream and downstream. In the measurements from 1999-2020, it looks as if this ‘dip’ is filling up. However, if one extracts only the measurements of the first years, it becomes clear that it is first eroding and then filled up by a sedimentation front arriving from upstream, that might have been caused by the construction of the fixed layer at Sint Andries in that was finished in 1998. We need to see whether the model reproduces that sedimentation front as well, once it is able to run for longer periods.

Downstream of km 935, the modelled bed level stays relatively stable, despite the decreasing transport rates. Modeled and observed development are similar.

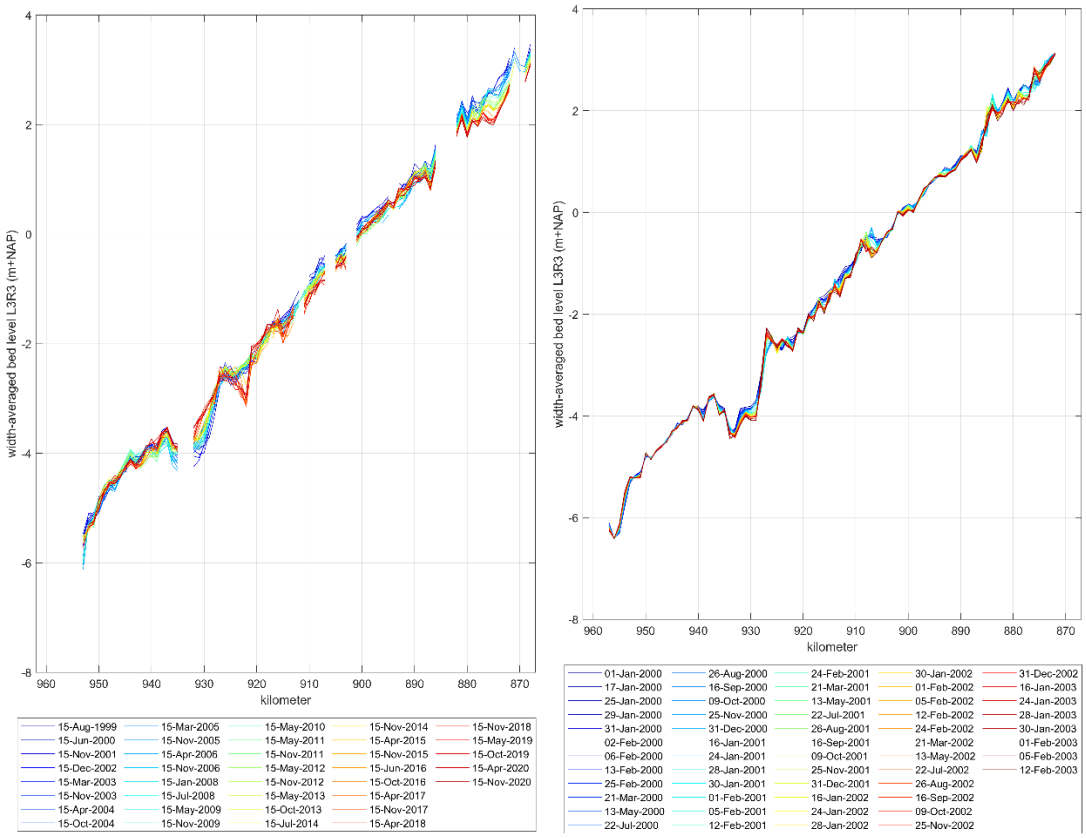

Figure 9.6 Trend in width-averaged (R3L3) and km-averaged bed levels along the Waal. Left: observed (1999-2020); right: modelled using the IRM transport formula and settings (2000-2003). Note that the simulation covers a much shorter period than the observations. That’s because the simulation crashes after about 3 years at the moment. We are working on a solution.

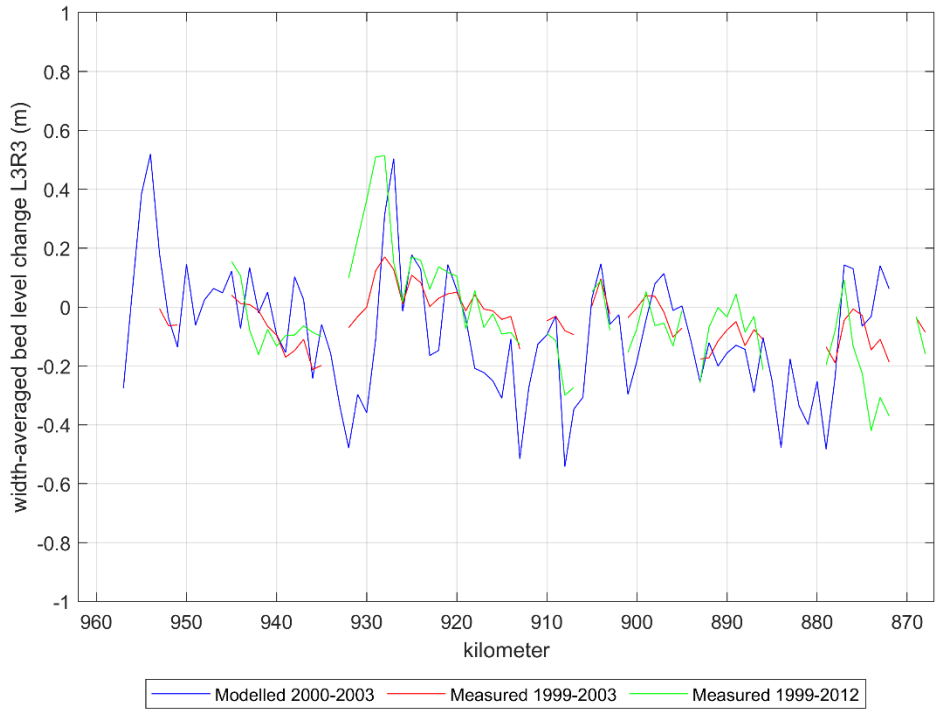

Figure 9.7 Total width-averaged (R3L3) and km-averaged bed level change between January 2000 and February 2003 compared to measurements.

9.3.3 Celerity of bed disturbances

Figure 9.8 presents the evolution of bed elevation along the Waal in time. Some migrating bed disturbances can be identified in the figure, especially in the Boven-Waal (km 868-886) and Midden-Waal (km 887-915). As far as can be judged from the rather short simulation, these migrate with a speed of approximately 1 km/y as expected. Longer simulations, by preference with a trench, need to confirm this conclusion. First simulations with trenches are running at the moment.

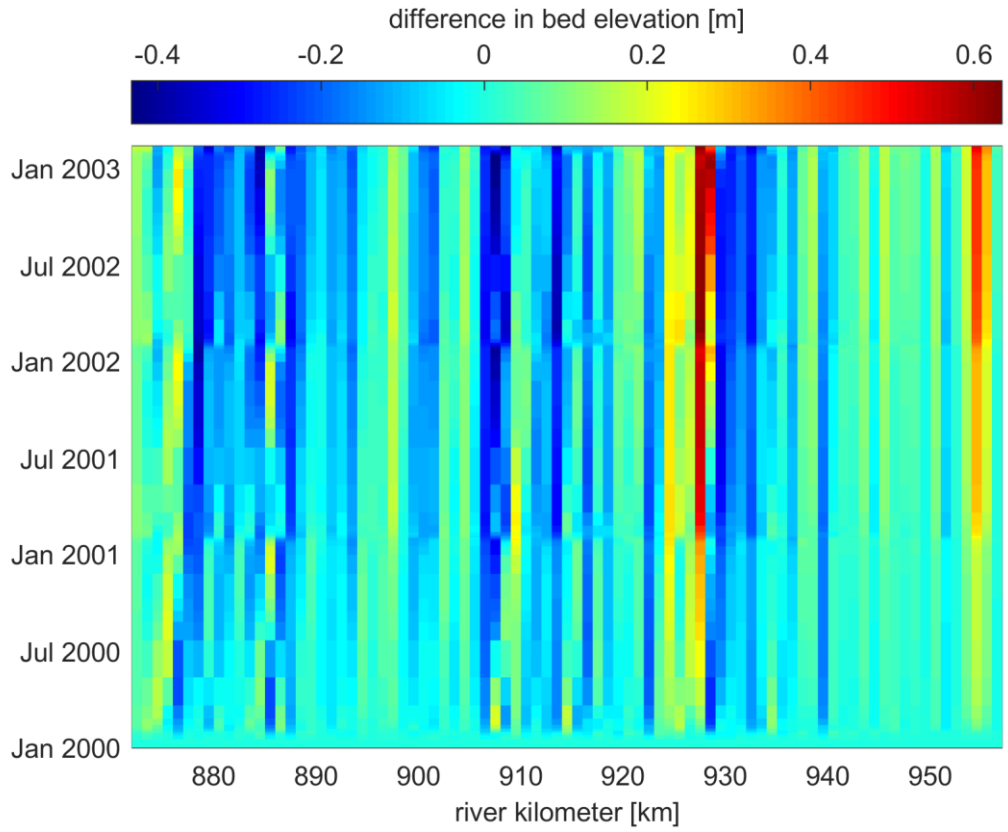

Figure 9.8 Evolution in time of the difference in bed elevation with respect to the start of the simulation.

9.3.4 Grain size distribution changes

Figure 9.9 shows the development of grain sizes after 3 years of simulation. The D_{50} is varying around the initially imposed rolling mean values, approximately keeping the initially imposed gradient. This gives trust in the performance of the model. However, the variations around the initial values seem rather high and fall outside the range of observed values shown in Figure 9.5 at several locations. The main observations on local behavior are:

- Downstream of the fixed layers at Nijmegen (km 883.1-885.0) and Sint Andries (km 925.0-928.2) and the bottom vanes at Erlecom (km 873.2-876.0) significant coarsening takes place due to strong erosion. This is visible on the left side and the river axis. During fine-tuning of the model it needs to be investigated how this behavior can be improved.
- The fining upstream of the fixed layer of Nijmegen and the bottom vanes at Erlecom (left side, km 879-883 and km 870-873) is also visible in the measurements.
- The outer bend at Tiel (km 912-km 918, right side) becomes rather coarse compared to the measurements. The modelled D50 in the sharp outer bends at Bemmel and Doornenburg (right side around km 873 and km 880) still falls within the range of the measurements. The coarsening in the less sharp bends at km 889 and km 898 is clearly too strong.

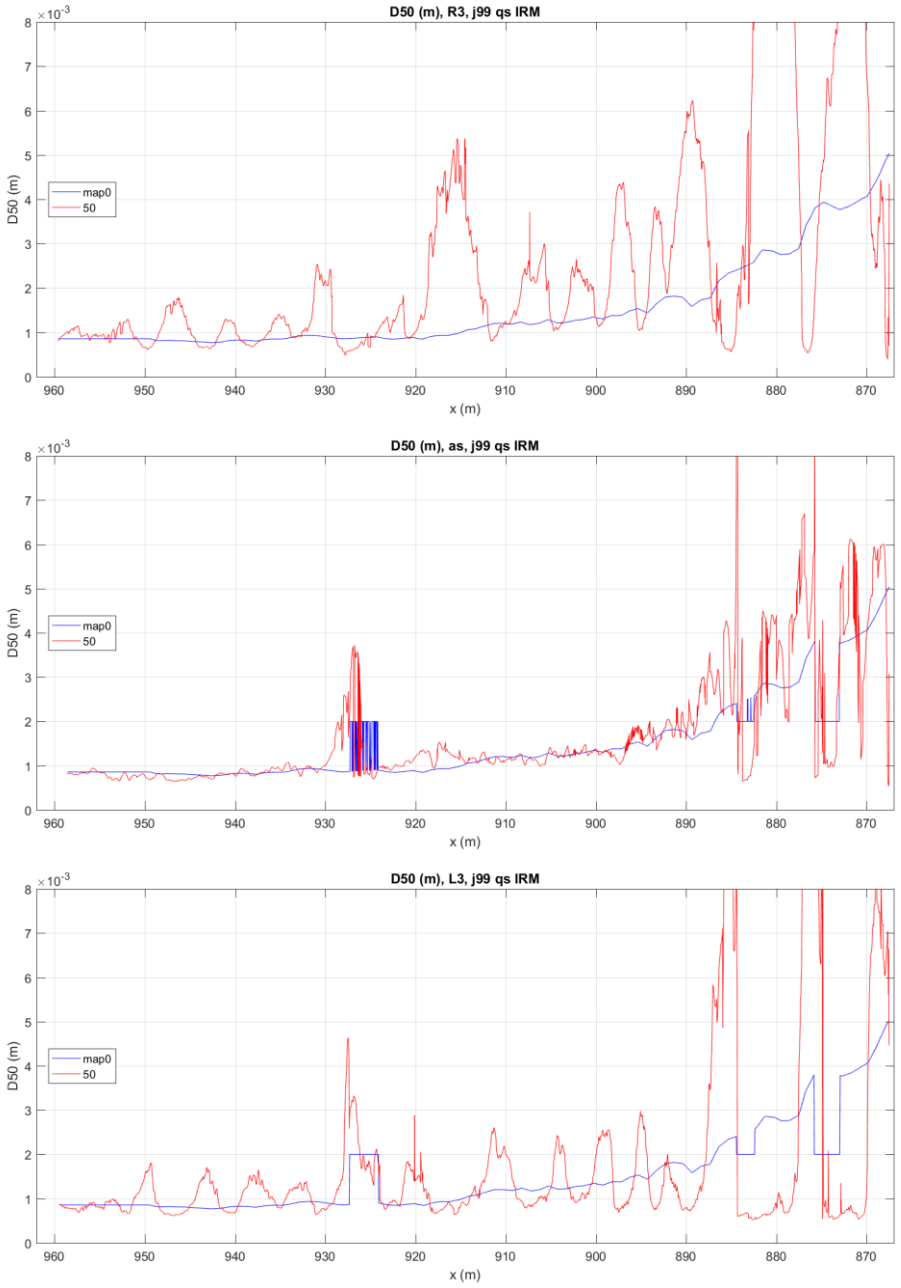

Figure 9.9 Mean sediment diameter D_{50} after a bit more than 3 years of simulation (red line, after 50 discharge steps) compared to the initial value (blue line).

9.4 Recommendations for following calibrations steps

Based on these first calibration results, the following steps are recommended for the next phase of this project:

- Repeat the simulations after proper spin-up of the model to see which part of the bed level and composition development is due to spin-up.

- Briefly analyze the sensitivity of sediment transport to the parameters of the transport formula, looking separately at the sand and gravel fractions since these use different transport relations at the moment. This can be done with the tool developed for offline calibration. In the IRM project, a similar analysis is currently carried out for the old DVR model (not yet reported). Insights from that study can be taken account, so that the analysis for the new model can be kept brief.
- Based on the findings of the offline analysis, more appropriate settings of the transport formulation can be tested with morphological model runs.
- If needed, the initial bed composition needs to be changed.
- Introduce a smooth gradient in main channel roughness to stay closer to the hydrodynamic results of the calibrated original model.
- Add dredging and dumping to the model and compare volumes to available data.
- Once the model is sufficiently calibrated for the long-term and on the larger scale, proceed to a detailed 2D calibration.

10 Developments for the application of the model

10.1 Simulation management tool (SMT)

At the current state of model construction, we use the so-called “Simulation Management Tool” (SMT) to start and manage a simulation. This tool was originally developed for the previous model (named the DVR model) and has been adapted for working with D-HYDRO during set-up of the Maas model (Ottevanger & Chavarrías, 2022). It starts a series of simulations with each a constant discharge at the upstream boundary and constant water level downstream. In each discharge step, a different appropriate morphological factor can be used to speed-up simulations (section 10.2). Furthermore, the SMT contains functionality to start each discharge step with initial conditions that are already well spun-up. The calculation of morphological changes starts from this steady state.

The combination of steps with constant boundary conditions, largest possible morphological factors and best possible restart of each simulation resulted in an optimal reduction of simulation times for the DVR model (Yossef et al., 2008).

The SMT environment has been set-up for both the Waal and the IJssel model and was used to run the simulations presented in this report. The discharge hydrograph that was used is presented in Figure 4.11.

At a later stage, we intend to check if different levels are needed or even if a different procedure (e.g. a “real” hydrograph instead of a schematized hydrograph) can be used as model forcing. The following section 10.2 shows which morphological factors can be used for the steady state discharges in the SMT setup.

The SMT was furthermore adapted to prevent problems with simulation periods that need to be a multiple of the ‘User timestep (DtUser)’ in D-HYDRO. For the discharge hydrograph that we use at the moment, a User Timestep of 12 s works best, because even for high morphological factors (e.g. 100) the resulting simulation periods in seconds are multiples of 12. Furthermore, D-HYDRO was modified to allow for simulation periods specified in seconds that use restart files[4].

10.2 Optimizing simulation times

10.2.1 Using a morphological scale factor

A morphological scale factor is used to scale up morphological activity. A morphological factor of 100 means that the effect of 1 minute of flow upon morphology (both bed level and sediment composition) is multiplied by 100 before morphological updates are performed. In this way simulation time can be reduced significantly. Effectively, the use of a morphological factor means that a much shorter flow time can be used to simulate a certain morphological time. For long-term river-morphological simulations with varying discharges it is important that in the reduced flow time still all the regular variations in discharge (in the correct sequence) are introduced: this means that the time-scale of the flow hydrograph as shown in Figure 4.11 is ‘squeezed’ to the short flow time.

[4] This turned out to be a problem due to the date mentioned in the restart file, which needs to be exactly the same as the start time of the simulation it is used in.

Looking at the flow time scale, it is clear that this squeezing causes the flood waves to become much steeper (shorter duration), which leads to a different propagation of these waves (more attenuation, different celerity) than without squeezing. For instance, for morphological factors higher than 10, and model lengths over 100 km, this effect can noticeably affect the morphological results.

To prevent this, we apply the more or less quasi-steady approach that was used in the DVR model as well (section 10.1). With this approach, morphological factors can be chosen much higher without losing accuracy.

Apart from this flow-unsteadiness problem, the morphological factor is also constrained for assuring numerical stability.

10.2.2 Test simulations

To evaluate the stability and accuracy of bed level development, simulations were run with increasing morphological factor and the j19_6 schematization. Sloff et al. (2009) tested morphological factors for the graded sediment domains (Boven-Rijn, Waal, Pannerdensch Kanaal) of the DVR model in Delft3D4. They used values between 1.440 (for discharges of up to approximately 1.400 m^3/s at Lobith) and 120 (for discharges of 3.800 m^3/s at Lobith and higher). Up to this speed-up, bed level development in the model remained approximately the same as in simulations without a morphological factor. For D-HYDRO, new tests need to be made, since it uses a different numerical approach. Van Dongeren et al. (2018) found that simulations for a test case in the Western Scheldt could get instable already for morphological factors of 25. These simulations used fixed time steps, though, that did not fulfill the stability criterion of a Courant number below 0.7 that is applied in our simulations. Furthermore, this was a tidal test case that is expected to behave differently than the Rhine branches. Therefore, tests for the Waal are now being made using morphological factors of 1, 2, 10, 50 and 100.

To assess the influence of the morphological factor on bed level development, three trenches were added to the initial bed level. Simulations were then run with and without trenches in order to compare the movement of the trenches for different morphological factors. The trenches are approximately 1 m deep and are introduced across the entire width of the morphologically active part of the main channel. They are located in the Boven-Waal (km 879.5), the Midden-Waal (km 900), and the Beneden-Waal (km 942), see Figure 10.1. Results for these are shown in the following paragraph.

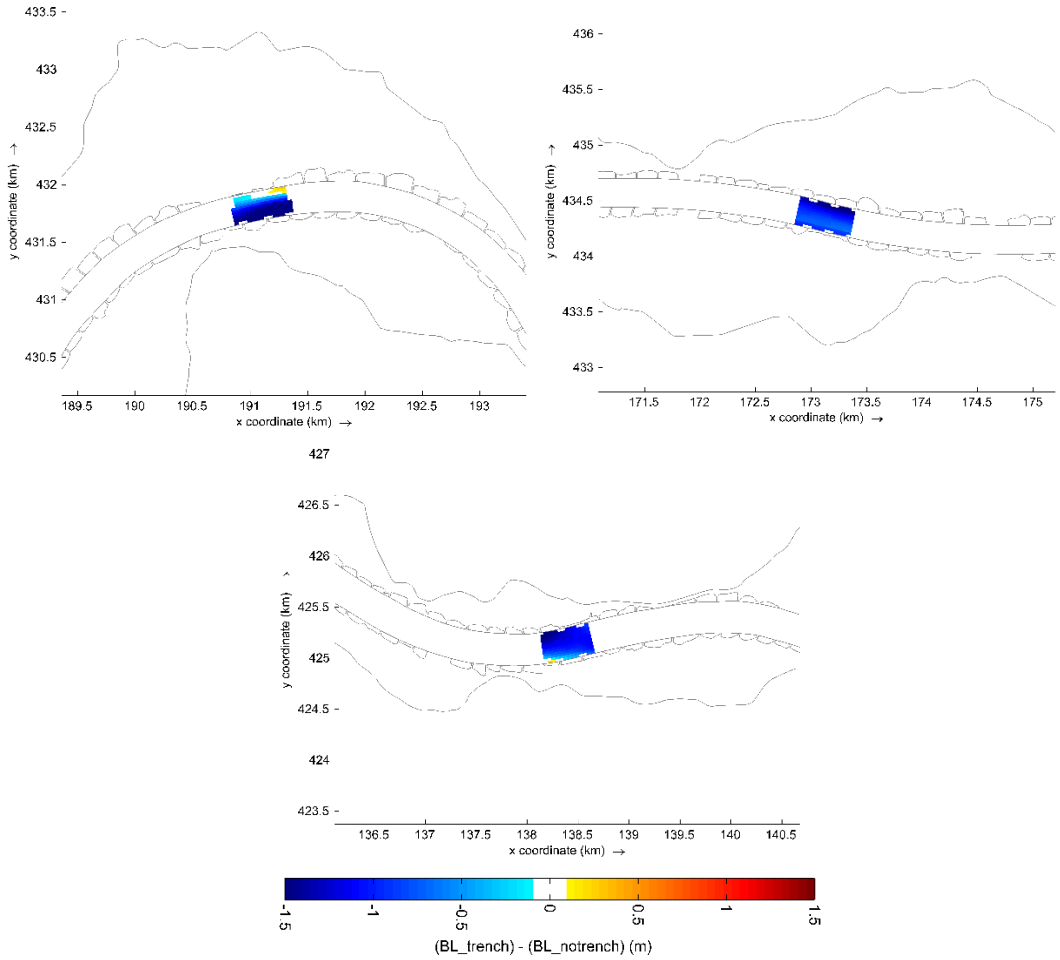

Figure 10.1 Initial location and depth of the trenches. Top left: Boven-Waal around km 880, top right: Midden-Waal around km 902, bottom: Beneden-Waal around km 942.

Since morphological changes are larger at higher discharges, the maximum value for the morphological factor is expected to be discharge dependent. Therefore, simulations with constant discharges in combination with the different morphological factors were run. Trench movement was assessed separately for each discharge. The next step in this analysis would be to compare trench movement for simulations using the average yearly discharge hydrograph presented in Figure 4.11. These were not carried out yet, since it is not yet clear if the instabilities observed in the simulations with constant discharge were caused by a too high morphological factor or software issues.

10.2.3 Influence of the morphological factor on bed level development

The development of the trench is very similar for all morphological factors applied, and this holds for all discharges. Figure 10.2 and Figure 10.3 show this exemplarily for the discharges of 3.824 m³/s and 8.592 m³/s at Lobith. In these plots, the runs with a morphological factor of 2 are considered as a reference, because the ones with a factor of 1 take too long to run. The dashed and dotted lines for the higher morphological factors are hardly visible behind the solid lines for morfac = 2, because the differences are minor.

However, it is not possible yet to draw conclusions about stability. All simulations stop due to too small time steps at some stage, but there is no clear trend in stability.

For several discharges, the simulations with low morphological factors (morfac = 1 or 2) stop earlier than the ones with high morfacs. For the highest discharge, all simulations stop shortly after 1 month of simulation, independent of the morfac. It is suspected that there is still another issue regarding stability of the simulations. It might be related to non-natural bed level development at some locations in simulations with constant discharge, or to the fact that with the current default settings, after limiting the time step, sometimes D-HYDRO does not manage to let the time step grow again as soon as that would be possible according to the Courant criterion. We are currently analyzing these issues and have started a simulation with the standard yearly hydrograph that uses a discharge-dependent morphological factor.

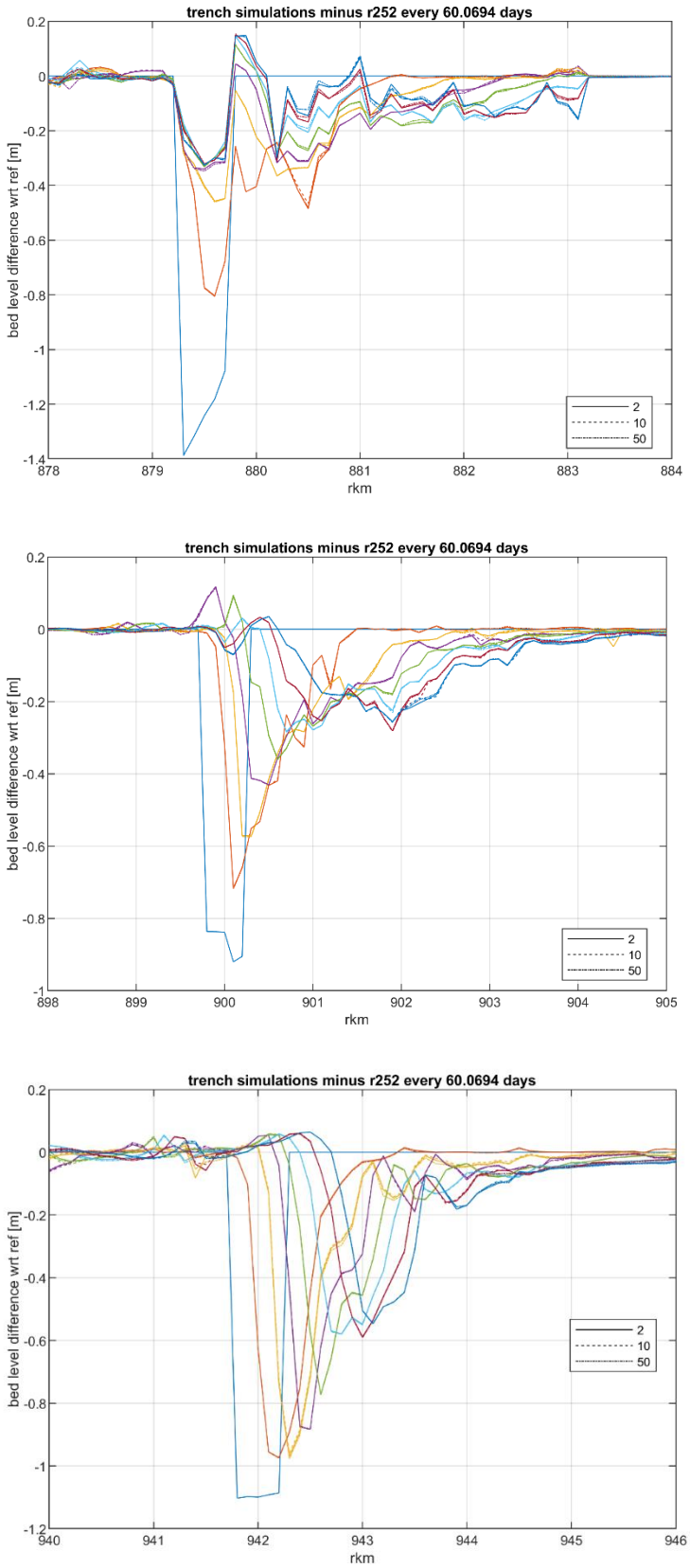

Figure 10.2 Development of the three trenches for simulations with Q_{Lobith} = 3.824 m³/s and a morphological factor of 2, 10 and 50. Results are plotted for every 60 days (different colours), the line style indicates the morphological factor used.

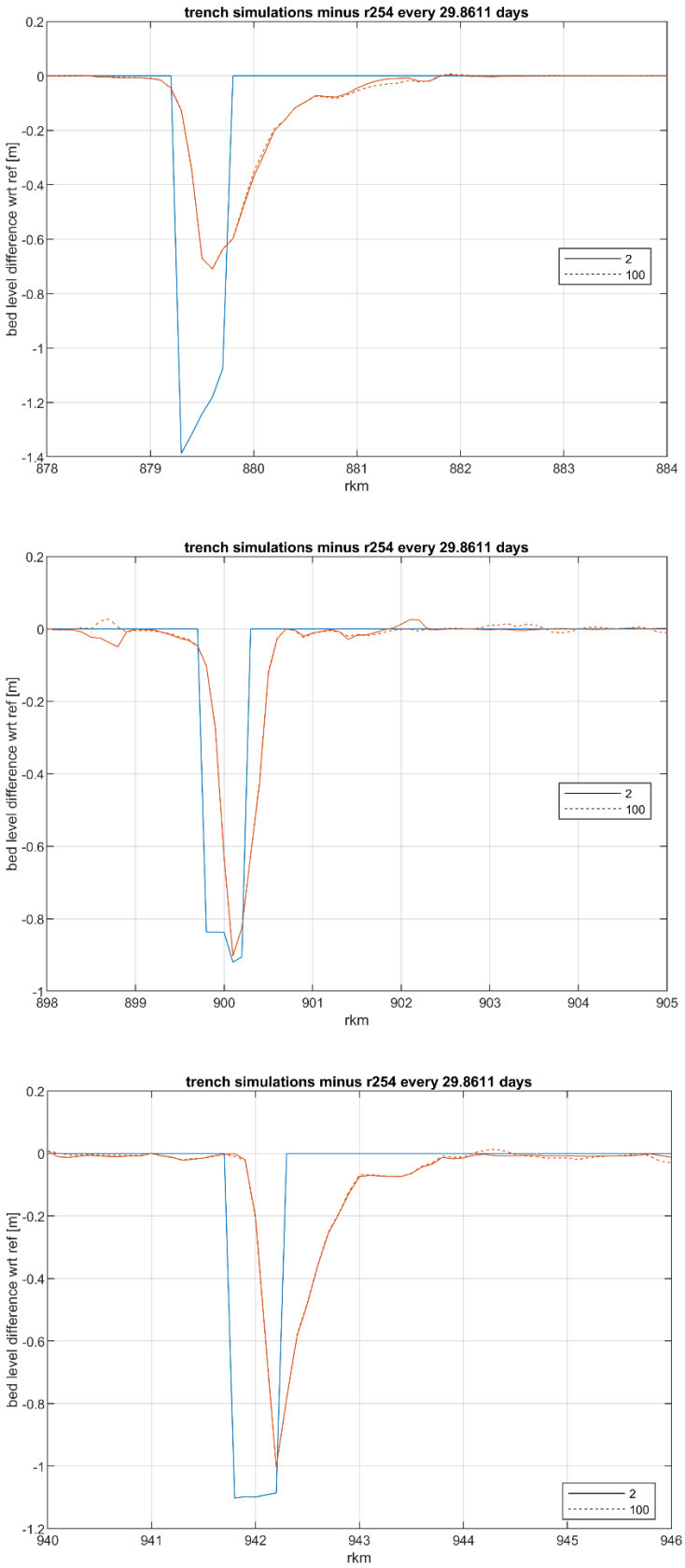

Figure 10.3 Development of the three trenches for simulations with Q_{Lobith} = 8.592 m³/s and a morphological factor of 2 and 100. Blue = initial trench; red = after 1 month. The line style indicates the morphological factor used.

10.3 Spin-up of grain sizes and bathymetry

10.3.1 Methodology for morphological spin-up

Modelled bed levels and composition will never exactly match the measured values. Deviations occur because of imperfections in model geometry and because not all physical processes are fully reproduced by the model. For example, an empirical formula is used for bed load transport, and the concept of vertical mixing is implemented in a simple way. At the beginning of a morphological simulation starting from initial (observed) bed levels and composition, bed composition and bed levels need time to adapt to these “model circumstances”. Changes will occur rather rapidly during that period and should not be taken into account in the analysis of morphological changes. Therefore, morphological spin-up is done as a separate step before the actual morphological simulations are carried out. The resulting bed level and composition are then used as initial values for the actual morphological simulations.

However, it is not possible to fully separate the spin-up, i.e. adaptation to model imperfections, from the “normal” morphological changes. During spin-up, also downstream propagation of sediment (waves) takes place. The latter is part of the changes that one wants to analyze, so the spin-up period should be chosen as short as possible.

There are several options how to spin-up the bed level and composition:

1) both together in one simulation
2) first the bed level in one simulation, then bed composition in another simulation, using the spun-up bed level as initial input
3) first the composition in one simulation, then bed level in another simulation, using the spun-up composition as initial input

In the DVR model, option 2) was chosen, using two simulations of 5 years each. The reason for this 2-step approach is that the development of bed level and bed composition strongly influence each other. It was believed that a correct bed composition could better be reached if the bed level was fixed to the initial, i.e. measured, bed level. Option 2) was preferred above option 3), because the bed composition is the more uncertain of the two parameters that need spin-up.

However, closer analysis of the result of the composition spin-up show that the resulting bed composition is not smooth, but contains unnatural stripes in maps of the resulting sediment composition that points to instable behavior. This does not happen if bed level update is also switched on. Therefore, for the new model it was decided to spin-up according to option 1), both bed level and composition together in the same simulation. Just as in the old approach, this is done in two steps, though, as explained by the flowchart in Figure 10.4. The first spin-up step produces adapted bed composition and bed level. Since it is possible that the change in bed composition during the first steps pushes the bed level too far off the observed level, a second spin-up simulation is run that uses the bed composition of the first spin-up step together with the observed (filtered) bed level as initial composition. The actual morphodynamic simulations then use both the bed levels and the composition resulting from the second step as initial values.

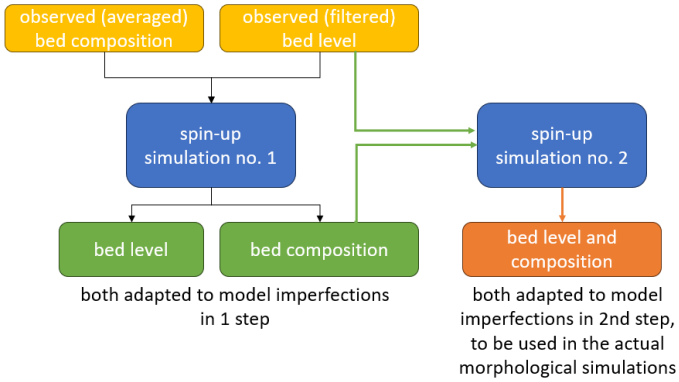

Figure 10.4 Flowchart of the process chosen to spin-up initial bed level and bed composition for the morphological simulations.

This approach was tested using the j19_6 morphodynamic schematization. A first spin-up run was carried out starting from the filtered bed level and the “rolling mean” sediment composition. Both sediment composition and bed level changed significantly during the first 1-2 years, depending on the location (Figure 10.5 and Figure 10.6). After that, the same discharge dependent pattern is seen every year, superposed by an approximately constant trend. The quick and irregular development during the first 1-2 years can be considered as the adaptation to model circumstances, i.e. the spin-up, while the yearly repeating pattern and constant trend are the actual morphological development. The resulting bed composition after two years was therefore imposed as initial composition in the second spin-up run.

Figure 10.7 shows a longitudinal profile of initial bed composition and composition after two years of the first spin-up step. It can be seen how e.g. the river bends have influenced the composition. Figure 10.8 compares the composition at the beginning and end of the second spin-up step. The changes during the second step are small, which proves that the spin-up during the first step was successful. Figure 10.9 presents the bed level changes during the second spin-up step. It shows that adaptations take place mainly on the smaller scale, while the medium-scale effects such as the transverse slope in bends stay similar as in the initial bed level. This means that imposing a reasonably spun-up bed composition in the simulation to spin-up the bed level indeed works well.

These figures demonstrate that the proposed two-step approach works well. Note that this is valid for the chosen concept for active layer thickness (constant thickness of 1 m, see section 6.1.1). If this concept is changed in future model versions, the approach for spin-up needs to be validated again. The expectation is that the 2-step approach in general will still work, but the simulation period might need to be changed.

The proposed approach for morphological spin-up results in two extra simulations of 2 year periods before the simulation of actual morphological developments can start. This is relatively short compared to the approach in the DVR-model, in which 2 simulations of 5 year periods were made.

The longitudinal plots also illustrate that both sediment composition and bed level are influenced by the upstream model boundary. This is analyzed in more detail in the following paragraph.

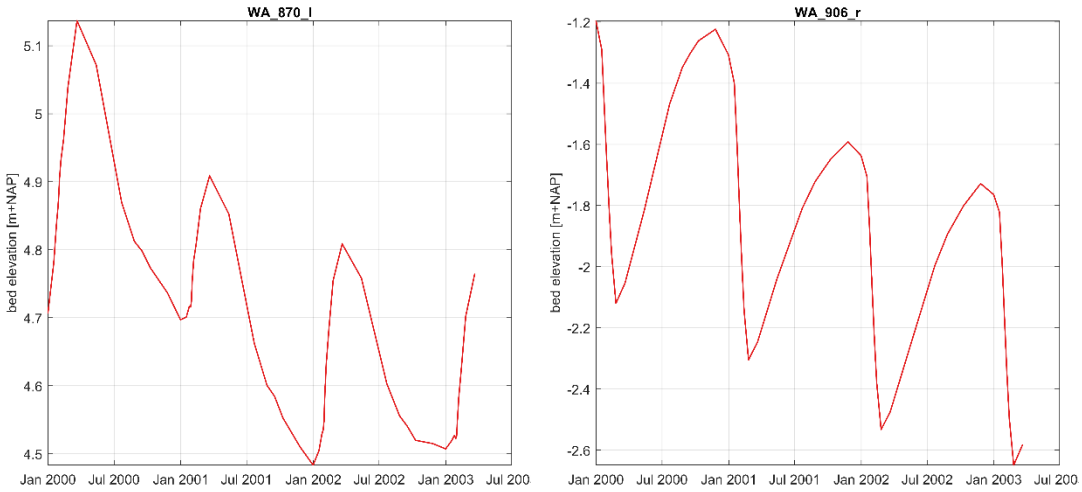

Figure 10.5 Bed level development at km 870, left side, and at km 906, right side, during first spin-up run.

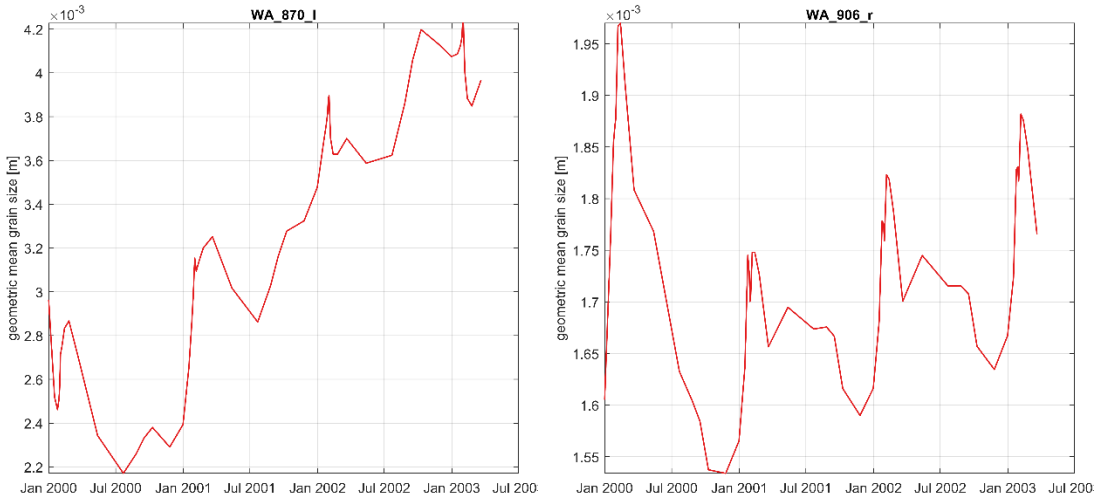

Figure 10.6 Grain size development at km 870, left side, and at km 906, right side, during first spin-up run.

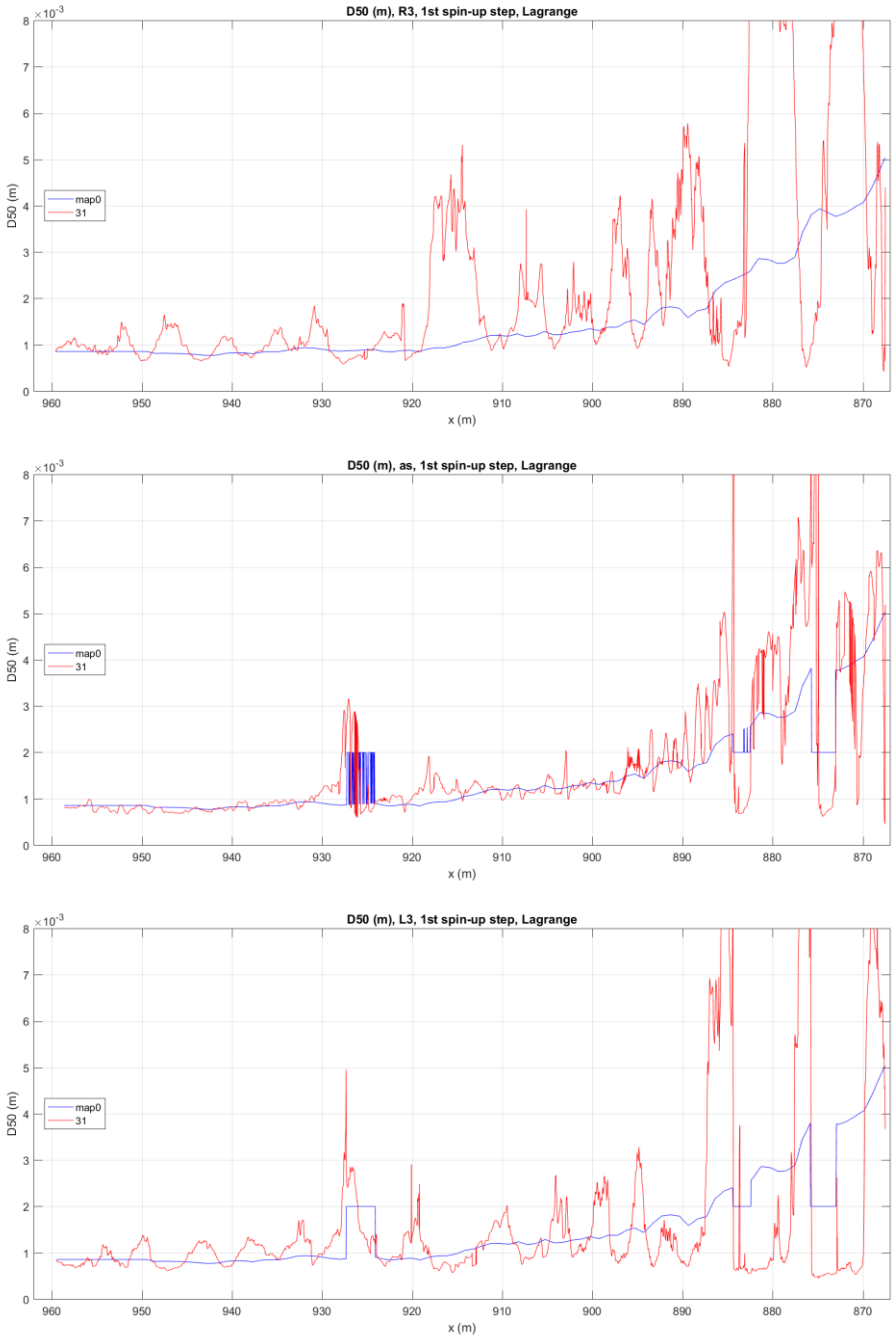

Figure 10.7 Red lines: Mean sediment diameter D_{50} after 2 years of spin-up (first spin-up step) with both bed level and composition update; blue lines: initial mean sediment diameter. Top: right side of the main channel (R3), middle: on the river axis, bottom: left side of the main channel (L3).

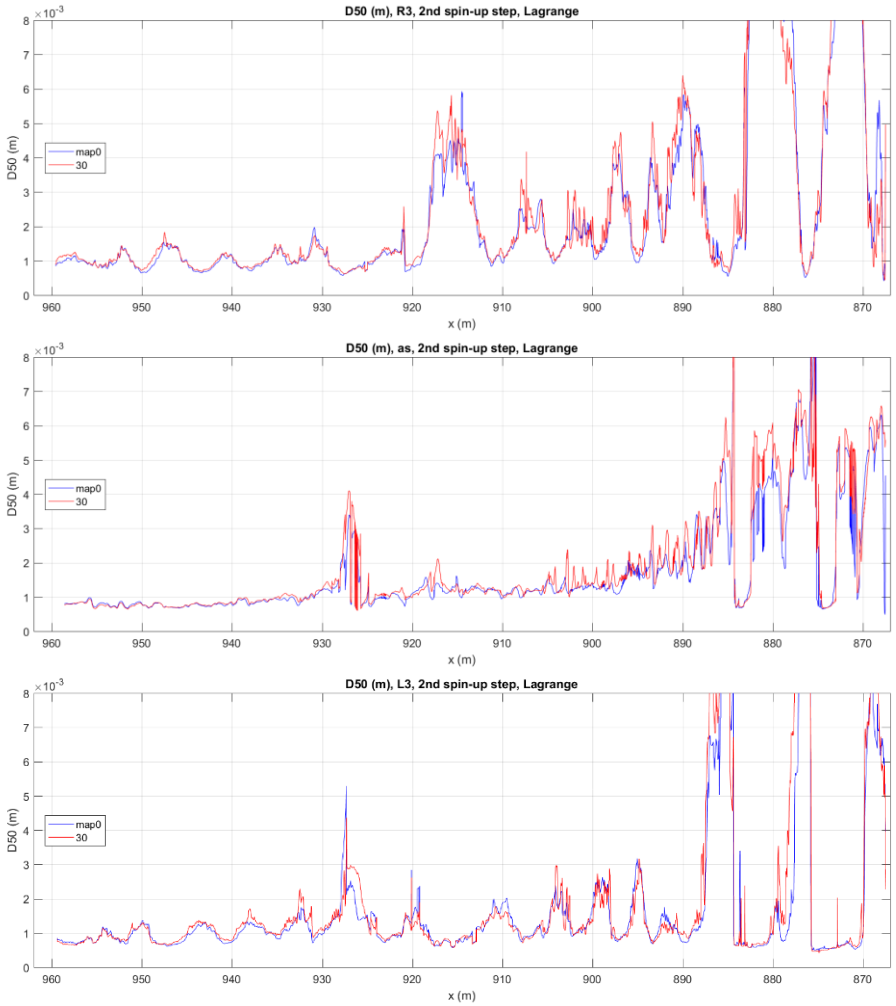

Figure 10.8 Red lines: Mean sediment diameter D_{50} after 2 years of spin-up (second spin-up step) with both bed level and composition update; blue lines: initial mean sediment diameter of the second spin-up step. Top: right side of the main channel (R3), middle: on the river axis, bottom: left side of the main channel (L3).

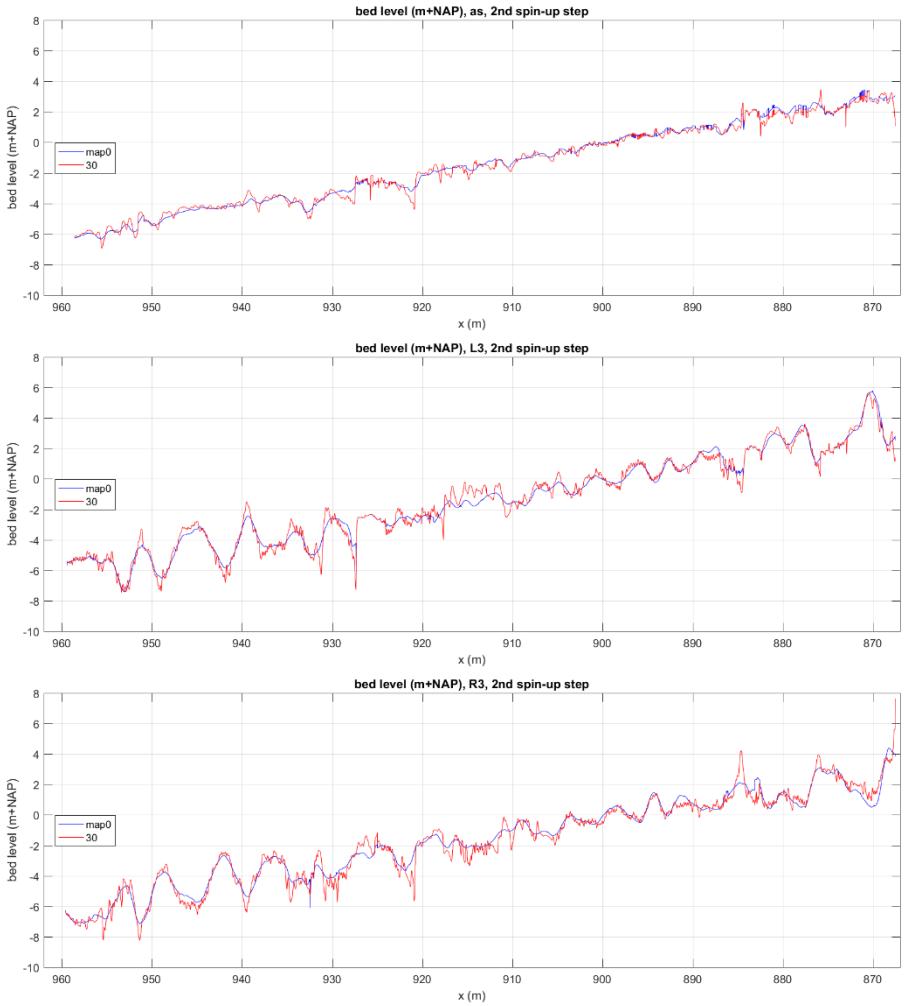

Figure 10.9 Red lines: Bed level after 2 years of spin-up (second spin-up step) with both bed level and composition update; blue lines: initial (filtered) bed level. Top: right side of the main channel (R3), middle: on the river axis, bottom: left side of the main channel (L3).

10.3.2 Bed level filtering and bed level after spin-up

To check the necessity of filtering the bed level (see section 4.3.2), the bed level that developed after morphological spin-up was compared to the initial filtered bed level and the bed level before filtering. Along the river axis (Figure 10.10), the unfiltered bathymetry contains the bed forms (river dunes) that are removed by the filtering, as intended. The morphological model cannot reproduce the process of forming bed forms explicitly, and the dunes do not reappear during the simulation. About 80 m to the left and right of the river axis, bathymetry is influenced by both dunes and stationary elements such as groyne flames (red lines in Figure 10.11 and map in Figure 10.12). These are filtered out in the initial bed level but partially reappear during the simulations, because the influence of the groynes is resolved by the model (blue and grey lines in Figure 10.11 and map in Figure 10.13). In principle, stationary bathymetry elements should not be filtered out. Since the groyne flames have a similar length scale as the river dunes, however, it is not possible to filter the one without filtering the other. Furthermore, the model is too coarse to represent the groyne flames in detail, so spin-up is needed anyway. Therefore, the current approach for filtering (section 4.3.2) is acceptable.

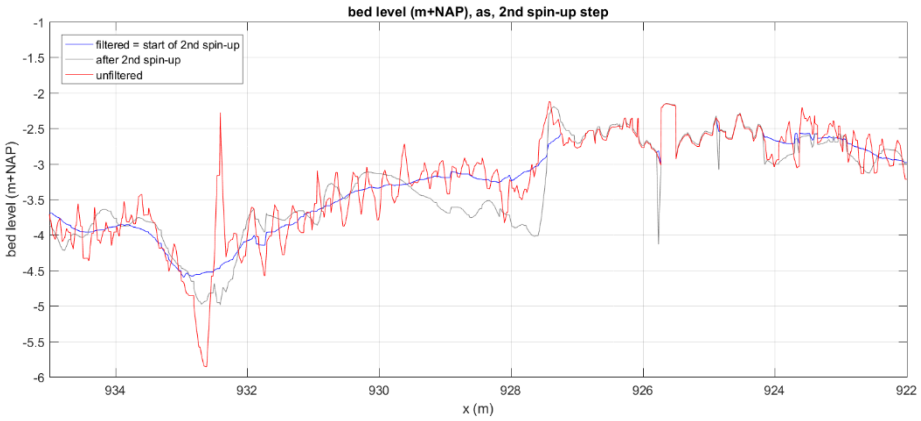

Figure 10.10 River bathymetry along a the river axis at the start (filtered bed, blue line) and end (grey line) of morphological spin-up compared to the unfiltered bathymetry (red line).

Figure 10.11 River bathymetry along lines 80 m to the left (L3) and right (R3) of the river axis at the start (filtered bed, blue line) and end (grey line) of morphological spin-up compared to the unfiltered bathymetry (red line).

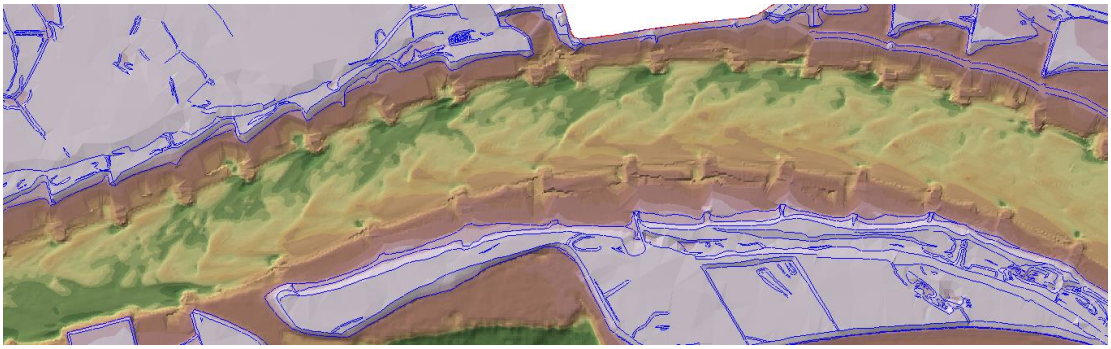

Figure 10.12 River bathymetry between km 930 and km 932 with bed forms in the middle of the main channel and groyne flames at the edges.

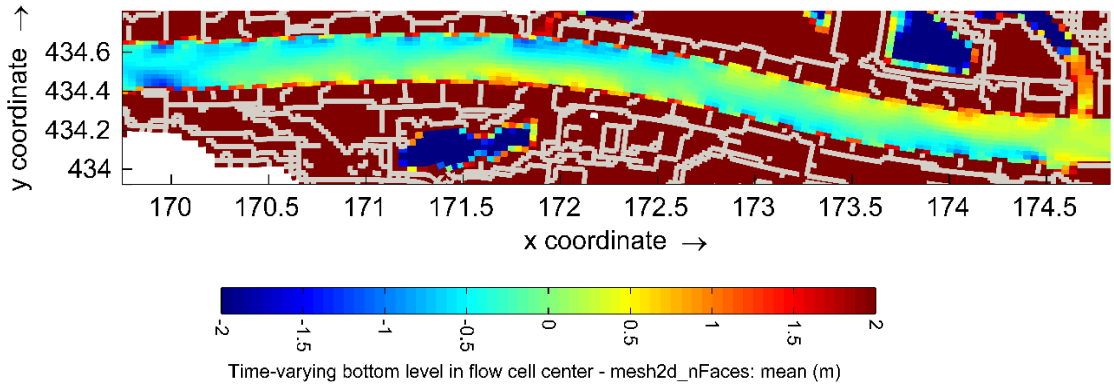

Figure 10.13 River bathymetry between km 890 and km 902 at the end of the morphological spin-up showing the influence of e.g. groynes on the modelled bathymetry.

10.3.3 Choice of underlayer type

Delft3D4 and D-HYDRO offer two options for defining sediment underlayers:

1) Lagrangian layers have a constant thickness specified by the user. Whenever sedimentation or erosion occurs, they are moved up or down respectively.
2) Eulerian layers have a varying thickness with a maximum thickness and a maximum number of layers. If sedimentation occurs on top of fully filled underlayers, the entire lowest underlayer is added to the final (thick) underlayer, and a new layer is created under the active layer to accommodate the sedimentation.

Since the sediment within an underlayer is fully mixed, Lagrangian layers are expected to cause more mixing of sediment than Eulerian layers. Therefore, Eulerian layers were used for the DVR model in Delft3D4. The same choice was made for the new model in D-HYDRO. However, when using Lagrangian layers in D-HYDRO, sedimentation results in the formation of several rather thin layers on top of each other, while the layers that existed initially are all moved to the final (thick) underlayer and fully mixed there. This issue is currently being investigated, and in the meantime we are using Lagrangian layers instead. When using Lagrangian layers, it is possible to use the thickness and composition of all sediment layers resulting from the spin-up as input for the actual morphodynamic simulations. In case of the Eulerian layers, it seems not desirable to use the composition and thickness of very thin layers in a simulation, because there was a risk of significantly limiting sediment availability locally. In the approach for the DVR model it was therefore decided to only use the spun-up composition and thickness of the first two layers (active layer and first underlayer). For the new model in D-HYDRO, this needs to be investigated further once it is clear if the behavior of the Eulerian layers can still be improved.

10.4 Making main channel roughness suitable for hydrodynamics and morphology

As shown in section, the 6th generation hydrodynamic model still contains abrupt changes in main channel roughness, which are inacceptable for morphological simulations. In their advice for the functional design of the 6th generation models, Spruyt et al. (2016) tested linear (first order) and second order transitions between roughness values over different lengths (2 km, 5 km, and 10 km). They saw hardly any influence of these transitions on the calibration result. For morphological models, such a transition should be as long as possible. In past projects, Deltares has used transition lengths of about 10 km. Spruyt et al. (2016) recommended to use transitions of 5 km length, since some of the river sections between measurement stations are too short to accommodate 10 km sections.

Finally, in the 6th generation hydrodynamic model transitions of 2 km length were implemented for the calibration factors, and no transitions were implemented for the base roughness (Figure 4.7). Figure 10.14 shows how sections with constant base roughness (red line) were derived from dune heights, which in reality have a much smoother variation. By preference, one would simply apply a rolling mean of this roughness value, just as we do for sediment composition. However, that does not match with the approach to use polygons with a roughness code in the trachytope functionality of Baseline and D-HYDRO.

Therefore, Baseline currently produces a transition represented by 10 polygons, along which the validity of the neighboring roughness sections is reduced/increased in steps of 10%. Simulations on fine grids show that this still produces visible steps in the resulting roughness values (Figure 10.15). These are not desirable for morphological simulations.

As alternative, we advise to define only the transition length by means of polygons in Baseline, and let the interpolation then be done as postprocessing step during the projection on the grid. In that way, the resolution of the steps in which roughness is increased or decreased can be made grid dependent, so that the variation is introduced smoothly per grid cell instead of per block of cells. And the transition lengths can be chosen in such a way that they nicely follow the natural variation in dune heights, as presented in Figure 10.16. For the calibration factor on top of the base roughness, transition lengths of at least 5 km should be chosen where possible.

Furthermore, attention is needed during calibration to not introduce unrealistic breakpoints in Q-S-relations. Changes in calibration factor should be linked to transitions on flow regime, such as the moment when flood plains start to become submerged. The offline analysis for the Waal has shown that this has been done well in the current hydrodynamic model.

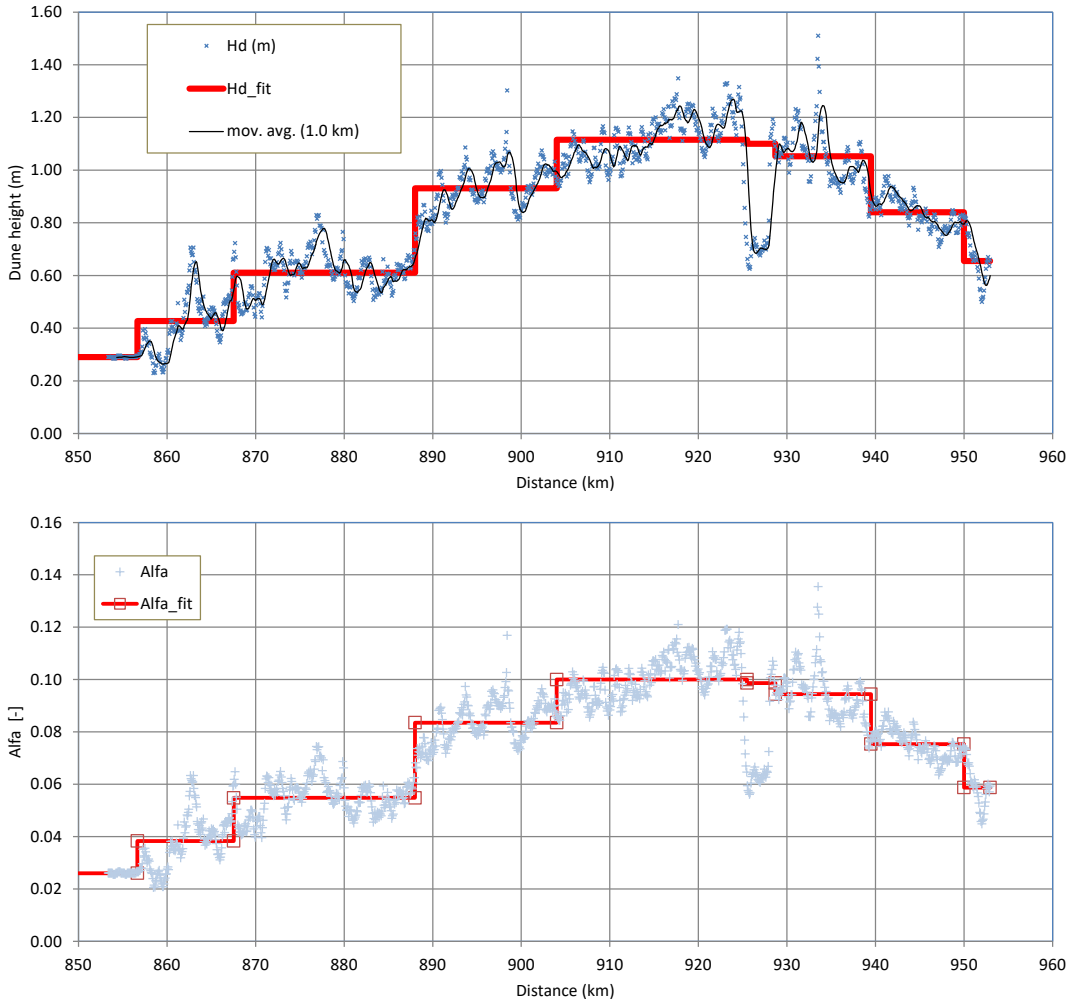

Figure 10.14 Sections of base roughness on Boven-Rijn and Waal in the 6th generation hydrodynamic model, with H_d = dune height, and Alfa the roughness coefficient in the Van Rijn formulation used in that model. Sections with fixed layers get a separate base roughness that is not presented in this figure. From: Kosters et al. (2022).

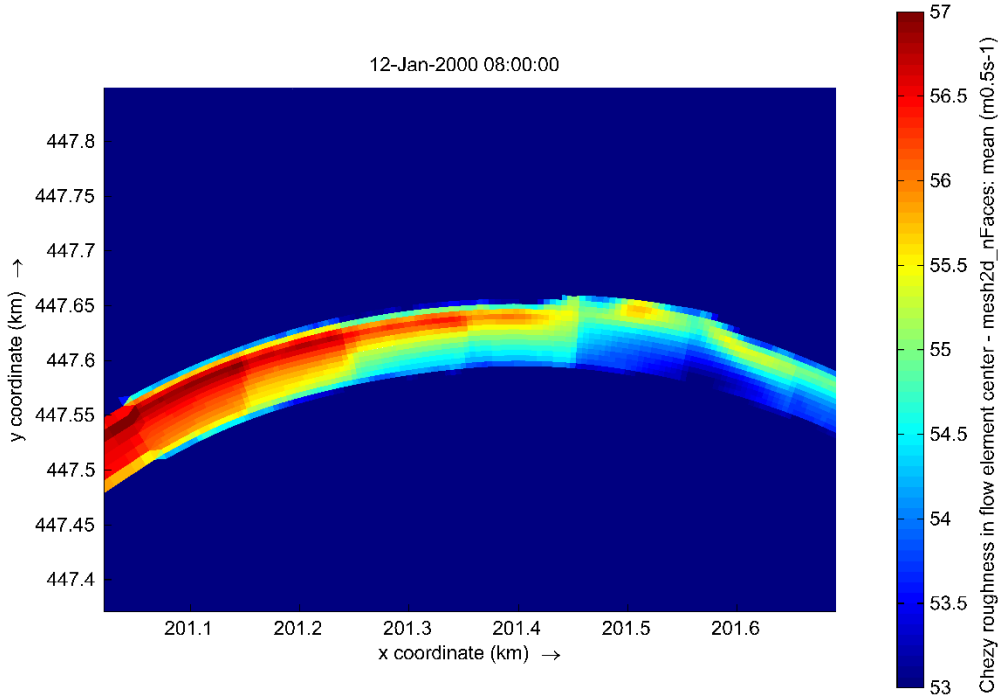

Figure 10.15 Chézy values at the IJssel close to De Steeg for a simulation of 2.000 m³/s at Lobith on a fine grid. The steps in the transition between roughness values are clearly visible.

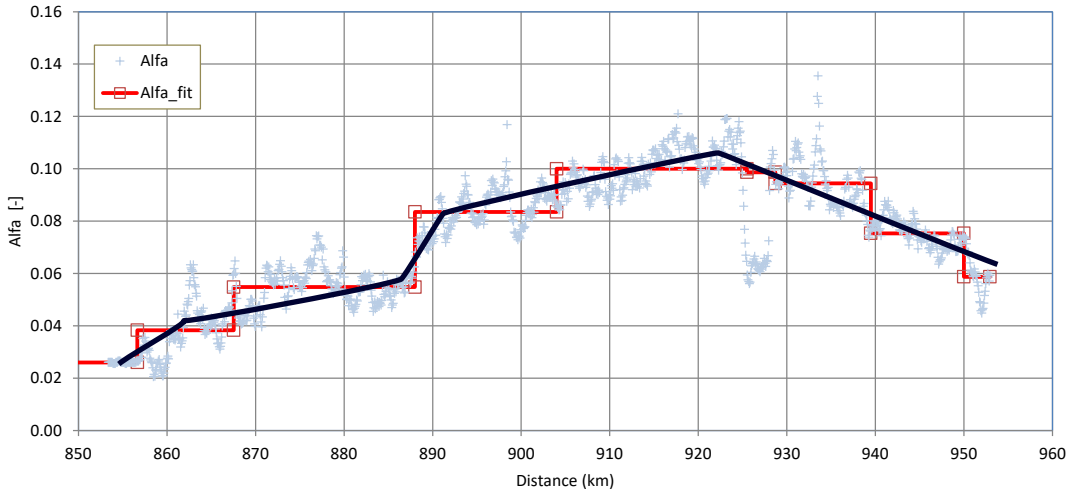

Figure 10.16 Base roughness estimate approximated by linear interpolation, choosing section length that fit the natural variation of dune heights (dark blue line).

10.5 Points of attention for further model development

10.5.1 Eddys in groyne fields and canal/harbour entrances

Because of the much finer grid compared to the DVR model, and maybe also because of the new approach for horizontal eddy viscosity, eddies form in the entrances of canals (e.g. ARK, see Figure 10.17) as well as in some of the groyne fields. This also happens in reality. However, it has never been validated how well the model represents these eddies with its current resolution, since the model was not intended to model these in detail.

In the groyne fields, it is expected that modelled eddies are not the same as real eddies because of insufficient grid resolution. Furthermore, 3D effects become important in groyne fields as soon as the groynes overtop. These cannot be represented by the 2D model.

The eddies in the current model result in strong sedimentation at the interface between main channel and the eddy (Figure 10.17). At the moment, we are testing a software version with a limiter for horizontal eddy viscosity to prevent this from happening.

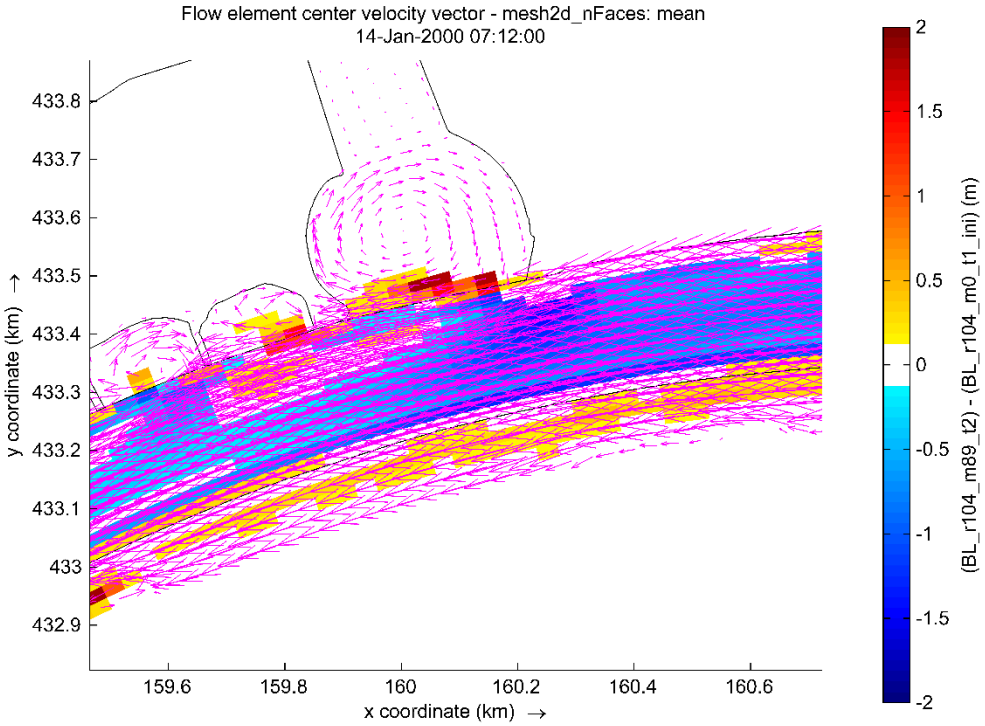

Figure 10.17 Cumulative erosion and sedimentation after 5,8 years around km 913 (mouth of ARK) as well as flow vectors for a discharge level of $Q_{Boven\text{-}Rijn}$ = 2.250 m³/s.

10.5.2 Bridge piers

The effect of bridge piers is clearly visible in the cumulative sedimentation and erosion. This is because the foundation of the bridge piers is partly included in the initial bed level, but these cells are not yet made non-erodible. Therefore, large erosion occurs in those cells in the first discharge step. When fine-tuning the model, we need to test if we can make these cells non-erodible, or if that leads to other undesired effects, e.g. too strong reaction of the bed level downstream of the fixed layer. In any case the model is too coarse and only 2D, so it will never be able to properly model scour processes at bridge piers.

10.5.3 Time step

At the moment, most simulations eventually crash because they reach the minimum allowed time step. Debugging some of them has shown that this happened although none of the computational cells was asking for a small time step. The reason was rather a “smoothness criterion” for the time step development, that prevented the time step to increase too fast after it had been low once. In our simulations, this leads to situations in which the time step did not manage to increase anymore, although that should have been the case. At the moment, we are testing the use of different settings within that smoothness criterium. In that way the time step should be increased faster. First results show that this indeed leads to less small time steps and later crash of the models. However, the reason why time steps are reduced at all need to be investigated further to make the model fully stable.

11 Conclusions and recommendations

A first version of the morphological model of the Waal (v0) was set-up based on existing 6th generation hydrodynamic models. Schematizations for three moments have been made: j99 (start of calibration period), j16 (start of validation period), and j19. The latter was used for a wide range of test simulations to test model performance and stability and find appropriate approaches for morphological spin-up, boundary conditions and morphological factors. First calibration runs have been carried out with j99. The results for width averaged bed level changes and sediment transport are promising. Local deviations between model behavior and reality need to be removed in the next phase during more detailed (2D) calibration.

Model stability has been an issue that seriously hampered progress. Several changes have been made to the software in order to improve stability and the workflow of model runs in the Simulation Management Tool (SMT). At the moment, we are still testing these. Looking at current model results, it seems that instabilities result from issues in the software rather than from the model schematizations. We did however identify points of attention in the schematization as well, that need to be looked at in more detail in the coming phase of model development.

The 6th generation hydrodynamic model was changed in several points to make it usable for morphological simulations. The most important one was the definition of main channel roughness. In the hydrodynamic model there are sharp transitions between different roughness values, which result in strong morphological reactions that do not occur in reality, where bed resistance usually has smooth gradients. In order to remove sharp transitions, and to decrease model complexity, the model is currently run using constant main channel roughness. A proposition was made on how to improve the approach to implement main channel roughness in future hydrodynamic models, so that they can be used for morphological simulations as well. These can be tested in the following phase, once the model is more stable and better calibrated.

In parallel to the Waal model, the first model version (v0) for the IJssel has been set-up in the same way as the one of the Waal. The simulations for hydrodynamic spin-up and validation are running at the moment, first morphological simulations are expected to start soon. The results will then be presented in a following report.

All steps in model development and the main steps in analysis of model results have been defined in Matlab scripts to make them reproducible and re-usable for model development for other branches or future scenarios. To make these accessible to future users, who will have to derive new model schematizations, it is recommended to group them in a clear workflow using software like Snakemake. In such a way, the order of the steps and input and output for/of each step are clearly defined. Snakemake also visualizes which steps have already been carried out, and which ones still need to be taken. Care should be taken to define which of the steps can be incorporated in future versions of Baseline, and how. These can then be kept outside the Snakemake workflow.

Table 11.1 recommends which steps to take next year. A strong focus should first lie on getting model results more stable, so that a proper calibration with long-term runs can be done. Test simulations with software and SMT improvements are already running and look promising, but it needs more simulations to definitely know if the issues are solved.

Table 11.1 Recommended steps to continue model development in 2024.

activity areas	associated activities	model version	steps for 2024
data collection	• Collection of all data needed to set-up a model, e.g. boundary conditions, calibration data hydrodynamics and sediment transport and morphology, bed composition, etc.	v0 v1	non- or less erodible layers Waal and IJssel v1 IJssel v0: 1D calibration data
morphodynamic model schematization: towards a well-working basic model (v0)	• set-up of a first running model including: a. dynamic river bed b. representative initial bed elevation (e.g. smoothing of bed forms) c. suitable roughness formulation for morphology d. sediment (grain sizes and sediment layers, with focus on active/upper layer) e. secondary flow f. first choice of transport formula and parameters (uncalibrated) g. non-erodible and less erodible layers h. suitable grid resolution • testing phase v0 model, identification of problems and modification of the schematization accordingly	v0	stability issues Waal v0 IJssel v0 testing phase
extending the basic model to a v1 model	• more sophisticated description of a. main channel roughness b. composition and thickness of underlayers, including non-erodible layers • set-up of a dredging and dumping module • testing phase v1 model, and iterative modification of model schematization if necessary	v1	Waal v1: dredging & dumping, main channel roughness
development of methodologies and tools for running the model	• approach and tools for model simulation (i.e. Simulation Management Tool) • strategy for model spin-up • strategy and tools for model evaluation and presentation of results • strategy and tools for simplification of model set-up and improving reproducibility	v0 v1	Waal v0/v1, IJssel v0: Snakemake workflows, analysis time dependent morfac
model calibration and validation	• calibration and validation strategy • adapting the hydrodynamic model to make it suitable for morphodynamic simulations • hydrodynamic validation • “offline” calibration giving a first estimate of morphological response based on the flow field in the hydrodynamic simulations • 1D morphodynamic calibration and validation (focusing on width-averaged, large-scale and long-term trends) • 2D morphodynamic calibration and validation (focusing on 2D patterns in the river bed, such as bank patterns and bend profiles) • validation of dredging and dumping module	v1	Waal v1: 1D and 2D calibration IJssel v0: hydrodynamic validation and start 1D morphological calibration
exploring model uncertainties	• influence of unknown physical variables (e.g. roughness in transport, bed composition, active layer thickness)	v1-v3	-

activity areas	associated activities	model version	steps for 2024
	• influence of model settings (e.g. initial geometry/composition and boundary conditions) or modelling concepts (e.g. Hirano model) • influence of simulation strategy and approaches (e.g. methods for optimizing simulation time, schematization of the hydrograph, choice of simulation period)		
development of modeling strategies and development for future use of the model	• identifying types of application and requirements • development of strategies for application of the model (e.g. choice of scenarios, choices for model settings and geometry, type of interventions) • identifying needs for further development of the model schematization (including needs for knowledge development and data requirements) • implementation and testing	v1-v3	-
verification of model application	testing the model application in test cases of a. effect of interventions b. planning study (“planstudie”) c. (long-term) forecast of system behaviour improvement of the model schematization, modeling strategies, methodologies and tools based on the outcomes of the test cases	v1-v3	-
Implementation of new functionality in D-HYDRO	• Identifying requirements of new functionality • functional design of needs • design of implementation • implementation and testing • updating user manuals	v2-v3	-

12 Literature

Becker, A. (2021), Slim suppleren Boven-Waal, rapport Deltares 11206792-014-ZWS-0001, Deltares, Delft, 156 pp.

Chavarrías, V., Busnelli, M. and Sloff, K. (2020). Morphological models for IRM. Rhine branches 1D. Deltares report 11206792-014-ZWS-0001.

Crebas, J. (2012). Stage-discharge relations for the downstream boundaries of the Rhine branches and river Meuse. Deltares memo d.d. July 12, 2012.

De Joode, A. (2022): Bodemparameters voorbereiding 2D model Rijntakken. 20 december 2022.

De Jong, J., Chavarrías, V. and Ottevanger, W. (2021). Eindevaluatie pilot Langsdammen in de Waal. Hydromorphological data and observations. Deltares report 11204644-018-ZWS-0001.

Engelund, F., and E. Hansen (1967): Monograph on sediment transport in alluvial streams. Tech. Rep., Hydraulics Laboratory, Technical University of Denmark, Copenhagen, Denmark.

Frings, R.M., G. Hillebrand, N. Gehres, K. Banhold, S. Schriever and T. Hoffmann (2019): From source to mouth: Basin-scale morphodynamics of the Rhine River. Earth-Science Reviews, Volume 196, ISSN 0012-8252, https://doi.org/10.1016/j.earscirev.2019.04.002.

Hirano, M. (1971): River bed degradation with armouring. Proc. Jpn. Soc. Civ. Eng. 195: 55-65. DOI: 10.2208/jscej1969.1971.195_55.

Gradussen, B. (2023). Validatie Waalmodel hoogwater 2021. Validatie afvoeren en stroomsnelheden in D-HYDRO. Deltares report 11209233-003-ZWS-0013.

Kosters, A., Spruyt, A.S. and Niesten, I. (2022). Ontwikkeling zesde-generatie Rijntakken model: Modelbouw, kalibratie en validatie. Deltares report 11206813-003-ZWS-0012.

Meyer-Peter, E., and R. Müller (1948): Formulas for bed-load transport. In: Proc. 2nd IAHR World Congress, 6-9 June, Stockholm, Sweden, pages 39-64.

Minns, T., A. Spruyt, D. Kerkhoven (2022): Specificaties zesde-generatie modellen met D-HYDRO. Generieke technische en functionele specificaties (v1-2023). Preliminary version, 22 december 2022.

Van der Maaten, L., and G. E. Hinton (2008), Visualizing data using T-SNE, Journal of Machine Learning Research, 9, 2579--2605.

Onjira, P. (2023), Living lab Rhine (LiLaR): Comparison of sediment measurement methods between the Netherlands and Germany, Tech. Rep., BfG.

Ottevanger, W., V. Chavarrías, S. Giri and E. van der Deijl (2021): Morphological model for the River Meuse. Model setup, input visualisation, and future steps. Deltares report 11206792-003-ZWS-0002, September 2021.

Ottevanger, W. and V. Chavarrías (2022): Morphological model for the River Meuse. Case Study for the reach Sambeek-Grave. Deltares report 11208033-002-ZWS-0003, December 2022.

Sieben, J., R. van der Veen, D.F. Kroekenstoel and M. Schropp (2005): Morfologsiche effecten Ruimte voor de Rivier in het Bovenrivierengebied. Tech. Rep. 20005.044X, RIZA, Directoraat-Generaal Rijkswaterstaat, Arnhem, The Netherlands.

Sieben, J., 2020. Overzicht afvoermetingen 2016-2019 project monitoring langsdammen. Tech. rep., Rijkswaterstaat.

Sieben, J., D. Beyer, M. Reneerkens (2023): Definitie calibratie perioden, RWS concept-memo 11-5-2023.

Sloff, K., A. Paarlberg, A. Spruyt, M. Yossef (2009): Voorspelinstrument Duurzame Vaardiepte Rijndelta. Continued development and application of morphological model DVR Part 2: model adjustment. Deltares report 1002069-002-ZWS-0005, June 2009.

Sloff, K. (2019): Prognose bodemligging Rijntakken 2020-2050. Trends voor scheepvaart en waterbeschikbaarheid. Deltares-rapport 1203738-005-BGS-0008, 20 december 2019.

Sloff, K. (2022): Ruimtelijke en temporele interpretatie van bemonstering bodemsamenstelling Rijntakken. Deltares report 11208033-012-ZWS-0001, 22 December 2022.

Spruyt, A. (2023): Plan voor ontwikkeling 2D morfologisch modelinstrumentarium van de Rijntakken in D-HYDRO. Functioneel en technisch ontwerp. Deltares report 11208033-014-ZWS-0001, 23 february 2023.

Spruyt, A., T. Minns, M. Yossef, D. Kerkhoven, F. Zijl, M. Genseberger (2016): Advies voor algemeen functioneel ontwerp voor de 6e-generatie modellen van RWS. Deltares rapport 1230071-011-ZWS-0009, December 2016.

Ten Brinke, W. (2019): Effecten morfologische ontwikkelingen op functies Rijn en Maas. Blueland Consultancy BV. Rapport B19.01, Oct. 2019.

Van der Wijk, R. (2022). Afleiden QH-relatie Rijn-Maasmonding voor Rijntakken en Maas. Deltares memo 11206813-006-ZWS-0008.

Van Dongeren, A., Marlies van der Lugt, Bjorn Röbke, Cilia Swinkels, Arjen Luijendijk, Emiel Moerman, Matthijs Gawehn (2018): Delft3D FM morphology. Results of testing. Deltares report I1000394-002.

Ylla Arbós, C., A. Blom, S. van Vuren, R.M.J. Schielen (2019): Bed level change in the upper Rhine Delta since 1926 and rough extrapolation to 2050. Delft University, Nov 2019.

Yossef, M. F. M., H. R. A. Jagers, S. van Vuren and A. Sieben (2008): Innovative techniques in modelling large-scale river morphology." In M. Altinakar, M. A. Kokpinar, ˙Ismail Aydin, S¸ evket Cokgor and S. Kirgoz, eds., Procedings of the 4th International Conference on Fluvial Hydraulics (River Flow), 3-5 September, Cesme, Izmir, Turkey. Kubaba Congress Department and Travel Services, Ankara, Turkey.

A Grain size interpolation using the T-SNE algorithm

This Appendix describes how an initial sediment composition is derived from the 2020 measurement campaign data using the T-SNE algorithm (van der Maaten and Hinton, 2008) and predictions via mixture modelling using logistic regression output as weights. This analysis employs statistical and Machine Learning techniques to predict the grain size distribution of sediments along the examined part of the river Waal. The analysis is based on performing inference using existing sieve curve data retrieved from the same stretch of the river to train the selected models and the using them for prediction of the sieve curve over the same stretch of the river. The analysis employs simple techniques and so aims to detect only baseline spatial patterns of the grain size distribution.

A dataset of features is composed by retrieving the passing percentage per of the 22 sieve diameters and the D_{50}, which is considered a good indicator of sieve curve behavior. As a result, the feature vectors live in a 23-dimensional plane. The T-SNE algorithm is used to project features in a 2D embedding, enhancing manipulation ease (Figure 12.1). The purpose of selecting the T-SNE for dimensionality reduction is that the algorithm aims to distinct neighboring points in the 23-dimensional plane from points that lie far apart.

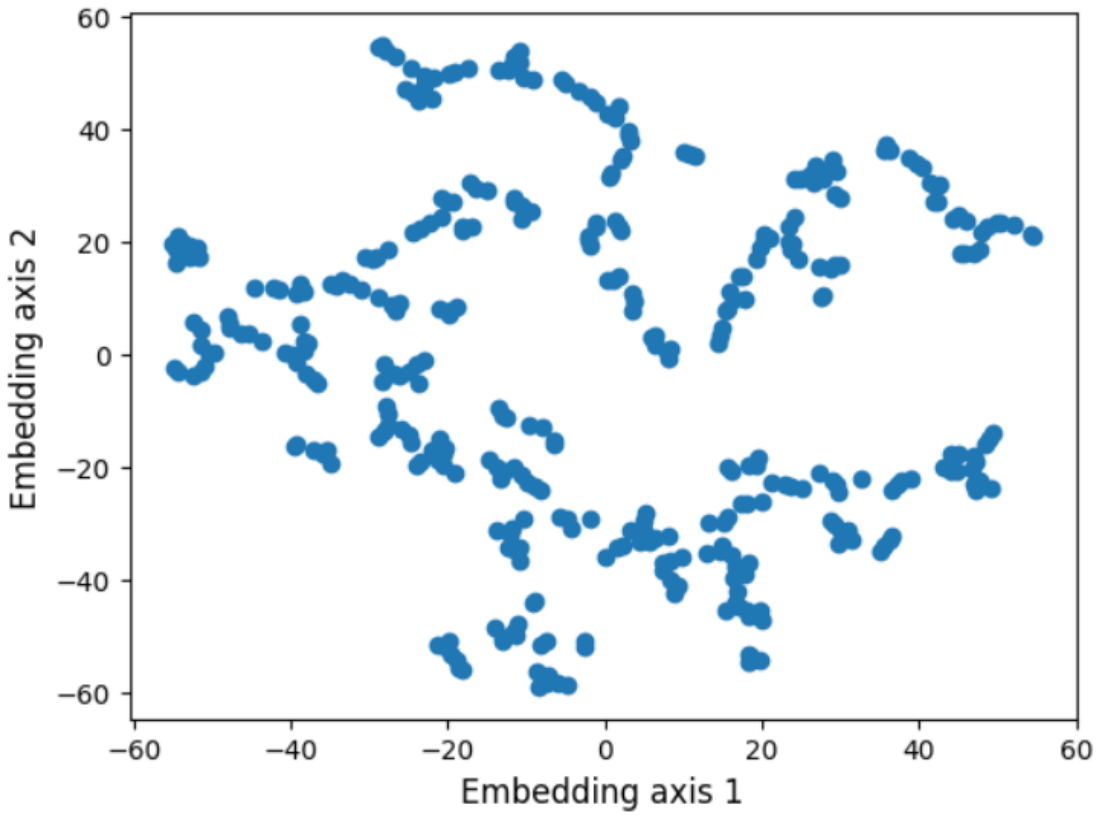

Figure 12.1: 2D embedding of the dataset achieved by the T-SNE algorithm.

Following, agglomerative clustering was used to achieve grouping of points in a hierarchical fashion (Figure 12.2). Since the analysis aims to identify baseline spatial patterns of the grain size distribution, a small number of clusters is used.

Eventually, this selection leads to clustering with lower local variance. More clusters could be added in a more sophisticated approach to the problem, probably in later iterations. Figure 12.3 shows the generated clusters of the feature vectors in the 2D embedding of the T-SNE algorithm.

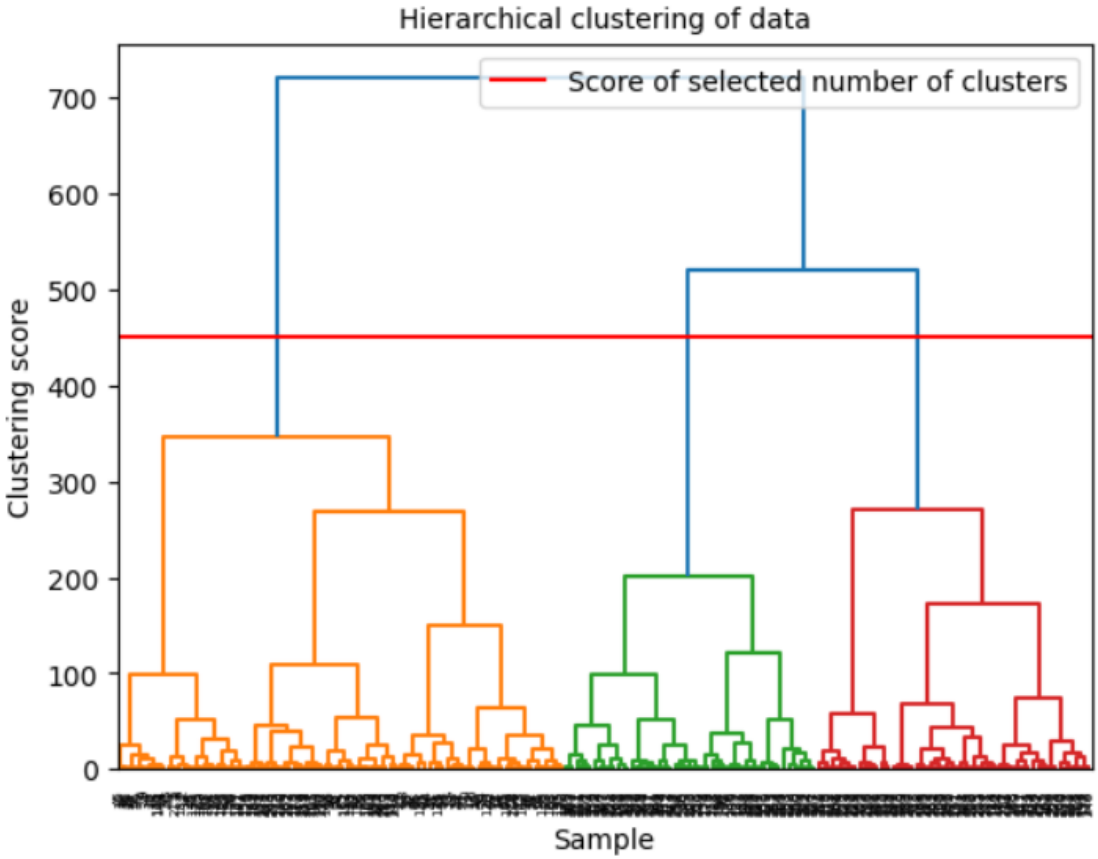

Figure 12.2: Dendogram of agglomerative clustering and selected number of clusters.

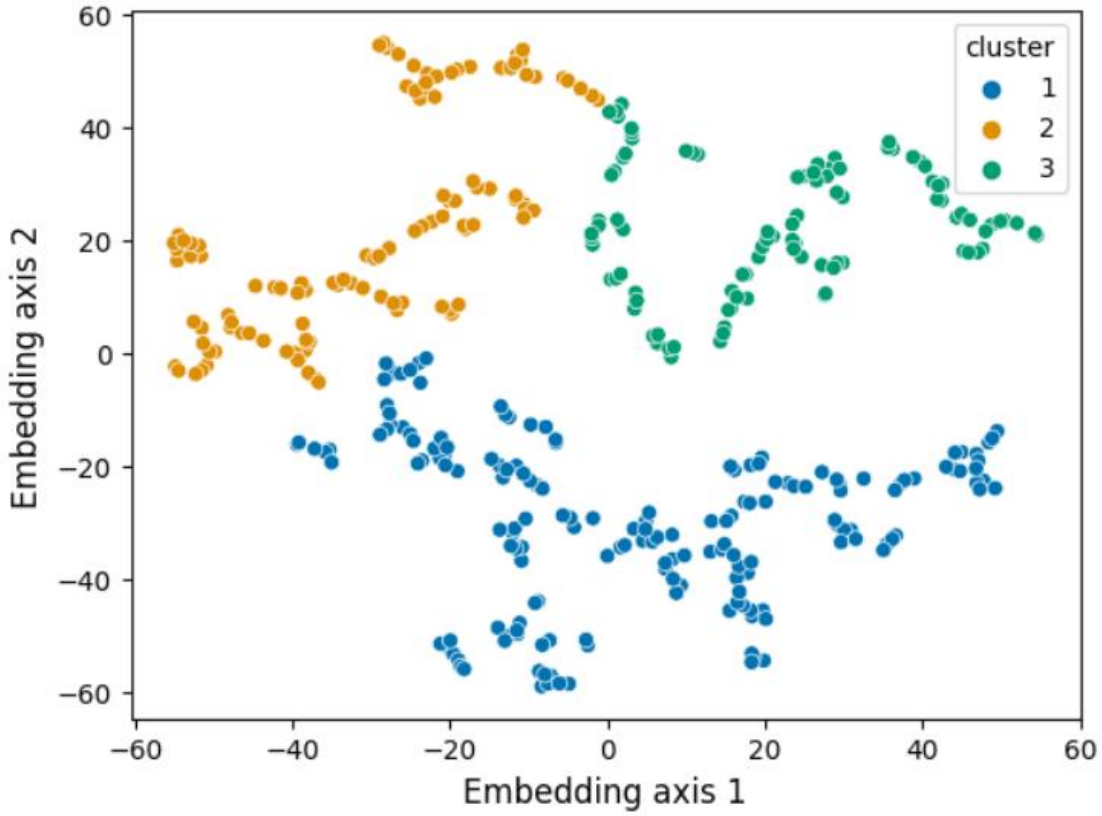

Figure 12.3: Selected clustering visualized on the 2D embedding.

Figure 12.4 shows the sieve curves and cumulative sieve curves per cluster. It also visualizes their statistics in boxplots and the mean and 95% confidence interval of the cumulative curves. Inspecting the cumulative curves shows that the clusters represent distinct behaviors: the first one favors larger diameters, the second favors low sieve diameters and third one has a more uniform distribution of grains. The mean curves of the clusters will be used as basis for prediction.

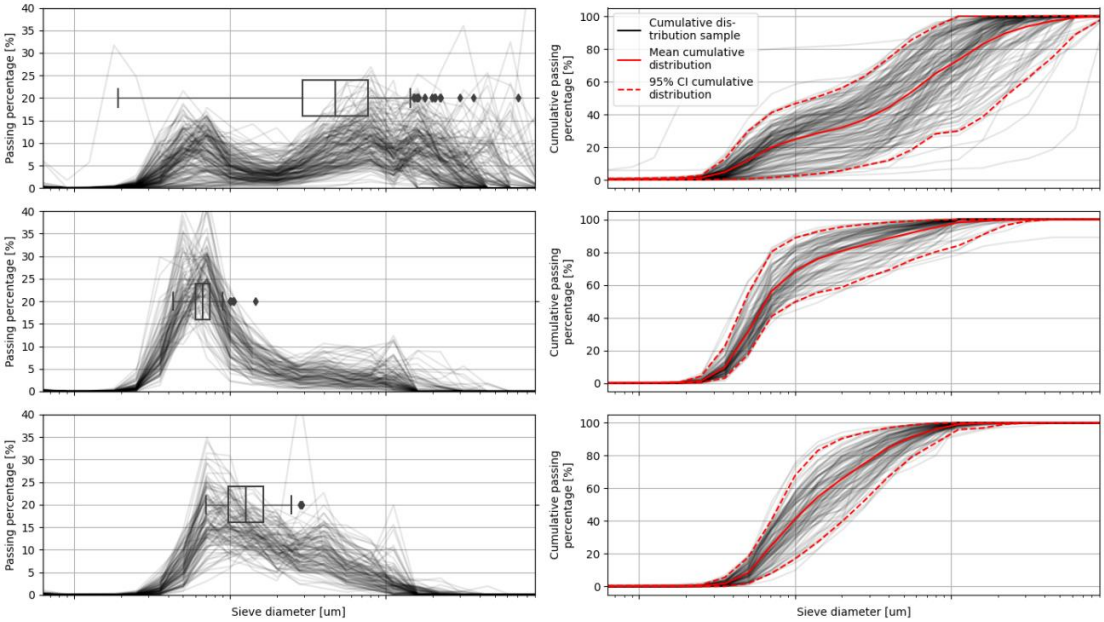

Figure 12.4: Sieve curve distribution (left) and cumulative sieve curve distributions (right) per cluster, along with their important statistics.

A logistic regression scheme is used to determine the probability of all points along the river stretch participating in each of the clusters. This part of the analysis used as features: the river chainage, the transversal locations of the points, the curvature of river meanders per at each chainage and the river flow along the river cross-section. Cross-validation of the logistic regression model suggests that only the three first features convey useful information. Thus, the 3-featured logistic regression model is selected as the fittest and produces a prediction of the clusters as shown in Figure 12.5.

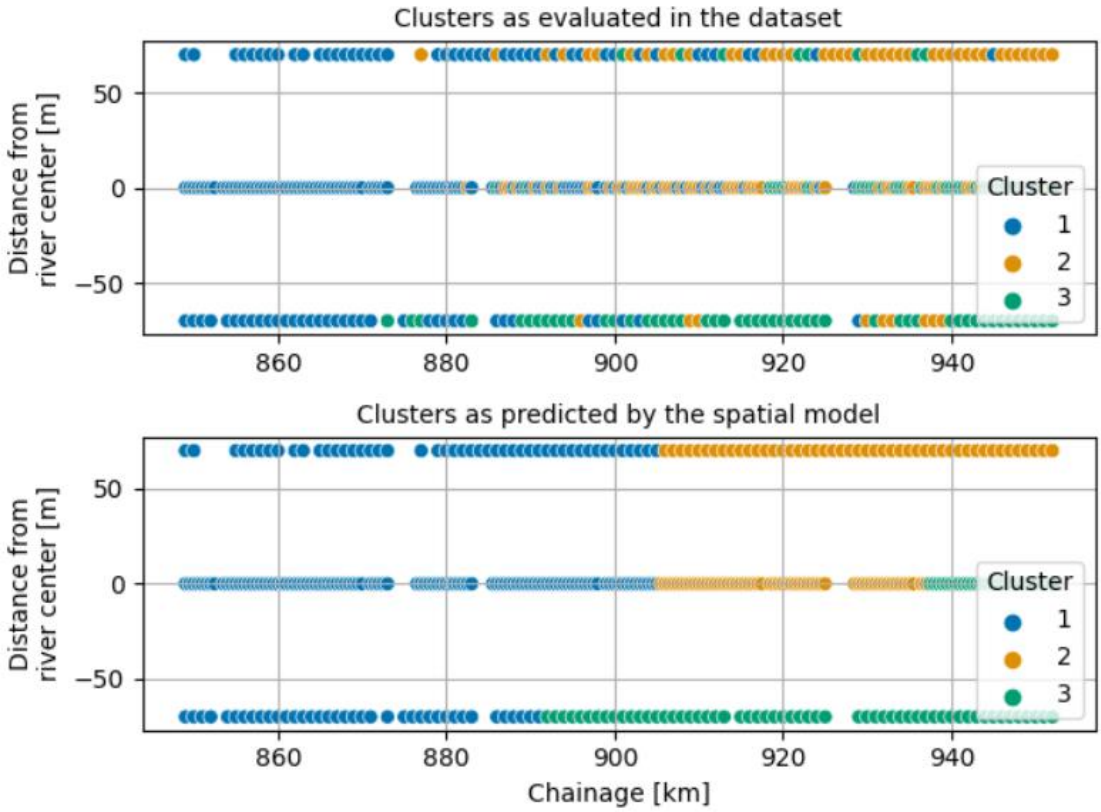

Figure 12.5: Clusters per river location (up) and prediction of clusters (bottom).

The next step is to establish a predictive model. In order to avoid discontinuities of prediction, a mixture model is adopted. The predicted sieve curve is taken as the weighted average of the mean sieve curve of the clusters, weighted by the probability of each river point to participate in each of the clusters, as estimated by the logistic regression model. The predicted sieve curve per location is compared to the actual sieve curve in Figure 12.6. While the analysis provides a decent approximation, it can be found lacking because using a mixture model with the cluster means disables predictions that lie outside the envelope of the means curves. This occurs because the mixture only focuses on the mean curves of the clusters, instead of their full distribution in order to reduce the prediction to a deterministic outcome.

Ultimately, the analysis established a spatial model for grain size distribution prediction. Inference has aimed in identifying the baseline spatial pattern. A s a result, predictions only describe this pattern. Among others, further developments could include the use of models more advanced than logistic regression to describe a greater part of the dataset's variance and improve the predictions achieved by the adopted mixture model.

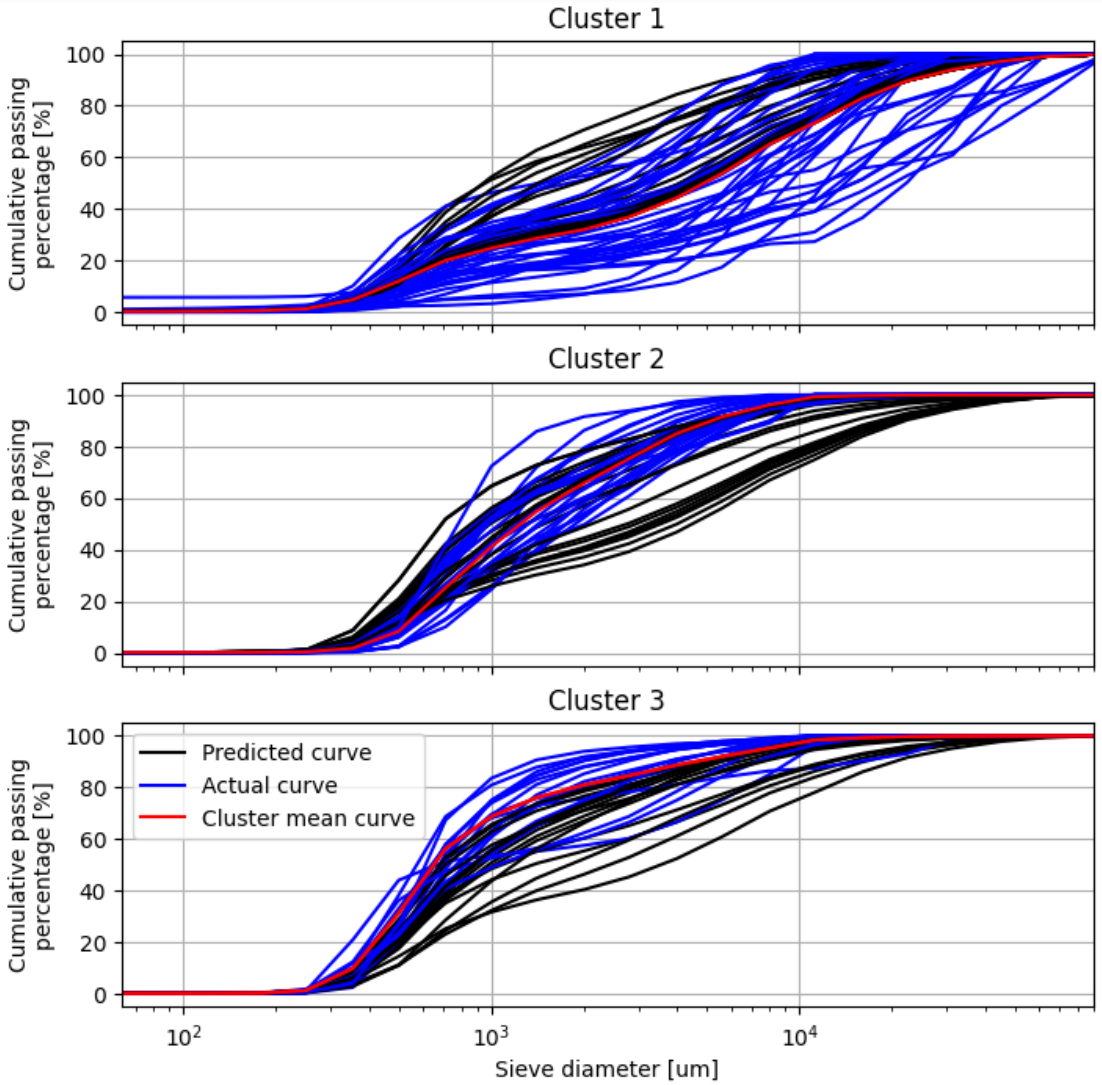

Figure 12.6: Comparison of the predicted and actual cumulative sieve curves per river location.

B List of measures j95 to j99

```
# ********************************************************************************
#
#  De naam voor deze variant is  : baseline-rijn-j99_6-v1
#  De basis voor deze variant is : baseline-rijn-j95_6-v1
#
# ********************************************************************************
#
#  RWS Oost-Nederland
#  11 juli 2023
#
#  Met deze maatregel_lijst kan een selectie van de beschikbare wijzigingen
#  tussen 1995 en 1999 ingemixt worden. De volgorde van de maatregelen is
#  oplopend in de tijd en er is rekening gehouden met de inmixvolgorde. Het
#  resultaat van deze variant geeft de actuele situatie weer van de Rijntakken
#  voor het jaar 1999.
#
#  Vanwege de inmixvolgorde is maatregel wl_bkriber_a2 onder modelmaatregelen
#  geplaatst.
#
# ********************************************************************************
#
#  Actualisatiemaatregelen
#
# ********************************************************************************
#
../../rijn-maatr_6/act/wl_ewijkse_a1
../../rijn-maatr_6/act/wl_passew_a2
../../rijn-maatr_6/act/wl_vlaagan_a3
../../rijn-maatr_6/act/wl_gameren_a3
../../rijn-maatr_6/act/wl_breemw_a4
../../rijn-maatr_6/act/wl_stdhees_a1
../../rijn-maatr_6/act/wl_zbhgt99_a1
#
# ********************************************************************************
#
#  Modelmaatregelen
#
# ********************************************************************************
#
../../rijn-maatr_6/mod/wl_bkriber_a2
#
# ********************************************************************************
#
#  Einde lijst
#
# ********************************************************************************
```

C Calibration factors hydrodynamic model

```
#------------------------------------------------------------------
2002 DISCHARGE WL_868.9_QO_Waal # instead of BR_862.7_QR_Lobith-
Pannkop (not included in model)
2002 0800 1.051
2002 1580 0.889
2002 2700 0.943
2002 5350 1.093
2002 7200 1.108
#------------------------------------------------------------------
2003 DISCHARGE WL_876.6_QR_Pannkop-Nijmegen # Pannkop-Nijmegen
2003 0800 0.948
2003 1580 0.942
2003 2070 0.969
2003 2700 0.969
2003 5350 0.998
2003 7200 0.943
#------------------------------------------------------------------
2004 DISCHARGE WL_894.8_QR_Nijmegen-Dodewaard # Nijmegen-Dodewaard
2004 0800 0.854
2004 1580 0.907
2004 2700 0.94
2004 5350 0.942
2004 7200 0.897
#------------------------------------------------------------------
2005 DISCHARGE WL_910.4_QR_Dodewaard-Tielwaal # Dodewaard-
Tielwaalkm911
2005 0800 0.848
2005 1580 0.936
2005 2700 1.001
2005 5350 1.03
2005 7200 0.981
#------------------------------------------------------------------
2006 DISCHARGE WL_924.3_QR_Tielwaal-Zaltbommel # Tielwaalkm911-Varik
2006 0900 0.883
2006 1580 0.982
2006 2700 1.076
2006 5350 1.033
2006 7200 0.892
#------------------------------------------------------------------
2007 DISCHARGE WL_924.3_QR_Tielwaal-Zaltbommel # Varik-Sintandries
2007 0900 0.883
2007 1580 0.982
2007 2700 1.076
2007 5350 1.033
2007 7200 0.892
#------------------------------------------------------------------
2008 DISCHARGE WL_924.3_QR_Tielwaal-Zaltbommel # Sintandries-
Heesselt
2008 0900 0.883
```

```
2008 1580 0.982
2008 2700 1.076
2008 5350 1.033
2008 7200 0.892
#-----------------------------------------------------------------------
2009 DISCHARGE WL_924.3_QR_Tielwaal-Zaltbommel # Heesselt-Zaltbommel
2009 0900 0.883
2009 1580 0.982
2009 2700 1.076
2009 5350 1.033
2009 7200 0.892
#-----------------------------------------------------------------------
2010 DISCHARGE WL_934.6_QR_Zaltbommel # Zaltbommel-Vuren
2010 1000 0.806
2010 1600 0.999
2010 2700 1.108
2010 5350 1.114
2010 7200 1.005
#-----------------------------------------------------------------------
2011 DISCHARGE WL_934.6_QR_Zaltbommel # Vuren-Merwedekop
2011 1000 0.851
2011 1600 0.82
2011 2700 0.871
2011 5350 1.208
2011 7200 1.146
#-----------------------------------------------------------------------
# 2012 DISCHARGE PK_872.5_QR_Pannkop-IJsselkop # Pannkop-Pannerden
2012 1.0 # calibration factor is discharge dependent but cross-
section PK_872.5_QR_Pannkop-IJsselkop is not included in model
```

D Bed level changes 2019 – 2022 simulation

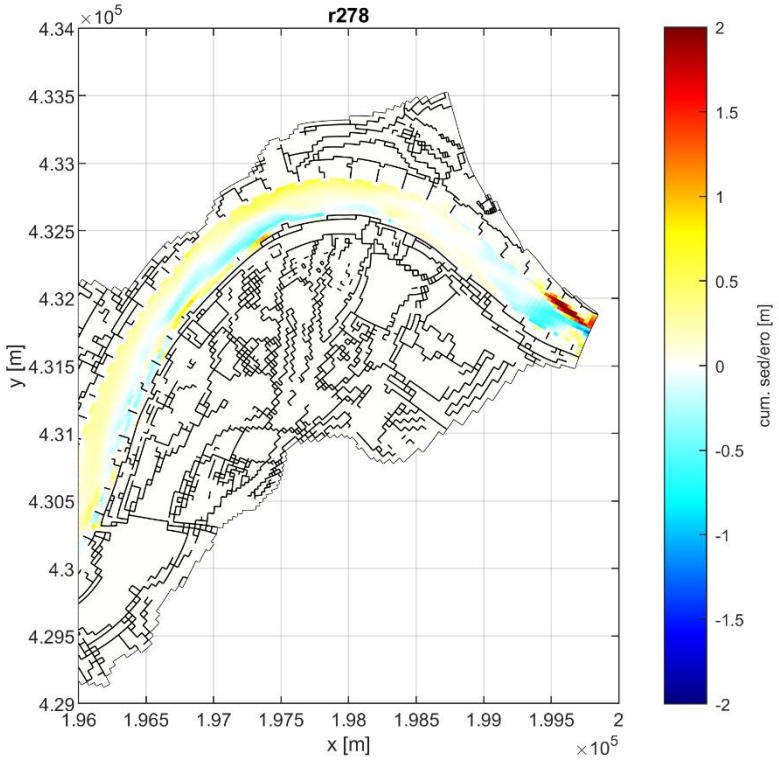

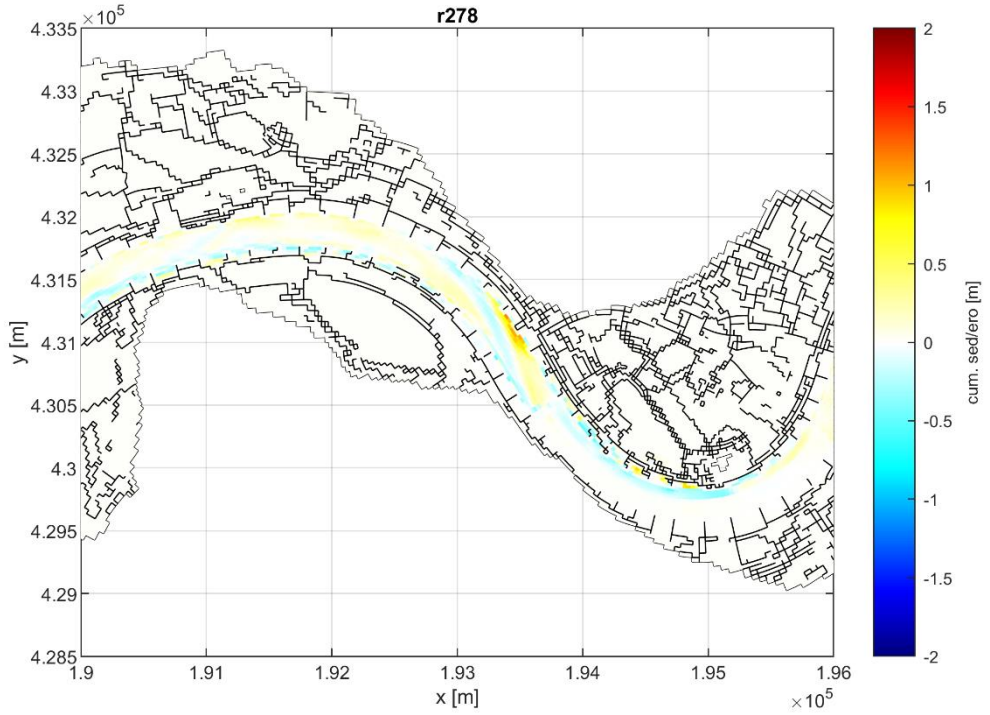
r278
×10^5
4.335
4.33
4.325
4.32
4.315
4.31
4.305
4.3
4.295
4.29
4.285
y [m]
1.9
1.91
1.92
1.93
1.94
1.95
1.96
x [m]
×10^5
2
1.5
1
0.5
0
-0.5
-1
-1.5
-2
cum. sed/ero [m]

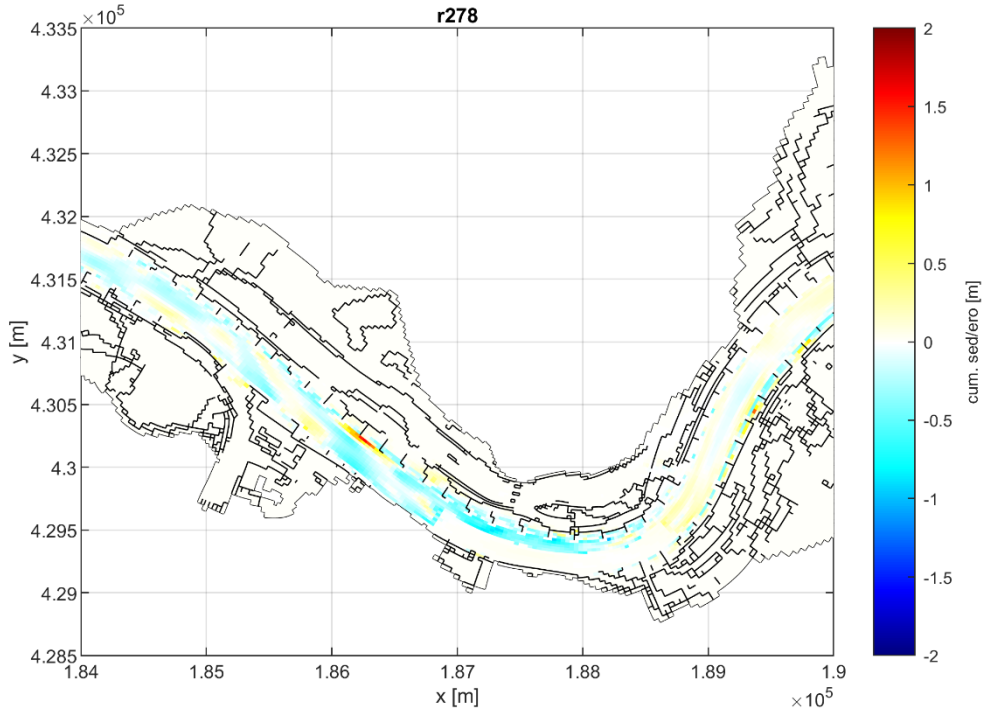
r278
×10^5
4.335
4.33
4.325
4.32
4.315
4.31
4.305
4.3
4.295
4.29
4.285
y [m]
1.84
1.85
1.86
1.87
1.88
1.89
1.9
x [m]
×10^5
2
1.5
1
0.5
0
-0.5
-1
-1.5
-2
cum. sed/ero [m]

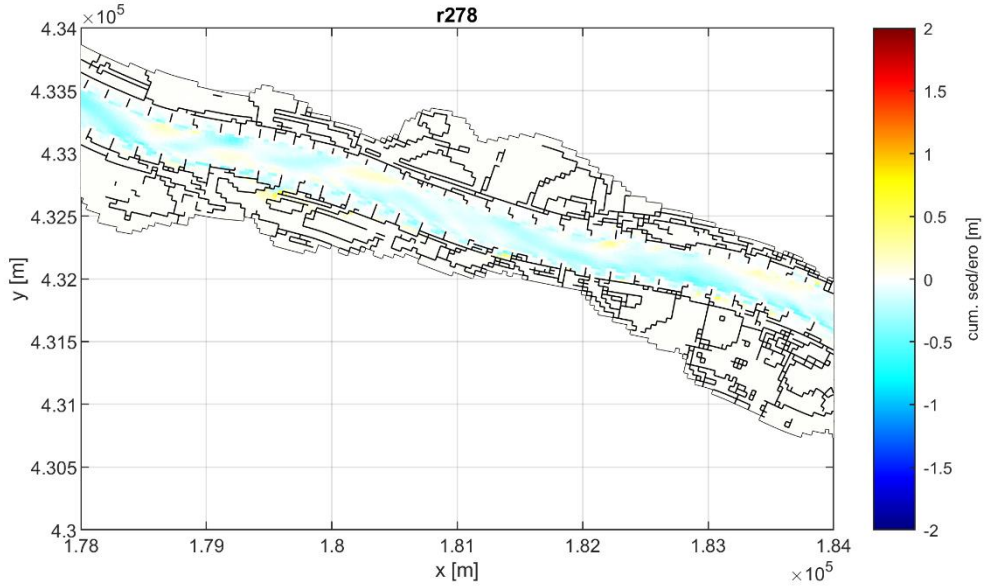
r278
×10^5
4.34
4.335
4.33
4.325
4.32
4.315
4.31
4.305
4.3
y [m]
1.78
1.79
1.8
1.81
1.82
1.83
1.84
x [m]
×10^5
2
1.5
1
0.5
0
-0.5
-1
-1.5
-2
cum. sed/ero [m]

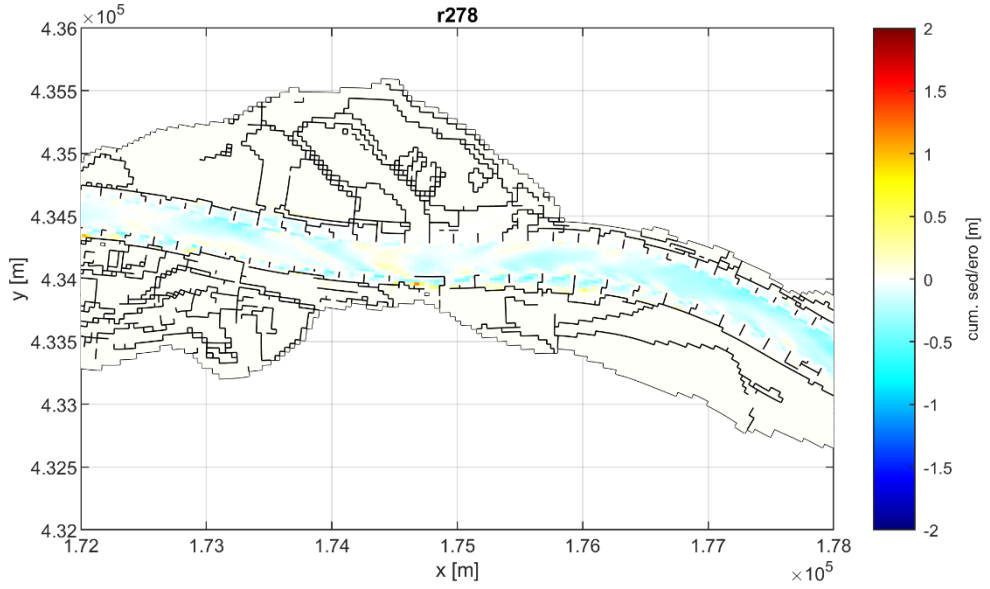
r278
×10^5
4.36
4.355
4.35
4.345
4.34
4.335
4.33
4.325
4.32
y [m]
1.72
1.73
1.74
1.75
1.76
1.77
1.78
x [m]
×10^5
2
1.5
1
0.5
0
-0.5
-1
-1.5
-2
cum. sed/ero [m]

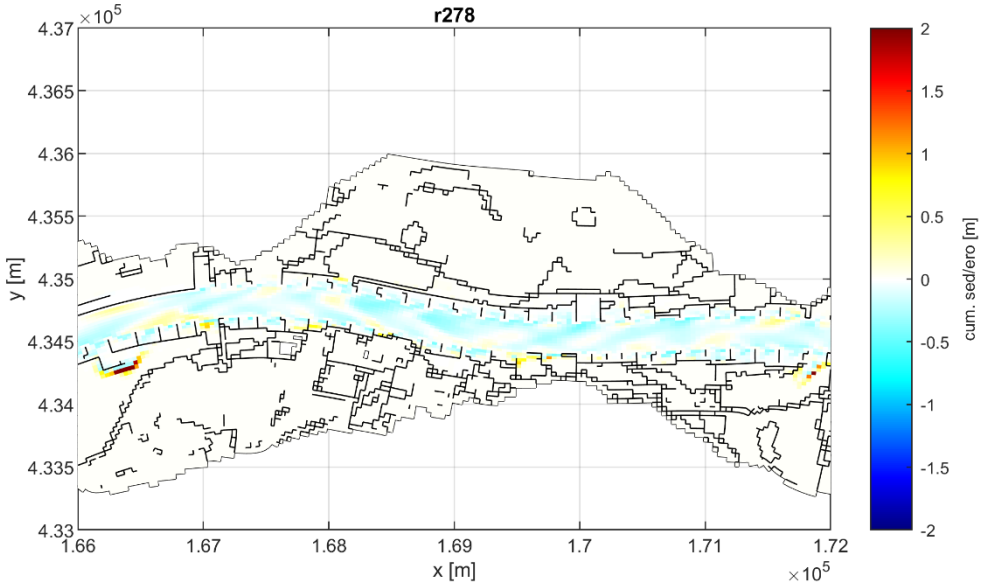
r278
×10^5
4.37
4.365
4.36
4.355
4.35
4.345
4.34
4.335
4.33
y [m]
1.66
1.67
1.68
1.69
1.7
1.71
1.72
x [m]
×10^5
2
1.5
1
0.5
0
-0.5
-1
-1.5
-2
cum. sed/ero [m]

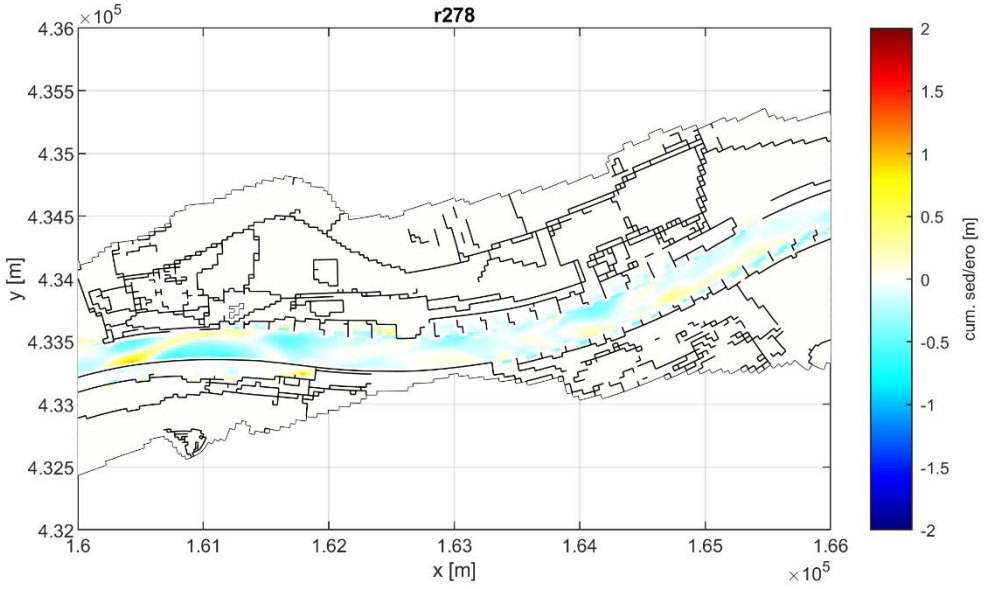
r278
×10^5
4.36
4.355
4.35
4.345
4.34
4.335
4.33
4.325
4.32
y [m]
1.6
1.61
1.62
1.63
1.64
1.65
1.66
x [m]
×10^5
2
1.5
1
0.5
0
-0.5
-1
-1.5
-2
cum. sed/ero [m]

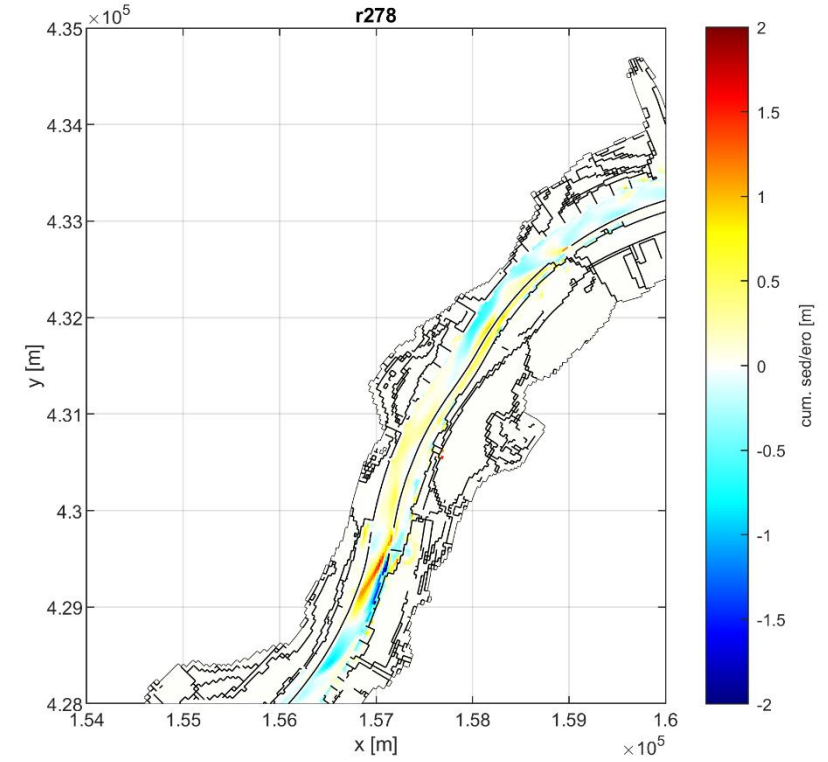
r278
×10^5
4.35
4.34
4.33
4.32
4.31
4.3
4.29
4.28
y [m]
1.54
1.55
1.56
1.57
1.58
1.59
1.6
x [m]
×10^5
2
1.5
1
0.5
0
-0.5
-1
-1.5
-2
cum. sed/ero [m]

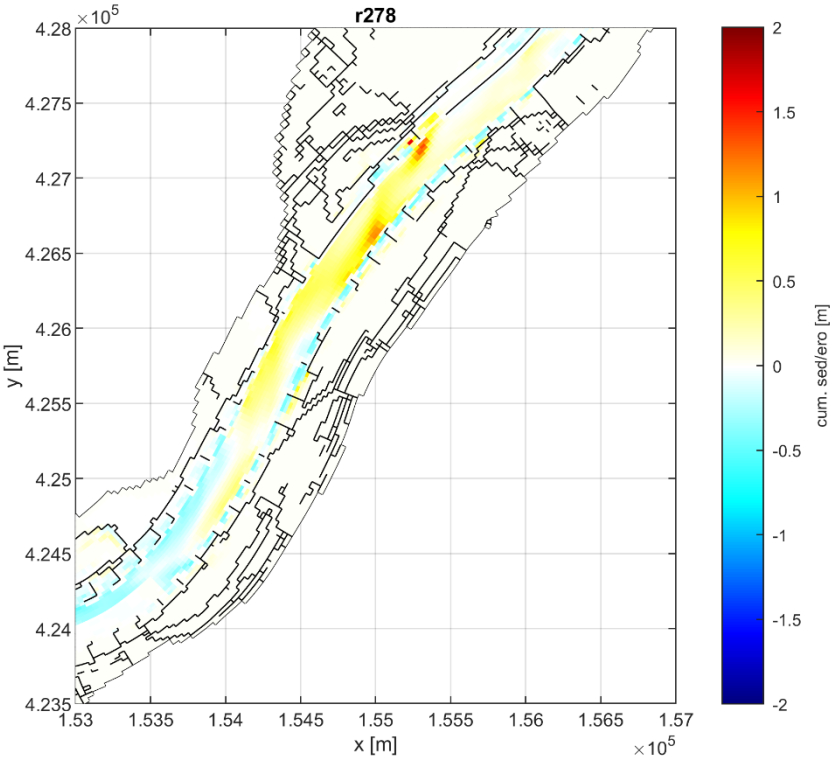
r278
×10^5
4.28
4.275
4.27
4.265
4.26
4.255
4.25
4.245
4.24
4.235
y [m]
1.53
1.535
1.54
1.545
1.55
1.555
1.56
1.565
1.57
x [m]
×10^5
2
1.5
1
0.5
0
-0.5
-1
-1.5
-2
cum. sed/ero [m]

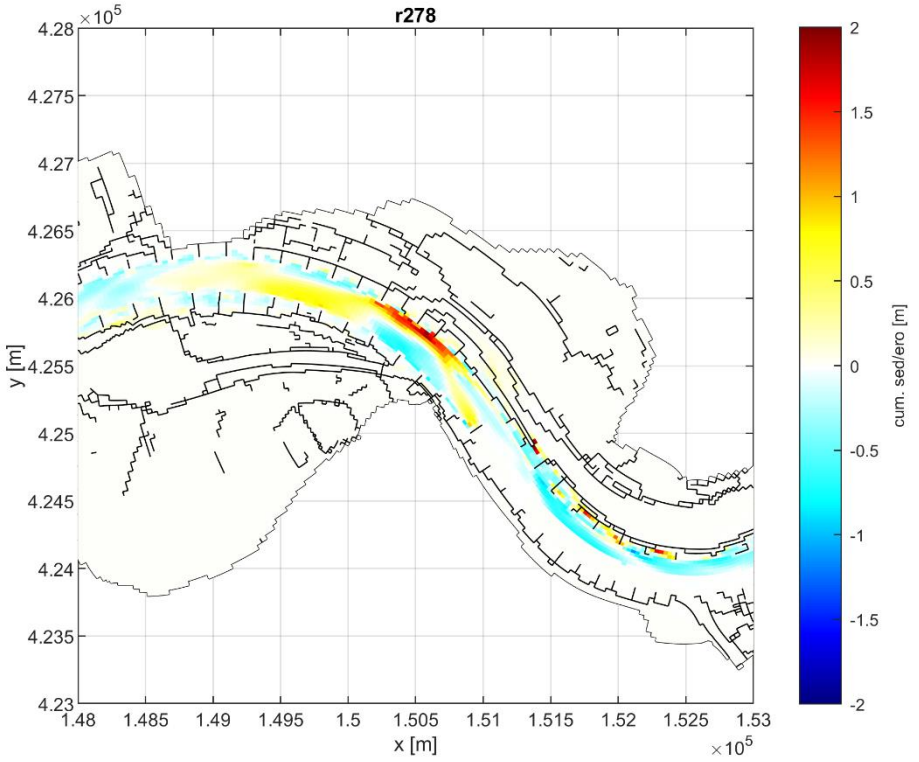
r278
×10^5
4.28
4.275
4.27
4.265
4.26
4.255
4.25
4.245
4.24
4.235
4.23
y [m]
1.48
1.485
1.49
1.495
1.5
1.505
1.51
1.515
1.52
1.525
1.53
x [m]
×10^5
2
1.5
1
0.5
0
-0.5
-1
-1.5
-2
cum. sed/ero [m]

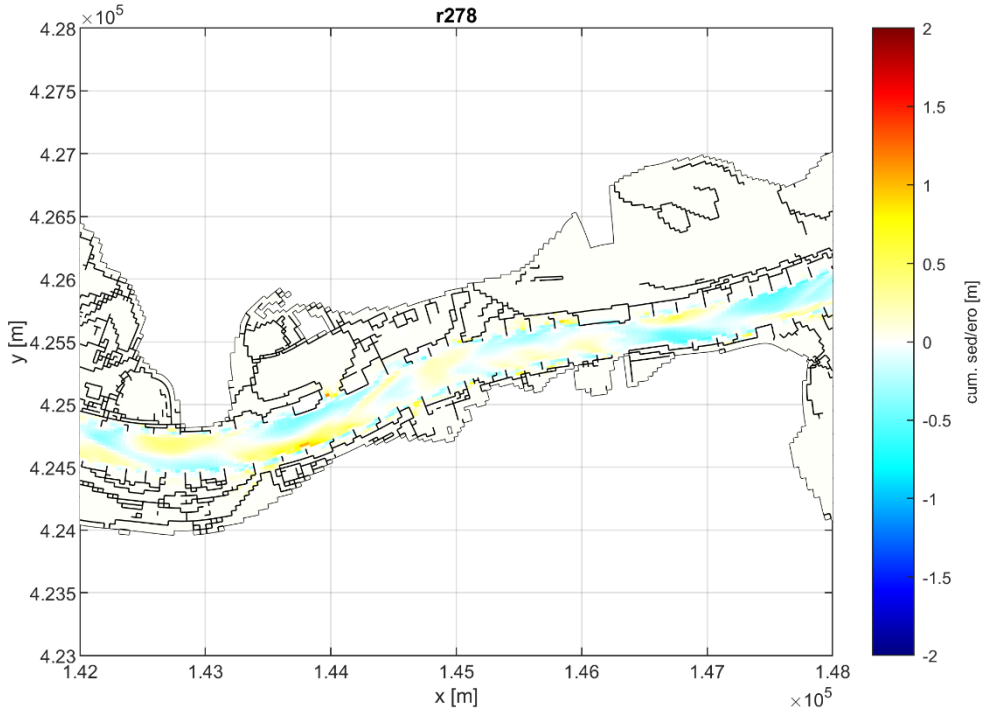
r278
×10^5
4.28
4.275
4.27
4.265
4.26
4.255
4.25
4.245
4.24
4.235
4.23
y [m]
1.42
1.43
1.44
1.45
1.46
1.47
1.48
x [m]
×10^5
2
1.5
1
0.5
0
-0.5
-1
-1.5
-2
cum. sed/ero [m]

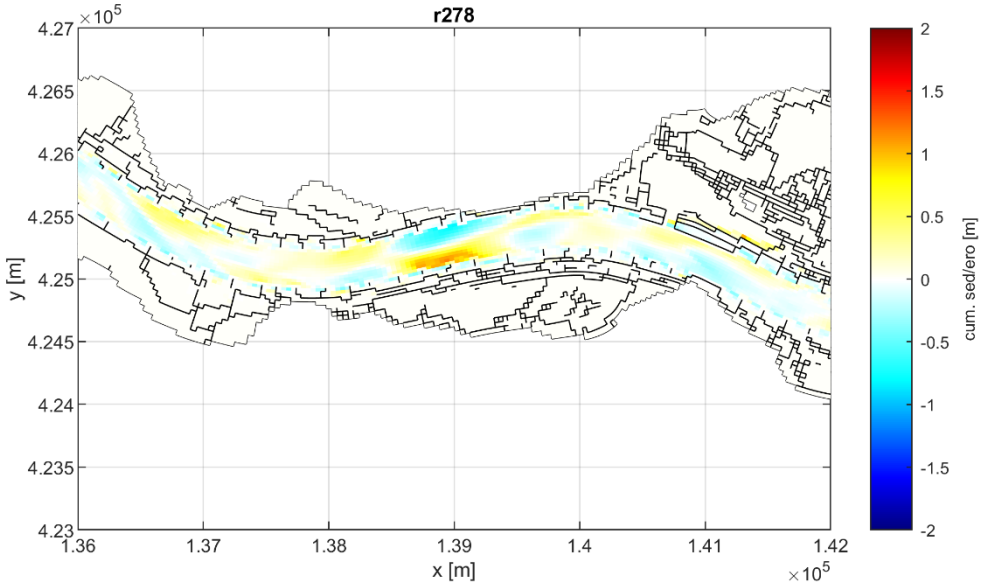
r278
×10^5
4.27
4.265
4.26
4.255
4.25
4.245
4.24
4.235
4.23
y [m]
1.36
1.37
1.38
1.39
1.4
1.41
1.42
×10^5
x [m]
2
1.5
1
0.5
0
-0.5
-1
-1.5
-2
cum. sed/ero [m]

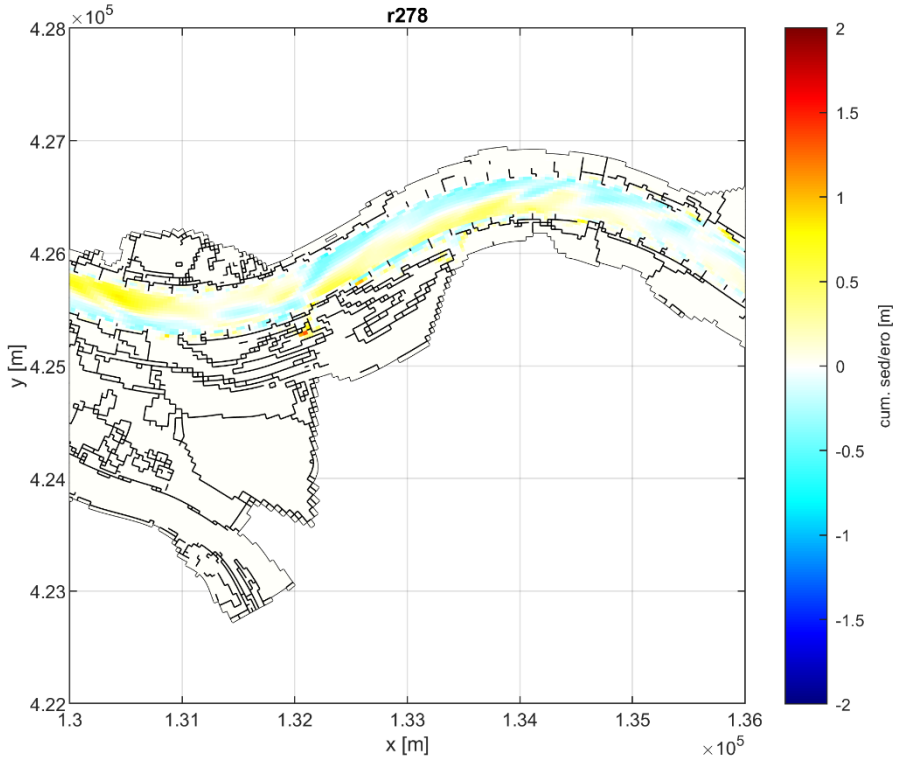
r278
×10^5
4.28
4.27
4.26
4.25
4.24
4.23
4.22
y [m]
1.3
1.31
1.32
1.33
1.34
1.35
1.36
×10^5
x [m]
2
1.5
1
0.5
0
-0.5
-1
-1.5
-2
cum. sed/ero [m]

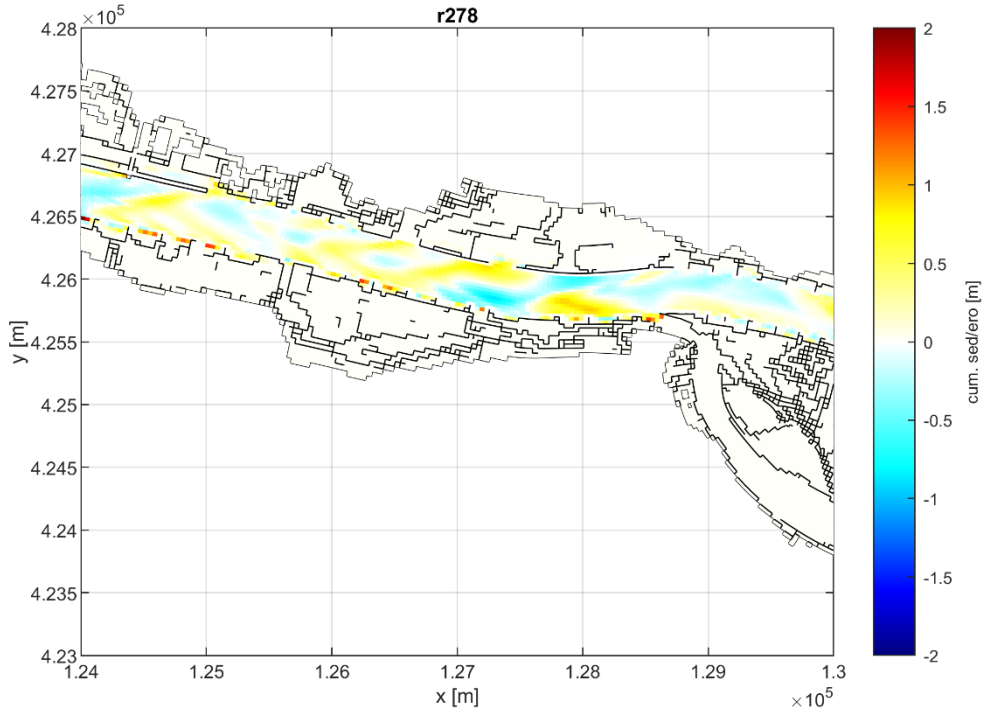
r278
×10^5
4.28
4.275
4.27
4.265
4.26
4.255
4.25
4.245
4.24
4.235
4.23
y [m]
1.24
1.25
1.26
1.27
1.28
1.29
1.3
x [m]
×10^5
2
1.5
1
0.5
0
-0.5
-1
-1.5
-2
cum. sed/ero [m]

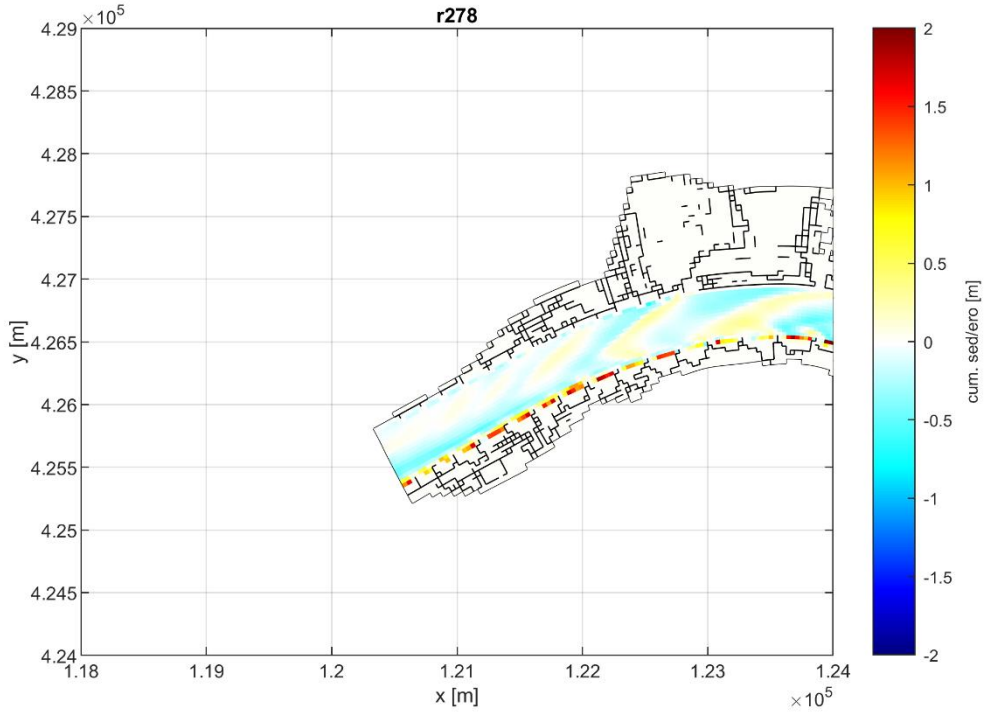
r278
×10^5
4.29
4.285
4.28
4.275
4.27
4.265
4.26
4.255
4.25
4.245
4.24
y [m]
1.18
1.19
1.2
1.21
1.22
1.23
1.24
x [m]
×10^5
2
1.5
1
0.5
0
-0.5
-1
-1.5
-2
cum. sed/ero [m]

Deltares is een onafhankelijk kennisinstituut voor toegepast onderzoek op het gebied van water en ondergrond. Wereldwijd werken we aan slimme oplossingen voor mens, milieu en maatschappij.

Deltares

www.deltares.nl